DECLINE CURVE ANALYSIS FOR UNCONVENTIONAL RESERVOIR SYSTEMS — VARIABLE PRESSURE DROP CASE

A Thesis

by

PATRICK WILLIAM COLLINS

Submitted to the Office of Graduate and Professional Studies of
Texas A&M University
in partial fulfillment of the requirements for the degree of

MASTER OF SCIENCE

Chair of Committee,	Thomas A. Blasingame
Committee Members,	Peter P. Valkó
	Lee L. Lowery
Head of Department,	A. Daniel Hill

December 2016

Major Subject: Petroleum Engineering

ABSTRACT

The premise of this work is the development, validation, and application of a methodology to forecast production data in unconventional reservoirs where variable rate and pressure drop producing conditions are typically observed. In unconventional reservoirs, it is not common practice to maintain or even arrive quickly upon a constant flowing bottomhole pressure which is the primary assumption for the application of traditional time-rate decline curve analysis. As a result, the application of traditional time-rate relations to these cases yields misleading results at best.

The methodology presented herein involves the application of the rigorous convolution/superposition theory traditionally relied upon for pressure transient or production analysis. Empirical pressure drop normalized rate decline relations are utilized as a proxy for analytical models in the convolution integral and superposed with either measured or calculated flowing bottomhole pressure drop data for the well(s) in question. The ability to incorporate non-linearities such as compressible gas flow and pressure dependent permeability is investigated using pseudopressure transformations and the limitations are outlined clearly.

A three step workflow consisting of diagnostics, model calibration, and production forecasting is first developed before ultimately being validated and applied for a number of simulation and field data cases. The diagnostic stage of the workflow provides the foundation for the proceeding analysis by providing insight into prevailing performance signatures for the well in question. The primary tool for achieving this is the so called “qDb” plot, which is referenced throughout the work. Incorporation of diagnostics minimizes non-uniqueness and guides model parameter selection for the second stage of the workflow. Ultimately, production is forecast into the future according to any number of defined pressure drawdown schedules.

The validation examples in this work successfully demonstrate the workflow for a range of oil and gas cases with and without pressure dependent permeability introduced into the system. In each of the cases, the data was synthetic and was generated by a commercial simulator using unstructured Voronoi gridding. Validation was achieved using a total of five decline models that are relied upon throughout the work and detailed in dedicated Appendices.

Application examples were chosen to reflect representative field cases where the author has found the methodology to be useful from a practical standpoint. Each example aims to emphasize a different problem and outline the strength and limitations of the methodology applied to each. It is here noted that the primary weakness of the methodology is its ability to handle cases with high degrees of non-linearity.

This is evident when forecasting a high-pressure/high-temperature shale gas well where drawdowns are very high.

The work is rounded out with the conclusion that the approach introduced herein provides a useful tool for quickly forecasting production under variable pressure drop conditions for both producing and undeveloped wells. The methodology is particularly useful for scenarios where more detailed analytical and numerical modeling techniques may not be feasible analysis options due to data or time limitations.

DEDICATION

This work is dedicated to:

My grandfather Rip for instilling education as a value of the utmost importance. Only the greatest educator could achieve this posthumously.

My grandfather Ray for the life lessons, both sorrowful and joyous, that I learned from observing such a full life.

"Live and act within the limit of your knowledge and keep expanding it to the limit of your life."
—Ayn Rand, Atlas Shrugged

ACKNOWLEDGEMENTS

The author would like to thank the following for their contributions to this work:

Dr. Thomas A. Blasingame, chair of my advisory committee, for his unending patience, friendship, sense of humor, and insistence on quality work.

Dr. Peter P. Valkó for his advice, suggestions, and serving as a committee member.

Dr. Lee L. Lowery for teaching me how to learn and earn a grade for the first time in my life during CVEN 305 and for serving as a committee member.

My professional colleagues Dilhan Ilk, Nima Hosseinpour-Zonoozi, and Matías Fernández Badessich for their suggestions, encouragement, and support.

My wife Elizabeth who took this journey with me. It wasn't exactly how we drew it up but your unending support, patience with the late nights, and gentle encouragement got us through it.

TABLE OF CONTENTS

Page

LIST OF FIGURES

Page

Page

LIST OF TABLES

CHAPTER I

INTRODUCTION

1.1 Introduction

Decline curve analysis, generally defined as the process of extrapolating only time-rate production data into the future using an empirical mathematical model is one of the most commonly used techniques for estimating ultimate recovery from a producing well or reservoir. Arps' (1945) exponential and hyperbolic decline models, the most commonly used decline models within the petroleum industry, are applied by calibrating a set of model parameters controlling the forecast shape until a best fit of the prevailing flowrate trend is achieved and appropriate application of these models is subject to the following list of assumptions adapted from Lee and Wattenbarger (1996):

- The extrapolation of a curve (*i.e.* rate-time model) through the historic production data is an adequate representation of future production trends.
- Current operating conditions and field development will continue without substantial changes which may affect the model extrapolation into the future.
- The well is producing from an unchanging drainage area with no-flow boundaries (i.e. boundary dominated flow).
- The well is producing against a constant bottomhole flowing pressure.

Production from conventional reservoir systems often occurs according to the above assumptions; however, most of them are violated in low to ultra-low permeability systems where there is a lack of historical analogs and considerable uncertainty regarding long-term well performance. Each of the points deserves attention in its own right, but the final point forms the focus of this work, specifically in the context of unconventional reservoirs where extended periods of variable pressure drawdown conditions are common due to choke management practices, pump capacity limitations, concerns about geomechanical effects, and prevailing market conditions. The primary goal is to present a workflow for incorporating flowing pressures into a traditional decline curve analysis workflow thus providing a simple forecasting technique for wells exhibiting variable pressure drop conditions that would otherwise require more rigorous analytical or numerical model based production analysis.

The aim of this work is achieved by using the superposition principle used in analytical model based production analysis with pressure drop normalized empirical decline curve relations serving as an approximation of the unknown constant pressure rate response. A three step process consisting of data

diagnostics, history matching using superposition, and production forecasting is thoroughly developed allowing consistent application. The methodology is first validated using a series of synthetic examples generated with a reservoir simulator where the system under consideration is known. It is noted that the methodology is able to adequately capture the sustained rate trends for cases with and without non-linearities using pseudopressure transformations where appropriate. Following validation, select oil and gas field examples are analyzed demonstrating practical applications.

1.2 Objectives

The primary objectives of this work are:

- To develop and validate a methodology combining the superposition principle and empirical constant pressure rate solution approximations enabling the incorporation of flowing pressures into decline curve analysis workflows.
- To extend the workflow to incorporate nonlinearities in the form of compressible gas flow and pressure dependent permeability while documenting any potential limitations.
- To demonstrate the technique applied to unconventional well production cases exhibiting variable-rate/variable-pressure drop conditions.

1.3 Statement of the Problem

Production forecasting in low to ultra-low permeability unconventional reservoir systems presents many challenges to the practicing engineer. In addition to having a limited understanding of the flow physics governing these complex systems, many of the traditionally used techniques for forecasting in conventional systems render themselves invalid. This is especially true when care is not taken when applying empirical decline relations which, at the time of this writing, are the industry standard for forecasting production for reserve evaluations.

Particular care is warranted when applying the most commonly used decline model, namely the Arps' decline relation. This statement is justified by carefully observing the list of assumptions outlined in section 1.1 where an argument can be made that each point is violated in unconventional systems. A lack of historical analogs, uncertainty regarding flow regime changes and timing, and a limited understanding of the contacted drainage area make it challenging to establish confidence that any particular model adequately represents future production behavior. Furthermore, choke management strategies, re-stimulation of wells, infill drilling, and artificial lift installations, among other practices, lead to constantly evolving field developments which makes comparing forecasts from year-to-year a challenge. Extremely low permeabilities coupled with multi-stage hydraulic fracture treatments lead to long term transient linear

flow regimes which is in stark contrast to the boundary dominated flow requirement outlined in Arps' original work. The reality of long term transient flow amplifies the non-uniqueness of the curve fitting procedure. Each of the above points deserves attention in its own right; however, the assumption of a constant bottomhole flowing pressure is the primary focus of this work.

The introduction of practice based approaches, such as the so-called modified hyperbolic relation and a slew of modern decline relations, have all been developed to mitigate some of the problems associated with forecasting time-rate production data in unconventional systems. Most of these models were developed to address specific flow regimes or operational conditions and at this stage all must be considered empirical relationships. Full theoretical treatment of five such models is provided in Appendices A through E. While the petroleum literature is replete with such "built-for-purpose" models, minimally addressed are in-depth workflows aiming to incorporate flowing pressures into a straightforward empirical decline curve analysis process. This is particularly important, regardless of the empirical model chosen, due to the common practice of managing pressure drawdown in unconventional wells which leads to a period of sustained production rates and violates a key assumption of decline curve analysis. **Figure 1.1**, shown below, depicts such a case for an unconventional shale oil well.

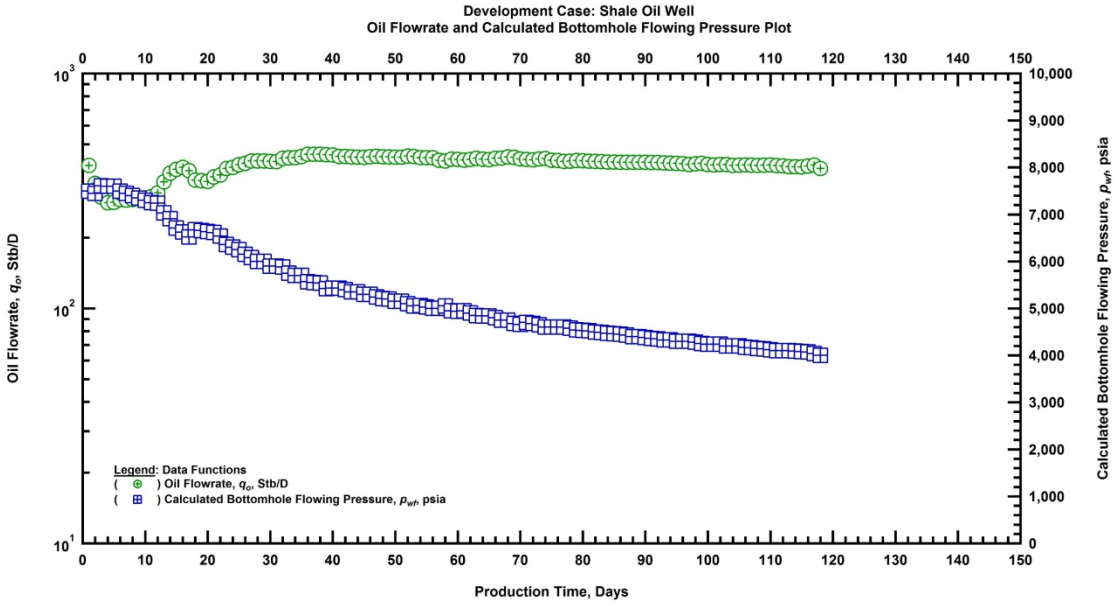

Figure 1.1 — Time-Rate-Pressure Production Data for Illustrative Development Case

Reasons for managing the pressure drawdown are wide ranging and are often due to surface facility limitations, pump capacity, the impact of in-situ stress on completion integrity, concerns about fluid

property changes, and prevailing market conditions to name a few. The most commonly employed method for forecasting this well with an aim of estimating remaining reserves would be to observe the time-rate data on a semi-log plot and vary the parameters of the modified hyperbolic Arps' decline relations (either manually or using a regression routine) until an adequate match is reached. **Figure 1.2** demonstrates this process where two widely different time-rate decline curve matches are overlain on the oil production data shown previously.

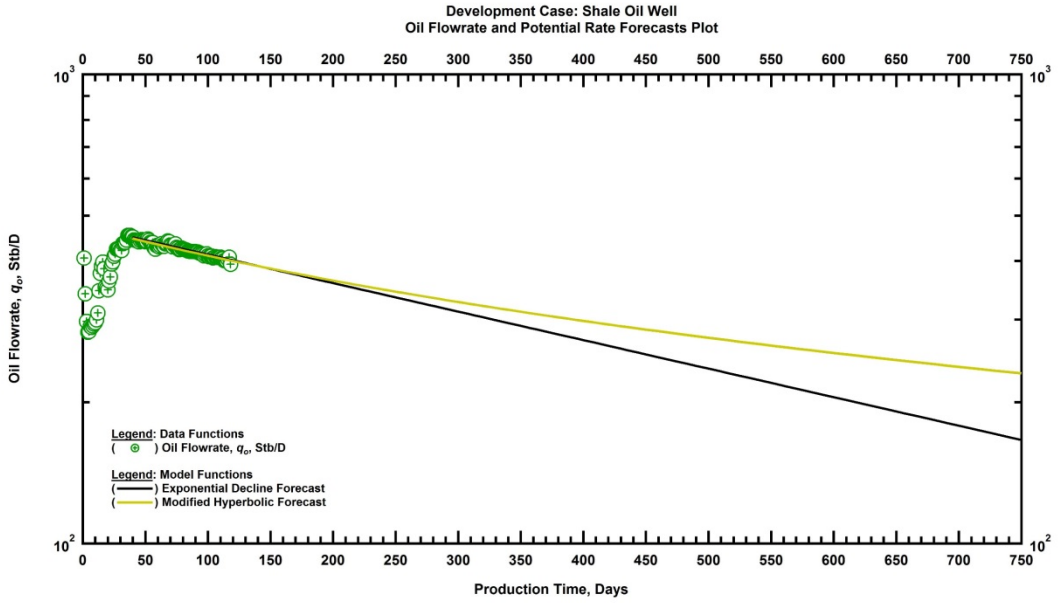

Figure 1.2 — Illustrative Development Case ─ Oil Flowrate and Potential Rate Forecasts

Table 1.1 below summarizes the model results and recovery values for the time-rate examples shown above. The range of both parameters and estimated ultimate recovery (EUR) values exhibited by the two production forecasts, both of which could be argued to be correct based upon only this semi-log plot of rate-time, illustrates the non-uniqueness of this exercise. It is clear in this case that using the semi-log plot in isolation has to potential to provide misleading production forecasts.

Table 1.1 — Illustrative Development Case ─ Time-Rate Decline Curve Analysis Results

Decline Model	q_i (STB/D)	D_i (1/D)	b (dim.less)	D_{lim} (percent/year)	EUR_{30yr} (Mstb)
EXP	475	0.0014	-	-	336
M.HYP	475	0.0016	1.3	10	899

Non-uniqueness is an unfortunate fact of life in reservoir engineering which is inherently an inverse problem, meaning we know inputs and outputs but have to try and characterize the system governing the observed response. This non-uniqueness is compounded by the short production history and the lack of clear decline trends as a result of the choke management practices for many wells. The workflow presented herein is intended particularly to address the practical need to forecast production from wells exhibiting variable pressure drawdown early (*e.g.* a few weeks to a few years) in the life-cycle of the well using easily taught and applied decline curve concepts.

The stated aims are achieved through a combination of Duhamel's principle (*i.e.* convolution integral), which provides the theoretical foundation for analytical model-based production analysis techniques, and pressure drop normalized formulations of empirical decline relations presented in the petroleum literature. The former part of the combination, namely the convolution integral, provides the fundamental reservoir engineering principle utilized in this work and is presented below in a time-step discretized form.

$$q(t) = \sum_{k=1}^{u} (\Delta p_{wf,k} - \Delta p_{wf,k-1})(q_{cp}(t_u - t_{k-1})) \quad \text{.....(1.1)}$$

where Δp_{wf} corresponds to the flowing bottomhole pressure drop at a particular time step and q_{cp} typically corresponds to an analytical solution to the diffusivity equation describing flow in porous media assuming a constant pressure at the sandface for the well in question. The primary assumption in this work involves the convolution kernel, or q_{cp}, in Equation 1.1. Instead of relying upon constant pressure rate solutions to the diffusivity equation (*i.e.* analytical models) the assumption is made that empirical relations utilized for standard decline curve analysis workflows can be normalized by a pressure drop term and serve as adequate proxies for the constant pressure rate response, q_{cp}, in the convolution integral. Equations 1.2 through 1.6 below provide these relations for the hyperbolic (HYP), power-law exponential (PLE), stretched exponential (SEM), Duong (DNG), and logistic growth (LGM) models, respectively.

$$q_{cp}(t) \approx \frac{q(t)}{\Delta p_{wf}(t)} = \left(\frac{q}{\Delta p}\right)_i \frac{1}{(1+bD_i t)^{1/b}} \quad \text{.....(1.2)}$$

$$q_{cp}(t) \approx \frac{q(t)}{\Delta p_{wf}(t)} = \left(\frac{\hat{q}}{\Delta p}\right)_i \exp[-\hat{D}_i t^n - D_\infty t] \quad \text{.....(1.3)}$$

$$q_{cp}(t) \approx \frac{q(t)}{\Delta p_{wf}(t)} = \left(\frac{\hat{q}}{\Delta p}\right)_i \exp[-(t/\tau)^n] \quad \text{.....(1.4)}$$

$$q_{cp}(t) \approx \frac{q(t)}{\Delta p_{wf}(t)} = \left(\frac{q_1}{\Delta p}\right)_i t^{-m_{DNG}} \exp\left[\frac{a_{DNG}}{1-m_{DNG}}(t^{1-m_{DNG}} -)\right] \quad \text{.....(1.5)}$$

$$q_{cp}(t) \approx \frac{q(t)}{\Delta p_{wf}(t)} = \left(\frac{K}{\Delta p}\right)_i \frac{n_{LGM}\, a_{LGM}\, t^{(n_{LGM}-1)}}{(a_{LGM} + t^{n_{LGM}})^2} \quad \text{.....(1.6)}$$

Combining equation 1.1 with equations 1.2 through 1.6 allows for the incorporation of pressure drop changes throughout time into a decline curve analysis workflow. The end result of the methodology is the ability to history match rate changes that occur as a result of pressure changes and forecast future production trends based on various prescribed future pressure schedules. As the convolution integral assumes linearity, special consideration is given to pseudopressure transformations to at least partially linearize systems exhibiting gas production and pressure dependent permeability.

Figure 1.3 depicts the end result of the variable pressure decline curve workflow using the power-law exponential decline relationship which is fully derived in Appendix B. Two separate pressure extrapolation profiles were used to demonstrate the methodologies ability to incorporate different pressure drawdown assumptions when forecasting production. **Tables 1.2** and summarizes the results for the power-law exponential decline model where it can be seen that the model parameters are in line with what may be expected for wells flowing against a constant bottomhole pressure and the estimated ultimate recovery values are heavily dependent upon the pressure profile assumption chosen.

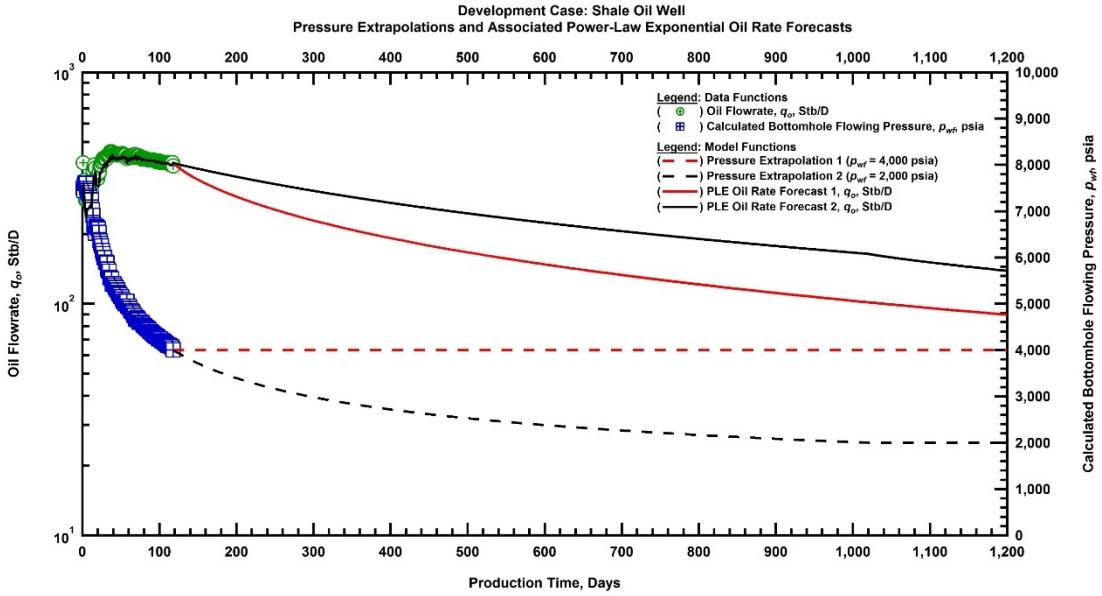

Figure 1.3 — Illustrative Development Case ─ Pressure Extrapolations and Power-Law Exponential Rate Forecasts

Table 1.2 — Illustrative Development Case ─ Power-Law Exponential Variable Pressure Decline Curve Results

Decline Model	$(q/\Delta p)_i$ (STB/D/psia)	D_i (1/D)	n (dim.less)	D_∞ (1/D)	EUR_{30yr} (Mstb)
PLE (p_{wf} forecast #1)	0.375	0.52	0.25	-	479
PLE (p_{wf} forecast #2)	0.375	0.52	0.25	-	701

1.4 Validation and Application

A complete development of the workflow in question is provided in the proceeding sections. Simulation examples, where the inputs and outputs of the reservoir system(s) being analyzed are known, validate the technique. Proof-of-concept is proven using a black oil simulation with no introduced non-linearities. Subsequently, the method is extended to accommodate non-linearities in the form of compressible gas flow and pressure dependent permeability. Each simulation is constructed in a manner reflective of typical unconventional oil and gas systems.

Following validation, application examples are demonstrated using field production data from various unconventional plays. The workflow is strictly followed to demonstrate repeatability and practical limitations. The assumptions are clearly outlined and demonstrated for all of the application examples.

1.5 Summary and Conclusions

Incorporation of flowing pressures into decline curve analysis techniques is achieved by developing a complete workflow consisting of diagnostics, decline model calibration, and forecasting based on a prescribed future pressure drawdown. The technique is found to be an effective and easily applied method to quickly forecast wells exhibiting variable pressure drop conditions. The workflow is particularly applicable to unconventional oil or gas production where constant bottomhole flowing pressures are typically not quickly achieved and the effect of different pressure extrapolation assumptions on the forecast behavior is desired for reserves forecasting or operational planning.

A diagnostic and differentiation procedure to assess the applicability of the method as a whole, evaluate the consistency of the production data, identify the presence of any non-linearities, and determine prevailing flow regimes is outlined as a necessary first step of the workflow. Specialized plots and numerical differentiation routines are used to achieve these goals. The convolution integral typically used for analytical model based production analysis and pressure transient analysis provides the fundamental reservoir engineering principle for the workflow. The main assumption of the work is that a pressure drop normalized empirical decline relation is a valid approximation of an analytical solution to the diffusivity equation and may thus serve in its place as the convolution kernel for superposition calculations. The chosen model is calibrated using diagnostic “qDb” plots and, after achieving an appropriate match of the data, production is forecasted assuming any number of pressure extrapolation realizations.

The workflow is validated using a series of synthetic examples meant to emulate typical unconventional production systems. Cases with and without non-linearities are analyzed in order to investigate possible extension and limitations of the method. Following validation, the method is demonstrated for a variety of field cases. Limitations when using pseudo-pressure transformations, particularly those incorporating pressure dependent permeability, are noted for high pressure drawdown cases. Widespread applicability of the workflow for unconventional production systems is suggested through the validation and field examples.

CHAPTER II

LITERATURE REVIEW

The overall objective of this work is the development of a methodology for forecasting production data from unconventional reservoir systems exhibiting nearly constant production rates due to continuously declining pressure drop conditions early in the life of a well. Prior to discussing the work to date addressing that particular problem, a discussion of both classical and modern developments related to time-rate decline curve analysis as well as semi-analytical/analytical model based production analysis is warranted in order to provide a foundation for the developments proposed. Special emphasis will be placed on practical techniques for forecasting production data in unconventional reservoir systems. The literature reviewed in this work is categorized according to the following subsections:

- Time-Rate Decline Curve Analysis
- Semi-Analytical/Analytical Model Based Production Analysis
- Variable-pressure Decline Curve Analysis

2.1 Time-Rate Decline Curve Analysis

Decline curve analysis (DCA), or the extrapolation of only time-rate production data into the future, is one of the most commonly used techniques in the petroleum industry to estimate ultimate recovery (EUR) for producing wells. Various techniques for forecasting production data have been proposed and applied since the early twentieth century; however, in the modern sense of the word decline curve analysis refers to the calibration of a time-rate model to a single well (or multiple wells) and extrapolating production to an abandonment limit yielding an estimate of ultimate recovery. This section provides an overview of classical decline curve analysis as a means of forecasting production data in conventional plays and modern techniques developed specifically to address production forecasting challenges in unconventional reservoir systems.

Lewis and Beal (1918) were among the first practitioners to recognize the importance of developing dependable, quick, and easily applied forecasting methods for estimating reserves early in the life of a well or field. In pursuit of this goal the authors examined available data from two different Oklahoma fields and observed that the percentage rate decline versus time data exhibited power-law trends, or straight-lines, when plotted on logarithmic coordinates. They concluded that this straight line behavior, along with plots of cumulative percentage decline, could be used to adequately forecast future production. The authors acknowledged the use and outlined the limitations of reserve estimates via volumetric techniques,

analogy methods, and production curve forecasting. Interestingly, the authors also provided an early look into probabilistic forecasting by examining the statistical nature of their forecast results.

Cutler (1924) later provided an extensive overview of production forecasting techniques during the 1920's. Similar to Lewis and Beal, he observed the decline behavior of a large number of wells produced with little or no production curtailment. His primary deduction was that the percentage rate decline was often variable which contrasted with the constant behavior observed by Lewis and Beal. He concluded that the rate decline could be modeled by a mathematical equation of the hyperbolic class by shifting production data through trial and error until a straight line trend is established.

The concepts of the loss-ratio and loss-ratio derivative were introduced by Johnson and Bollens (1927) giving the observations of prior authors a mathematical context. The definition of the loss-ratio is presented below as:

$$\frac{1}{D(t)} = -\frac{q(t)}{dq(t)/dt} \quad \text{.....(2.1)}$$

Where $1/D(t)$ is the loss-ratio, $q(t)$ the flowrate, and t production time. By extension, the derivative of the loss-ratio is defined as follows:

$$b(t) = \frac{d}{dt}\left[\frac{1}{D(t)}\right] = -\frac{d}{dt}\left[\frac{q(t)}{dq(t)/dt}\right] \quad \text{.....(2.2)}$$

In this case b represents the derivative of the loss-ratio. Their forecast approach involved tabulating these ratios using finite difference numerical differentiation, extrapolating the corresponding trend according to the observed ratio behavior, and back-calculating the future rate profile. The authors confirmed the observations of prior engineers by mentioning that the ratio trends often display power-law behavior. These revelations provide a crucial piece of the foundation for both classic and modern decline curve analysis techniques.

Prior to Arps' (1945, 1956) seminal works, the majority of the effort in the realm of production forecasting was focused on plotting rate, cumulative production, or associated ratio data in various coordinate systems searching for an easily extrapolated straight line behavior. Arps formally synthesized prior work by defining the now ubiquitous exponential and hyperbolic declines in mathematical terms for both rate versus time and rate versus cumulative production expressions. The rate versus time exponential decline, using modern nomenclature, is given below as:

$$q(t) = q_i \exp\left[-D_i t\right] \quad \text{.....(2.3)}$$

where q_i is the initial flowrate of the model and D_i represents the initial nominal decline rate. This equation is the mathematical manifestation of the constant percentage decline concept alluded to by prior researchers. In other words, Eq. 5 was derived based on *observations* by Arps and others that the loss ratio, defined by Equation 2.1, exhibited near constant behavior. Additionally, Arps also provided the following formulation of the rate versus time hyperbolic decline which is shown below.

$$q(t) = \frac{q_i}{\left(1 + bD_i t\right)^{1/b}} \quad \text{.....(2.4)}$$

where the *b* parameter represents the Arps' hyperbolic decline exponent. This equation provides a mathematical basis to the apparent hyperbolic nature, or the observed deviation from a constant percentage decline behavior noted by Cutler (1924). The hyperbolic derivation was based on an *observation* that the loss-ratio derivative, defined by Equation 2.2, exhibited constant behavior for some wells. As a result a single *b* factor is used to describe the production decline throughout the history of a well when using the hyperbolic model in its traditional sense.

In conjunction with his derivations, Arps formally outlined a set of assumptions governing the practical applicability of the exponential and hyperbolic relations. The list below, adapted from Lee and Wattenbarger (1996), summarizes these assumptions:

- The extrapolation of a curve (*i.e.* rate time model) through the historic production data is an adequate representation of future production trends.
- Current operating conditions and field development will continue without substantial changes which may affect the model extrapolation into the future.
- The well is producing from an unchanging drainage area with no-flow boundaries (*i.e.* boundary dominated flow).
- The well is producing against a constant bottomhole flowing pressure.

In addition to these formal assumptions Arps noted that the hyperbolic *b* parameter should range between 0 and 1 due to the unbounded nature when the hyperbolic exponent is greater than or equal to unity.

In direct contrast to Arps' prior suggestions that the hyperbolic *b* exponent should fall between 0 and 1, Maley (1985) demonstrated that a *b* value greater than unity could adequately fit production data from tight gas wells. This observation, while strictly empirical, can be confirmed as one of the first addressing and questioning, the applicability of classical decline curve analysis for unconventional reservoirs. The author also noted that care must be taken to avoid unreasonable estimates of ultimate recovery due to the unbounded nature of the mathematical model.

Rushing *et al*. (2007) delved further into the topic of forecasting production data in tight reservoirs as part of a comprehensive simulation study where they observed that extrapolating rates during transient flow using an unbounded hyperbolic equation ($b > 1$) resulted in significant overestimates of estimated ultimate recovery (EUR). As an additional point of significance, they also observed that the b value tended to decrease as a function of time. These observations were further elaborated on in the work of Lee and Sidle (2010) which discussed the significance of these observations as they relate to reserve estimation.

An in depth discussion of the cause of b-parameters greater than unity is warranted due to its direct relevance to the challenge of forecasting production data in unconventional reservoir systems. Okouma *et al.* (2012) provide a comprehensive discussion on the practical aspects of decline curve analysis in unconventional reservoirs where horizontal wells with large multi-stage fracture stimulations are the development norm. The authors note that these wells typically exhibit linear, bi-linear, or multi-fractured flow signatures early on in their productive lives. The following equation corresponds to linear flow which is characterized by a half slope trend when production rate versus time is plotted on logarithmic coordinates. Linear flow is indicative of very high conductivity fractures.

$$q(t) = \frac{a_{LF}}{\sqrt{t}} \quad \text{.....(2.5)}$$

where a_{LF} is a lump linear flow model parameter. Similarly, quarter slope trends in raw data are often indicative of bi-linear flow resulting from low or very low conductivity fractures. The following equation summarizes this behavior.

$$q(t) = \frac{a_{BLF}}{\sqrt[4]{t}} \quad \text{.....(2.6)}$$

where a_{BLF} is a lump bi-linear flow model parameter. The authors also mentioned occasional third slope behavior when analyzing field data and termed this the multi-fracture flow regime. The equation describing this regime is as follows.

$$q(t) = \frac{a_{MFF}}{\sqrt[3]{t}} \quad \text{.....(2.7)}$$

where a_{MFF} is a lump multi-fracture flow model parameter.

Observing Eqs. 7, 8, and 9 it is immediately evident that each is a power-law representation of the rate as a function of time. The practical implications are realized by showing that Arps' hyperbolic relation (Eq. 2.4) can be reduced to a power-law equation for certain circumstances. Okouma *et al.* (2012) made the

following observations, showing that Arps' hyperbolic equation could be reduced to the power-law relations presented above.

- Substituting b=2 into Eq. 2.4 (assuming $bD_it >> 1$) yields the linear flow relation (Eq. 2.5).
- Substituting b=4 into Eq. 2.4 (assuming $bD_it >> 1$) yields the bi-linear flow relation (Eq. 2.6).
- Substituting b=3 into Eq. 2.4 (assuming $bD_it >> 1$) yields the multi-fracture flow relation (Eq. 2.7).

These observations help explain why Arps' hyperbolic relation often adequately fits production data from fractured wells early in their production history. The authors acknowledge that the hyperbolic relation can still be used as a practical tool as long as proper care is taken to constrain the relation to avoid excessive resource estimates.

Robertson (1988) introduced the so called modified hyperbolic decline which, at the time of this writing, is by far the most used method of constraining hyperbolic models with *b*-parameters greater than unity. This method is a practice based approach where early transient production data is fit using Eq. 2.4 with an appropriate *b*-parameter and at a later period in time an exponential tail, or terminal decline, is spliced to the hyperbolic portion to force the rate to eventually reach zero and bound the forecast. This method is a useful and practical method for constraining recovery estimates; however, there is a great deal of ambiguity surrounding the magnitude and switch point when applying the exponential tail. Without proper care, future recovery can be grossly over or under estimated.

The power-law exponential decline, which assumes that the *b*-factor trend (*i.e.* derivative of the loss-ratio) declines as a function of time, was derived by Ilk *et al.* (2008, 2009) in an attempt to better model fracture dominated flow in low/ultra-low permeability reservoirs. The rate versus time formulation is provided below.

$$q(t) = \hat{q}_i \exp[-\hat{D}_i t^n - D_\infty t] \quad \text{.....(2.8)}$$

where $\hat{q}_i$ is the initial rate coefficient, $\hat{D}_i$ the decline coefficient, n the time exponent, and D_∞ the terminal decline coefficient. Similar to Arps' models, the authors' derivation was based on observed behaviors of the loss-ratio (Eq. 2.1) and derivative of the loss-ratio (Eq. 2.2). Specifically, the model assumes that each decreases as a power-law function with time (*i.e.* straight line on a log-log plot). This observation is in-line with the early time flow regime behaviors that predominate in many fractured wells producing from unconventional formations. In an attempt to model the transition from transient (*e.g.* linear, bi-linear, etc.) flow to boundary dominated or depletion type flow the power-law exponential decline includes a terminal decline coefficient (D_∞) which forces the model to gradually transition to an exponential decline at later times.

Valkó (2009) later introduced the stretched exponential decline as part of a large scale database study of monthly production data from the Barnett Shale. While derived independently, the stretched exponential model and power-law exponential model are essentially the same aside from the inclusion of the D_∞ term included in the power-law exponential decline. The functional form of the stretched exponential decline model also finds use across scientific disciplines including modeling aftershock decay for electrical engineering applications [Kohlrausch (1854) and Kisslinger (1993)]. The rate-time formulation for the stretched exponential model is given below:

$$q(t) = \hat{q}_i \exp[-(t/\tau)^n] \quad \text{.....(2.9)}$$

where $\hat{q}_i$ is the initial rate coefficient, n the time exponent, and τ the time coefficient. While still empirical, the stretched exponential equation is essentially an infinite sum of exponential declines which could be thought to define the model in terms of fundamental reservoir engineering principles.

Duong (2011) developed his namesake model in a specific attempt to describe long-term linear flow performance. The rate time formulation of his model is displayed below.

$$q(t) = q_1 t^{-m_{Dng}} \exp\left[\frac{a_{Dng}}{(1-m_{Dng})}[t^{(1-m_{Dng})}-1]\right] \quad \text{.....(2.10)}$$

where q_1 is the initial rate coefficient and m_{Dng} and a_{Dng} are additional model parameters. Duong's model aims to model long term transient linear flow behavior and the author proposed a systematic methodology for calibrating the model parameters. Specifically, Duong's methodology utilizes a best-fit power law relation of the rate-cumulative ratio (q/G for gas production cases and q/N for oil) versus time data to establish the a_{Dng} and m_{Dng} from the intercept and slope, respectively.

Clark *et al.* (2011) proposed a decline curve model in the form of a generalized logistic growth model of the hyperlogistic class [Blumberg (1968)]. The authors noted the utilization of logistic growth functions for applications ranging from new product market penetration to the biomedical sciences. The formulation presented relies on the assumption that cumulative production grows logistically to a previously known or estimated initial hydrocarbon volume in-place. The rate versus time formulation presented below was obtained by taking the derivative of the cumulative production model proposed by the authors.

$$q(t) = \frac{dG_p(t)}{dt} = \frac{Kn_{LGM}a_{LGM}t^{(n_{LGM}-1)}}{(a_{LGM}+t^{n_{LGM}})^2} \quad \text{.....(2.11)}$$

where K is the carrying capacity, which in this case is a proxy for the hydrocarbon initially in place. The remaining two parameters are n_{LGM}, which is the time exponent, and a_{LGM} which is a model parameter. This model is analogous to the power-law and stretched sponential models shows good results when applied to transient flow regimes and decent results when attempting to model transitional flow regimes.

At this point each of the models presented above, with the exception of Arp's exponential decline, must be considered empirical. Each tends to focus on a particular flow regime or production characteristic (*e.g.* power-law flow regimes, boundary dominated flow, long-term linear flow, etc.) and all are subject to numerous assumptions. The most important assumption, common to all of the models, addressed in this work is that of a constant bottomhole flowing pressure throughout the life of the well. The aforementioned Okouma *et al.* (2012) reference provides an outstanding overview of the practical application of each of the time-rate decline models presented here. Additionally, a development of each of the models is included in the Appendices.

2.2 Model Based Production Analysis

Advances to empirical rate-time decline curve analysis methods presented in the previous section have come in the form of semi-analytical, analytical, and numerical model based production analysis (*e.g.* type curves, simulation software packages, etc.). Both approaches attempt to estimate ultimate recovery, resources in-place, and, whenever possible, well/reservoir characteristics governing production. Various authors have attempted to include the effect of variable rates and pressures into type curve analysis while software aided model based production analysis handles variable pressure drop conditions by using the convolution integral. Both topics will be addressed throughout this section.

While type-curves have long been utilized for the analysis of pressure transient data, their application as a means to forecast time-rate production data was introduced by Fetkovich (1980). The author introduced and applied a composite type-curve by splicing together analytical solution stems for the transient flow regime and the empirical hyperbolic decline solutions presented by Arps to model boundary dominated performance trends. Perhaps most importantly, the authors also provided an analytical derivation for the exponential decline and noted that this solution was common to both sides (*i.e.* transient and boundary dominated flow) of their proposed type-curve. Camacho and Raghavan (1989) attempted to show, with some degree of success, that the hyperbolic stems could be derived analytically for solution gas drive wells under boundary dominated flow. It is worth noting that Fetkovich's type curve assumes a well producing against a constant bottomhole flowing pressure in a bounded circular reservoir, although a re-initialization technique is proposed to account for variable pressure drop conditions.

Carter (1985) and Fetkovich *et al.* (1987) both extended the original Fetkovich paper to account for compressible gas flow. In their work, Fetkovich *et al.* used pressure-squared and pseudopressure transformations along with their original plotting functions to partially linearize the system thus allowing for the application of the liquid solutions to gas production scenarios [Wattenbarger and Ramey (1968) and Al-Hussainy *et al.* (1966)]. Carter, on the other hand, developed an independent type curve and thoroughly elaborated on the dependence of gas production on the magnitude of pressure drawdown which was briefly noted in the original Fetkovich work [Fetkovich (1980)]. The authors also note that the onset of boundary dominated flow was a necessary pre-requisite to partially avoid non-uniqueness of type-curve matches during the transient flow regime.

In order to completely linearize gas production systems, Fraim and Wattenbarger (1987) introduced a pseudotime definition accounting for changes in fluid properties with declining average reservoir pressure. The authors expanded upon previous pseudotime definitions where gas viscosity and compressibility were evaluated at the flowing bottomhole pressure [Agarwal (1979) and Lee and Holditch (1982)]. Pseudopressure and their pseudotime corrections were then used to apply the liquid Fetkovich type curves to gas production data. The authors also mentioned that pressure drop normalized rate data provided an adequate proxy for constant bottomhole pressure conditions as long as pressures were smoothly changing so as not to introduce excessive transient spikes.

Blasingame and Lee (1986) provided work attempting to use decline curve analysis as a tool for establishing reservoir characteristics for homogeneous, naturally fractured, and hydraulically fractured systems using the concepts of reservoir limits testing. There work relied on the analytical foundations of the exponential decline and is limited to wells producing a single phase (*i.e.* oil, gas, or water) against a constant bottomhole pressure and exhibiting boundary dominated flow. The authors later extended their work to systems producing under variable-rate/variable-pressure conditions using the concept of material balance time and material balance pseudotime for oil and gas production [Blasingame and Lee (1986, 1988)]. These works provide the foundation for the development of a series of type curves and diagnostic plots used for modern model based production analysis.

In order to mitigate one of the main practical hindrances of type curve analysis, namely non-uniqueness when matching solution stems to data, Blasingame *et al.* (1989) introduced the pressure integral and integral derivative diagnostic functions to assist in the analysis of noisy well tests. In follow up works, Blasingame *et al.* (1990) and Blasingame *et al.* (1991) thoroughly demonstrating the application of these plotting functions for various well/reservoir configurations. McCray (1990), and subsequently Blasingame *et al.* (1991), extended the integral and integral derivative techniques to the analysis of noisy production (*i.e.* time-rate-pressure) data. As a result of these works the authors developed a set of type

curves based on pressure drop normalized rate and material balance time and successfully demonstrated the ability of their methodology to handle variable-rate and pressure production under boundary dominated flow.

Formalized workflows, application examples, and unified type curves of the integral and integral derivative functions are provided in a string of subsequent works. Palacio and Blasingame (1993) extended the concepts to include material balance pseudotime and demonstrated the applicability of the liquid solution type curves for gas production cases. Doublet *et al.* (1994) provided a thorough demonstration of the application for oil production using both simulated and field production data. Additional type curve developments have been introduced for horizontal wells, various water influx scenarios, multi-well reservoir systems, fractured wells, and elliptical flow [Shih and Blasingame (1995), Doublet and Blasingame (1995), Marhaendrajana and Blasingame (2001), Agarwal *et al.* (1999), Pratikno *et al.* (2003), and Amini *et al.* (2007)]. The type-curve developments proposed in these works are extensively utilized in software aided analytical model-based production analysis packages.

Model-based production analysis, at its core, is based on analytical solutions to the diffusivity equation set up for a various well/reservoir conditions. The diffusivity equation for radial flow – a second order partial differential equation – is given below:

$$\frac{1}{r}\frac{\partial}{\partial r}\left[r\frac{\partial p}{\partial r}\right]=\frac{k}{\phi\mu c_t}\frac{\partial p}{\partial t} \quad \text{.....(2.12)}$$

where r is the radial distance measured perpendicular to the wellbore, p pressure, ϕ porosity, μ viscosity, c_t the total compressibility, and k the permeability of the system. Solutions to this equation assuming a constant rate inner boundary condition form the theoretical basis for pressure transient analysis while solutions based on a constant pressure inner boundary condition provide the same for production analysis. Both of these solutions can be related using Laplace transformation identities. For scenarios where variable-rate and variable-pressure drop conditions prevail Duhamel's principle, or the convolution integral, is used to generate the variable-rate pressure and variable-pressure rate response [Duhamel (1833)]. The convolution integral for the variable rate pressure response is given below as:

$$\Delta p_{wf}(t)=\int_0^t q(t-\tau)p'_{cr}(\tau)d\tau \quad \text{.....(2.13)}$$

where Δp_{wf} is the bottomhole pressure drop as a function of time and p'_{cr} is the unknown derivative of the constant-rate pressure solution. Similarly, the variable pressure rate integral is given below as:

$$q(t) = \int_0^t \Delta p_{wf}(t-\tau) q'_{cp}(\tau) d\tau \quad \text{.....(2.14)}$$

where q'_{cp} is the derivative of the unknown constant pressure rate solution. It must be noted that the rigorous application of the convolution integral requires system linearity. Linearizing transformations are required in order to apply Eqs. 2.13 and 2.14 to cases where non-linearities prevail (*i.e.* gas flow, multiphase production, geomechanical effects introducing pressure dependent permeability, non-Darcy flow, etc.). The most commonly used methods to do so, which are the aforementioned normalized pseudopressure and pseudotime, utilize Kirchoff transformations to account for changing gas properties as functions of pressure [Al-Hussainy *et al.* (1966), Fraim and Wattenbarger (1987)]. The definition for normalized pseudopressure is as follows:

$$p_{pn} = \left(\frac{\mu_g z}{p}\right)_r \int_0^p \frac{p}{\mu_g z} dp \quad \text{.....(2.15)}$$

where p_{pn} is the normalized pseudopressure, z is the real gas deviation factor, and the subscript r denotes a reference condition. The definition for pseudotime is given below as:

$$t_n = \left(\mu_g c_t\right)_r \int_0^t \frac{1}{\mu_g(\bar{p}) c_t(\bar{p})} dt \quad \text{.....(2.16)}$$

where $\bar{p}$ is the average reservoir pressure of the system. We note here the difficulty encountered when applying Eq. 2.16 to unconventional reservoir systems where estimates of average reservoir pressure are rarely available due to the unfeasibility of long-term build-up tests in systems characterized by ultra-low permeability.

In practice, model-based production analysis consists of calibrating model parameters, or solution variables (i.e. effective fracture half length, permeability, formation thickness, etc.), to generate relevant response functions using the superposition concepts outlined above. In other words assumed constant-rate pressure solutions are superposed with discrete rate changes and constant-pressure rate solutions are superposed with discrete pressure changes in order to generate variable-rate or variable-pressure responses in an attempt to history match the actual production data from a well. One of the main challenges an analyst faces is the issue of non-uniqueness. To address this, diagnostic plotting functions such as the "log-log plot" and Blasingame plot, which utilize the pressure integral and pressure integral derivative concepts discussed previously, and type curves are utilized to help guide the model calibration process. It is also worthwhile to mention that a thorough assessment of all available data (*e.g.* PVT reports, completion records, production notes, etc) should be performed as part of a diagnostic workflow in order

to ensure the greatest amount of consistency during the history matching process. Ilk (2010) provides a thorough overview of such a diagnostic process in addition to well performance analysis techniques in unconventional reservoir systems.

The number of parameters involved in the modelling process depends on the model used. Various models, or analytical solutions to the diffusivity equation, are readily available in the petroleum engineering literature and only those particularly relevant to the analysis of unconventional reservoir systems will be reviewed. As a starting point we must first realize and concede that we have only a rudimentary understanding of the complex production mechanisms and flow characteristics of unconventional reservoirs where we are dealing with permeability values on the order of 10-500 nd and pore throats approaching the size of the produced hydrocarbon molecules [Nelson (2009)].

For tight gas applications, vertically fractured well solutions are often utilized in accordance with the common completion technique used when developing these reservoirs. Ilk *et al.* (2007a) provide numerous field examples using analytical elliptical flow solutions to evaluate the effectiveness of waterfrac techniques. Their work expands on the list of fractured well and elliptical flow solutions already mentioned [Agarwal *et al.* (1999), Pratikno *et al.* (2003), and Amini *et al.* (2007)].

Attempting to address the uncertainty inherent in the analysis of unconventional reservoir systems Wattenbarger *et al.* (1998) and, concurrently, El-Banbi and Wattenbarger (1998) formalized the linear flow concept frequently relied upon to analyze fractured wells exhibiting long periods of transient linear flow. The authors created Cartesian plots of reciprocal production rate versus square root of time where an initial straight line trend is attributed to predominating linear flow. The slope of a best fit line through an initial flow trend is used to garner an estimate of the effective drainage area, or the so called stimulated reservoir volume (SRV). Deviations from the linear flow trend are attributed to fracture interference, geomechanical effects, SRV depletion, or skin effects. Best-fit intercepts not passing through the origin are attributed to lower fracture conductivity and skin effects. Numerous works in the petroleum literature have extended these concepts and outline comprehensive workflows to facilitate easy application to field production data.

The model upon which many other models are based, and which is often times used for the analysis of production data from shale oil and gas formations, is the simple multi-fractured horizontal well solution. van Kruysdijk and Dullaert (1989) were among the first to develop an analytical solution for multi-fractured horizontal wells by using the boundary element method. They noted the presence of an initial period of linear flow during which hydrocarbons flow from the formation to the fracture face in a perpendicular direction, followed by a period of compound linear flow due to the onset of fracture-to-fracture interference, and finally a period of pseudoradial flow. Soliman *et al.* (1990) addressed some of

the primary technical concerns when attempting to drill, complete, and produce a horizontal well with multiple hydraulic fracture stages. They developed an analytical solution as part of their investigation into the optimal number of fracture stages, appropriate wellbore placement, and the effect of fracture geometry as a result of formation stresses. Larsen and Hegre (1991, 1994) developed constant wellbore rate solutions for a variety of fracture conductivities, shapes, and configurations. Additionally, the authors present solutions to modeling open-hole completions where flow into the wellbore and fractures occurs simultaneously. The second work thoroughly discusses the progression of flow regimes expected for a typical multi-fractured horizontal well. The flow regimes mentioned for a multi-fractured horizontal well with circular transverse fractures were fracture radial flow, radial-linear flow, formation linear flow, and, finally, pseudoradial flow. There are numerous other horizontal well solutions available in the petroleum literature in addition to the references reviewed here [Guo and Evans (1993), Horne and Temang (1995), Chen and Raghavan (1997), Raghavan *et al.* (1997)].

Ozkan *et al.* (2009) presented the so called tri-linear flow solution for modelling multi-fractured horizontal well completions. This model assumes the presence of an inner reservoir, or SRV area, the footprint area of which is bounded by the effective fracture half-length and the lateral length of the well. The model also assumes an outer reservoir zone. The three linear flow paths that give the model its name occur from the outer reservoir linearly into the inner reservoir, from the inner reservoir linearly to the fracture face, and within the fracture linearly to the wellbore. This solution is useful when trying to account for additional flow contribution outside a minimally contacted stimulated reservoir volume or SRV. In addition to the usual challenges posed by non-uniqueness, difficulty arises when trying to characterize the model parameters of the outer reservoir zone.

2.3 Variable-Pressure Decline Curve Analysis

As mentioned previously, there is limited treatment of methodologies to incorporate variable pressure drop conditions into empirical decline curve workflows. While analytical or numerical modeling rigorously incorporates variable rate and pressure behavior using the convolution integral, the data to support the modeling effort is often not available and the process could be prohibitively time consuming due to the vast number of wells typical of unconventional field development. On the other hand, empirical models are easy to implement, easy to tie to an economic model, and widely understood by development stakeholders ranging from engineers and managers or operating companies, investment professionals, and regulatory bodies. The challenge, as outlined in section 2.1, is the reality that they assume a constant bottomhole pressure which is often not the case. As a result of the strength and weaknesses of both approaches there is a clear need for methodologies to incorporating pressures into a straightforward

empirical decline curve workflow to estimate reserves and field development planning for wells exhibiting variable pressure behavior early in their lives.

Lacayo and Lee (2014) proposed one such solution which involves forecasting the pressure drop, or pseudopressure drop, normalized rate data into the future using modified decline curve relations. They provided a workflow to establish a rate forecast by assuming a pressure profile into the future and back calculating the expected production rate from the forecasted pressure drop normalized rate trend. Their rationale for this approach is that pressure drop normalization of the rate data provides an adequate approximation to the constant pressure rate response. This assumption is regularly used in the industry when diagnosing performance trends and most acknowledge the necessity of consistent data and smoothly varying rates and pressures as a requirement for the assumption to be meaningful.

Ilk and Blasingame (2013) and Collins *et al.* (2014) provide the foundational basis for this work. In the former, the authors postulated that combining empirical decline curve analysis with superposition theory could provide a means to incorporate pressure into decline curve analysis techniques. They demonstrated the applicability for a single high-pressure/high-temperature shale gas well using the hyperbolic decline model and the power-law exponential decline model. The latter work extended the prior to include validation examples using a variety of simulation examples and an extended suite of decline models. In both cases, potential limitations surrounding non-linearities were documented.

CHAPTER III

DEVELOPMENT OF THE METHODOLOGY

The primary deliverable of this work is the development of an easily followed and practically applicable workflow for incorporating variable pressure drop operating conditions into traditional decline curve analysis approaches. This section introduces the theoretical foundations of the proposed workflow and illustrates in detail the development case presented in Chapter I of this document in order to provide a visual foundation. A framework consisting of three primary steps, listed below, forms the structure of the section and appropriate consideration and discussion will be dedicated to handling particular complexities expected in practical analysis.

- Production Data Diagnostics
- Model Calibration
- Production Forecasting

3.1 Production Data Diagnostics

The first step prior to beginning any production analysis procedure is a guided diagnostic analysis integrating all available data relevant for achieving a specified engineering question. This data may include, but is not necessarily limited to, time-rate-pressure production data – all fluid phases and bottomhole pressure being preferred – in addition to any auxiliary data that a given data collection program allows (*e.g.* PVT reports, vertical and/or horizontal logs, DFIT analysis, completion reports, etc.). The problems addressed and the outcomes expected are dictated on a case-by-case basis and may include data quality control, identification of prevailing flow regimes, monitoring of fluid phase ratios, and assessment of the impact of operational changes, to name a few.

With the need for a clear engineering goal in mind, it is here stated that the most critical outcome of production diagnostics in the context of this work is to gain an understanding of the characteristic reservoir signature of the individual well being analyzed. This understanding will be expressed by way of both quantitative and qualitative deductions all of which should lead to a clearly outlined conjecture prior to moving on to further stages of the analysis. The primary tools to achieve these tasks are plots of time, rate, and pressure production data along with so-called "qDb" plots of the reciprocal of the loss-ratio, $D(t)$, the loss ratio derivative, $b(t)$, and the pressure drop normalized production data. Each of these tasks will be addressed in the proceeding paragraphs.

The starting point for the diagnostic analysis of each of the cases presented in this work will begin with a semi-log plot of the major hydrocarbon phase flowrate and any available flowing pressure measurements (surface or bottomhole) versus production time. Diagnosing whether flowing pressures are variable or constant is a primary point of investigation. Additionally, data consistency, or whether pressure and rate changes agree with each other, is of primary importance for reasons that will be expanded upon in the following section. **Figure 3.1**, included below, depicts such a plot for the development example that will be followed throughout this section.

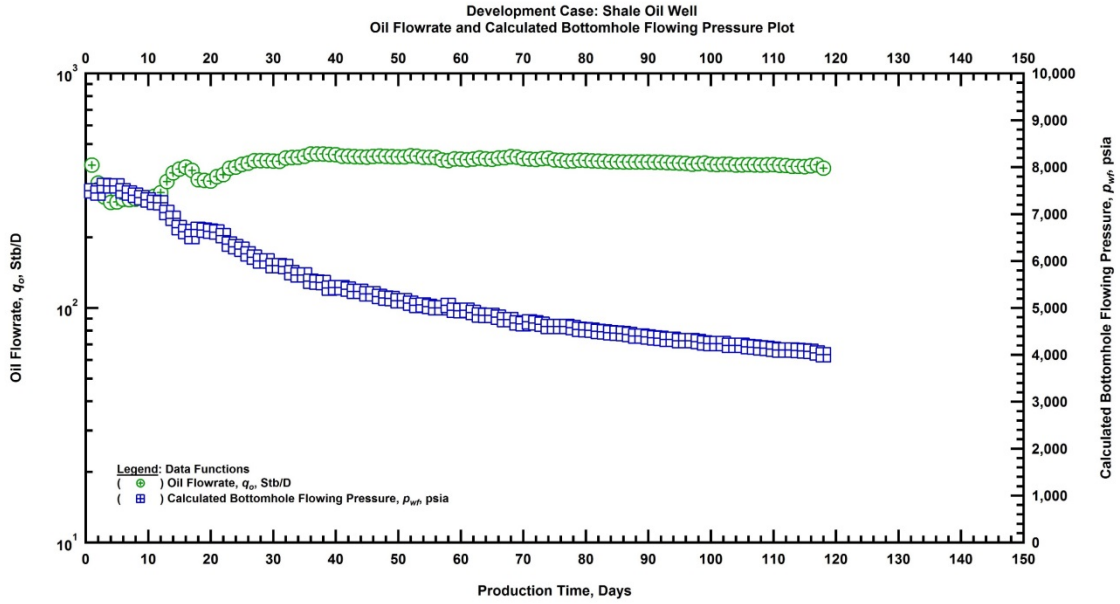

Figure 3.1 — Time-Rate-Pressure Production Data for Illustrative Development Case

It is clear from observing **Figure 3.**1 that the development example data set is highly consistent and the flowing pressure data is variable as opposed to constant, making this a wonderful illustrative example of a case where the methodology being developed is directly applicable. This basic quality control plot will also help when assessing operational changes such as installation or changes of wellbore tubulars or artificial lift. This has important implications when converting flowing surface pressure measurements to bottomhole values using either flow correlations or nodal analysis. As a final point, pressure drop normalization of the rate data forms a key pillar of the entire methodology, and as such, it is necessary to establish an estimate of the initial reservoir pressure at this stage of the workflow.

Following the initial data review described and depicted above, we move on to generating a modified version of the "qDb" plot introduced by Ilk *et al.* (2008, 2009). When this concept was introduced by Ilk

et al. as an integrated diagnostic and calibration tool, the reciprocal of the loss-ratio, $D(t)$, and the loss-ratio derivative, $b(t)$, — the equations defined by Johnson and Bollens (1918) are included below — were calculated from the rate data alone using the differentiation scheme introduced by Bourdet (1989).

$$D(t) = -\frac{1}{q(t)}\frac{dq(t)}{dt} \quad \text{.....(3.1)}$$

$$b(t) = \frac{d}{dt}\left[\frac{1}{D(t)}\right] = -\frac{d}{dt}\left[\frac{q(t)}{dq(t)/dt}\right] \quad \text{.....(3.2)}$$

By observing the raw rate data and the calculated derivative streams, deductions related to the reservoir signature can be made to better guide the model fitting process while somewhat mitigating the issue of non-uniqueness.

The utility of Eqs. 3.1 and 3.2, in relation to this work, is limited due to the assumption that the rate data alone accurately reflects the reservoir signature of the well subject to a single constant pressure drawdown. This is limiting for the cases of interest in this work such as the example provided in **Figure 3.1** where the pressure drop is highly variable with time. Addressing this limitation, it is proposed that the pressure drop normalized rate signature be observed for diagnostic purposes to approximate the equivalent constant pressure rate response. This, of course, is an approximation limited to smoothly varying rates and pressures but as a practice this technique is widely used throughout the industry. Accordingly, Eqs. 3.1 and 3.2 are modified below to account for this transformation.

$$\hat{D}(t) = -\frac{1}{q(t)/\Delta p(t)}\frac{d(q(t)/\Delta p(t))}{dt} \quad \text{.....(3.3)}$$

$$\hat{b}(t) = \frac{d}{dt}\left[\frac{1}{\hat{D}(t)}\right] = -\frac{d}{dt}\left[\frac{q(t)/\Delta p(t)}{d(q(t)/\Delta p(t))/dt}\right] \quad \text{.....(3.4)}$$

It is important to note here that rates must be normalized by real gas pseudopressures for incompressible flow in order to satisfy system linearity for superposition (the subject of the following section) and extract meaningful signatures when calculating derivative trends. In addition to compressible flow, additional non-linearities, such as geomechanical effects in the formation, are believed to be prevalent in unconventional systems. For this work these effects are captured by incorporating a pressure dependent permeability term in the pseudopressure definition when appropriate. The following two equations represent the above described forms of pseudopressure transformations respectively.

$$p_{pn} = \left(\frac{\mu_g z}{p}\right)_r \int_0^p \frac{p}{\mu_g z} dp \quad \text{.....(3.5)}$$

$$p_{pn} = \left(\frac{\mu_g z}{kp}\right)_r \int_0^p \frac{k(p)p}{\mu_g z} dp \quad \text{.....(3.6)}$$

where $k(p)$ is a placeholder for a functional relationship between permeability and pressure. Tables or custom functions can be used depending upon the availability of geomechanical lab data, however; in their absence correlations will suffice. For this work the exponential relationship proposed by Yilmaz and Nur (1991) and defined below is used exclusively to represent $k(p)$.

$$k(p) = k_i e^{-\gamma(p_i - p_{wf})} \quad \text{.....(3.7)}$$

where k_i represents the initial permeability of the system and γ is the permeability modulus defining the shape of the functional relationship. The limitations of the practical applications of Eqs. 3.6 and 3.7 will be discussed thoroughly in the validation and application chapters of this document.

Having discussed the theoretical foundations behind the modified "qDb" plot, which is the ultimate deliverable of the diagnostic step of this workflow, we now turn to the calculation procedure itself and present the result for the development example. Observing Eqs. 3.3 and 3.4, it is clear that a numerical differentiation routine must be relied upon to obtain the derivative signature of the raw pressure drop normalized rate signature. It must be noted here that some degree of regularization or data cleaning is likely required as numerical differentiation tends to accentuate any noise in the raw data. This will be covered in more detail in the application examples.

In this work, both the weighted finite difference routine proposed by Bourdet (1989) and a smoothing spline algorithm presented in a work by D.S.G. Pollock are used to calculate the derivative terms in order to. The purpose for using both techniques is to provide an estimate of the $D(t)$ and $b(t)$ signatures using two completely different numerical routines providing an additional element of trend granularity. This provides a degree of comfort given that the field production data tends to be riddled with noise and the pressure drop normalized rate data itself is only an approximation of the unknown constant pressure rate solution of the well. **Figure 3.2** below depicts the completed modified "qDb" plot for the development example.

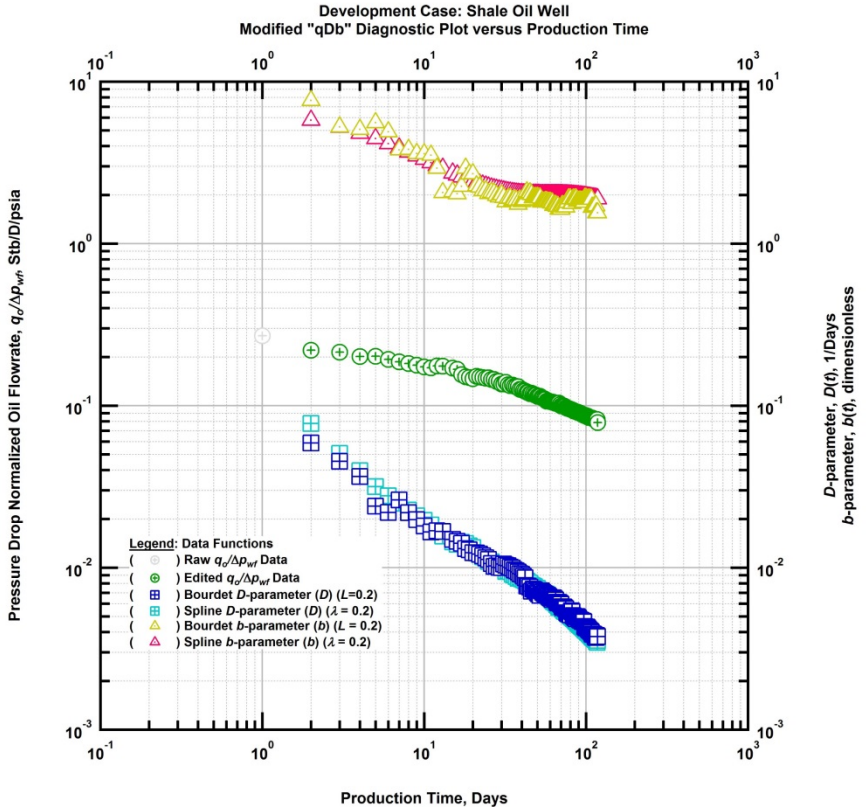

Figure 3.2 — Modified "qDb" Diagnostic Plot for Illustrative Development Case

The plot presented above provides a high degree of insight into the well performance for a particular case. As mentioned previously, the pressure drop normalized rate data provides an approximation for the constant pressure rate signature of the well with different slope trends providing insight into the prevalent flow regime(s). For instance, a half-slope would indicate linear flow while any departure would indicate a loss of productivity that would need further investigation to identify (*e.g.* well interference, reservoir boundaries, geomechanical effects, etc.).

The derivative terms, $D(t)$ and $b(t)$, are calculated from the edited pressure drop normalized rate stream using a degree of smoothing indicated by L and λ for the Bourdet and Spline routines, respectively. The signatures provide further verification of the prevalent flow regimes trends and aid in model choice and parameter calibration. For instance, in this well we see that after a period of well cleanup indicated by a slope less than one-half in the pressure drop normalized rate data, we see the establishment of what appears to be an approximate half-slope, indicative of linear flow. Theoretically this should correspond to a $b(t)$ signature of approximately two. When we observe the calculated $b(t)$ signature we see that indeed there is some stabilization of the data around two; however, one could interpret the overall trend as

declining throughout time suggesting a behavior more appropriate for a model such as the power-law exponential decline or logistic-growth model. The following section will work through this model fitting process in its entirety.

3.2 Model Calibration

The discussion no proceeds to the primary analysis portion of the workflow, namely superposing a calibrated pressure drop normalized decline curve model with a wells pressure drop history. As a starting point, the discussion necessarily begins with a brief theoretical discussion of model-based production analysis theory (*i.e.* well testing and rate-transient analysis) which is reliant upon analytical solutions to the diffusivity equation and the superposition integral. The diffusivity equation in radial coordinates, presented previously, is again included below.

$$\frac{1}{r}\frac{\partial}{\partial r}\left[r\frac{\partial p}{\partial r}\right]=\frac{k}{\phi\mu c_t}\frac{\partial p}{\partial t} \quad \text{.....(3.8)}$$

Solutions to this, or any other, second order partial differential equation require the selection of two boundary conditions and an initial condition. Pressure transient and production analysis, in general, concern themselves with solutions based on the specification of inner boundary and outer boundary conditions based on the wellbore and the reservoir properties and geometry, respectively. The inner boundary condition is the primary interest of this work and as a general rule, solutions (or models) are based on the assumption of either a constant sandface rate or a constant bottomhole flowing pressure. The solutions are relatable in the Laplace domain with the solutions subject to a constant rate traditionally being used for well-test analysis and the solutions subject to a constant wellbore pressure being used for production analysis. As outlined in Chapter 2 of this document, there is no shortage of available models in the petroleum literature representing various wellbore configurations (*e.g.* fractured wells, horizontal wells, etc.), reservoir phenomena (*e.g.* dual porosity, stimulated rock volume (SRV) models, homogeneous, etc.), and reservoir boundary conditions (*e.g.* infinite acting, faults, boundary dominated flow, etc.).

Stand-alone analytical solutions are limited in practical application due to the assumption of a constant wellbore producing condition (rate or pressure) throughout the producing life of the well. In their paper, van Everdingen and Hurst (1949) first comprehensively addressed the case of variable producing conditions for the handling wells producing from a reservoir with an active aquifer influx. The authors utilized the convolution integral, previously introduced, to apply standard analytical solutions to variable rate/pressure production data. The convolution integral formulated for modeling both continuously varying pressures and rates are presented below, respectively.

$$\Delta p_{wf}(t) = \int_0^t q(t-\tau) p'_{cr}(\tau) d\tau \quad \text{.....(3.9)}$$

$$q(t) = \int_0^t \Delta p_{wf}(t-\tau) q'_{cp}(\tau) d\tau \quad \text{.....(3.10)}$$

where p_{cr} represents a constant-rate pressure solution to the diffusivity equation and q_{cp} represent a constant pressure rate solution to the diffusivity equation. Given that continuous reading of rate and pressure data are not practically available, the continuous formulations are presented below in discretized form allowing the modeling of step changes in rate and pressure.

$$\Delta p_{wf}(t) = \sum_{k=1}^{u} (q_k - q_{k-1})(p_{cr}(t_u - t_{k-1})) \quad \text{.....(3.11)}$$

$$q(t) = \sum_{k=1}^{u} (\Delta p_{wf,k} - \Delta p_{wf,k-1})(q_{cp}(t_u - t_{k-1})) \quad \text{.....(3.12)}$$

Eqs. 3.11 and 3.12 form the theoretical foundation for modern model based pressure transient and production analysis where analytical model parameters (*e.g.* permeability, effective fracture half length, etc.) are calibrated iteratively based on diagnostic guidance in order to obtain a history match of the measured field data. It is crucial to note that the superposition principle is rigorous meaning that exact inputs yield exact outputs which justifies the data consistency efforts put forth in the foundational diagnostic analysis. A further caveat to application of the superposition principle is system linearity which only applicable for slightly compressible fluid flow. The pseudopressure transformation outlined in Eqs. 3.5 and 3.6 will be used to partially linearize the system for handling compressible flow or pressure dependent permeability, respectively.

It is important to emphasize that Eq. 3.12 is the primary fundamental reservoir engineering principle relied upon in this work. Already noted, however, is that the convolution integral only forms half of the methodology. To reiterate, the ultimate goal is the development of a methodology to incorporate variable pressure producing conditions into traditional decline curve analysis techniques which rely on constant bottomhole flowing pressures. In this work, the methodology is developed and demonstrated for the modified hyperbolic, power-law exponential, Duong, and logistic growth decline curve relations which are provided below for reference and developed thoroughly in Appendices A through E.

$$q(t) = \frac{q_i}{\left(1 + bD_i t\right)^{1/b}} \quad \text{.....(3.13)}$$

$$q(t) = \hat{q}_i \exp\left[-\hat{D}_i t^n - D_\infty t\right] \quad \text{.....(3.14)}$$

$$q(t) = \hat{q}_i \exp\left[-\left(\frac{t}{\tau}\right)^n\right] \quad \text{.....(3.15)}$$

$$q(t) = q_1 t^{-m} \exp\left[\frac{a}{1-m}(t^{1-m}-1)\right] \quad \text{.....(3.16)}$$

$$q(t) = \frac{Kant^{n-1}}{(a+t^n)^2} \quad \text{.....(3.17)}$$

While the above five models are exclusively focused upon in this work, it is important to note that any rate-time expression or tabulated rate-time data could be used as an alternative within the same workflow framework. The primary assumption of this entire work involves a slight modification of Eqs. 3.13 through 3.17. Particularly, it is assumed that pressure drop (or pseudopressure drop) normalization of the empirical models provides a valid approximation of an appropriate constant pressure rate analytical solution for the system under consideration. This assumption is presented mathematically as follows.

$$q_{cp}(t) \approx \frac{q(t)}{\Delta p_{wf}(t)} = \left(\frac{q}{\Delta p}\right)_i \frac{1}{(1+bD_i t)^{1/b}} \quad \text{.....(3.18)}$$

$$q_{cp}(t) \approx \frac{q(t)}{\Delta p(t)} = \left(\frac{\hat{q}_i}{\Delta p}\right)_i \exp\left[-\hat{D}_i t^n - D_\infty t\right] \quad \text{.....(3.19)}$$

$$q_{cp}(t) \approx \frac{q(t)}{\Delta p(t)} = \left(\frac{\hat{q}_i}{\Delta p}\right)_i \exp\left[-\left(\frac{t}{\tau}\right)^n\right] \quad \text{.....(3.20)}$$

$$q_{cp}(t) \approx \frac{q(t)}{\Delta p(t)} = \left(\frac{q_1}{\Delta p}\right)_i t^{-m} \exp\left[\frac{a}{1-m}(t^{1-m}-1)\right] \quad \text{.....(3.21)}$$

$$q_{cp}(t) \approx \frac{q(t)}{\Delta p(t)} = \left(\frac{K}{\Delta p}\right)_i \frac{nat^{n-1}}{(a+t^n)^2} \quad \text{.....(3.22)}$$

At this point it must be noted, that the assumed validity of Eqs. 3.18 through 3.22 as proxy models for analytical solutions may provide challenges. It is suspected that this assumption will prove adequate for cases where predominate flow regimes are evident; however, the empirical nature of the decline curve

relations cannot be emphasized enough and as such it is not expected that these relations will be able to adequately model complex flow scenarios (*i.e.* changing flow regimes, highly non-linear systems, etc.) in all cases. This will, of course, be investigated throughout the validation and application examples.

With the above assumptions in mind, Eqs. 3.18 through 3.22 can theoretically be substituted into Eq. 3.12 as the constant pressure rate equivalent convolution kernel. Doing so yields the following five expressions for modeling rate data exhibiting variable pressure drop conditions using solely decline curve relations.

$$q(t)=\left(\frac{q}{\Delta p}\right)_i\sum_{k=1}^{u}(\Delta p_{wf,k}-\Delta p_{wf,k-1})\frac{1}{(1+bD_i(t_u-t_{k-1}))^{1/b}} \quad \text{.....(3.23)}$$

$$q(t)=\left(\frac{\hat{q}}{\Delta p}\right)_i\sum_{k=1}^{u}(\Delta p_{wf,k}-\Delta p_{wf,k-1})\exp\left[-\hat{D}_i(t_u-t_{k-1})^n-D_\infty(t_u-t_{k-1})\right] \quad \text{.....(3.24)}$$

$$q(t)=\left(\frac{\hat{q}}{\Delta p}\right)_i\sum_{k=1}^{u}(\Delta p_{wf,k}-\Delta p_{wf,k-1})\exp\left[-\left(\frac{t_u-t_{k-1}}{\tau}\right)^n\right] \quad \text{.....(3.25)}$$

$$q(t)=\left(\frac{q_1}{\Delta p}\right)_i\sum_{k=1}^{u}(\Delta p_{wf,k}-\Delta p_{wf,k-1})(t_u-t_{k-1})^{-m}\exp\left[\frac{a}{1-m}\left[(t_u-t_{k-1})^{1-m}-1\right]\right] \quad \text{.....(3.26)}$$

$$q(t)=\left(\frac{K}{\Delta p}\right)_i\sum_{k=1}^{u}(\Delta p_{wf,k}-\Delta p_{wf,k-1})\frac{na(t_u-t_{k-1})^{n-1}}{[a+(t_u-t_{k-1})^n]^2} \quad \text{.....(3.27)}$$

Beyond the assumptions listed above, it is emphasized that, irrespective of their simplicity, the use of Eqs. 3.18 through 3.22 in the convolution integral assumes that the parameters themselves have some sort of physical meaning. This can only be explained at this point by considering the empirical parameters to be lump parameter approximations of the well and reservoir variable present in analytical solutions. Finally, the need for consistent, high quality, data for any time-rate-pressure analysis utilizing the convolution principle is duly noted. While not specifically useful as an analysis tool when data is inconsistent, the methodology still provides a degree of utility as a first order surveillance tool to check for data consistency.

Moving past the theoretical elements, the analysis process itself consists of calibrating a chosen decline model(s) using the rate-time history in conjunction with the modified "qDb" diagnostic plot described in the previous section. The pressure drop normalized rate, $D(t)$, and $b(t)$ data are matched by varying the model parameters for each model until an adequate match is achieved on the diagnostic plot. The $D(t)$

model trends are described mathematically for the hyperbolic, power-law exponential, stretched exponential, Duong, and logistic growth decline models as follows.

$$D(t) = \frac{D_i}{(1+bD_i t)} \quad \text{.....(3.28)}$$

$$D(t) = D_\infty + D_1 t^{-(1-n)} \quad \text{.....(3.29)}$$

$$D(t) = \frac{nt^{n-1}}{\tau^n} \quad \text{.....(3.30)}$$

$$D(t) = mt^{-1} - at^{-m} \quad \text{.....(3.31)}$$

$$D(t) = \frac{a(1-n)+(1+n)t^n}{t(a+t^n)} \quad \text{.....(3.32)}$$

Similarly, the $b(t)$ model trends are describe by the following mathematical expressions.

$$b(t) = b \quad \text{.....(3.33)}$$

$$b(t) = \frac{\hat{D}_i(1-n)nt^n}{\left(D_\infty t + \hat{D}_i nt^n\right)^2} \quad \text{.....(3.34)}$$

$$b(t) = \frac{(1-n)\tau^n}{nt^n} \quad \text{.....(3.35)}$$

$$b(t) = \frac{mt^m\left[t^m - a\ t\right]}{\left[at - mt^m\right]^2} \quad \text{.....(3.36)}$$

$$b(t) = \frac{a^2(1-n) - 2a(n^2-1)t^n + (n+1)t^{2n}}{[a(1-n)+(n+1)t^n]^2} \quad \text{.....(3.37)}$$

Once a match on the modified "qDb" diagnostic plot is achieved, the pressure drop normalized rate model as a function of time is superposed with the pressure drop data as a function of time in order to generate a model of the measured rate response subject to variable rate conditions in the wellbore. Small adjustments of the model parameters may need to be made in order to match the rate-time history as a part of an iteration process. **Figure 3.3** below provides a cartoon illustration of the superposition concept that is described above mathematically.

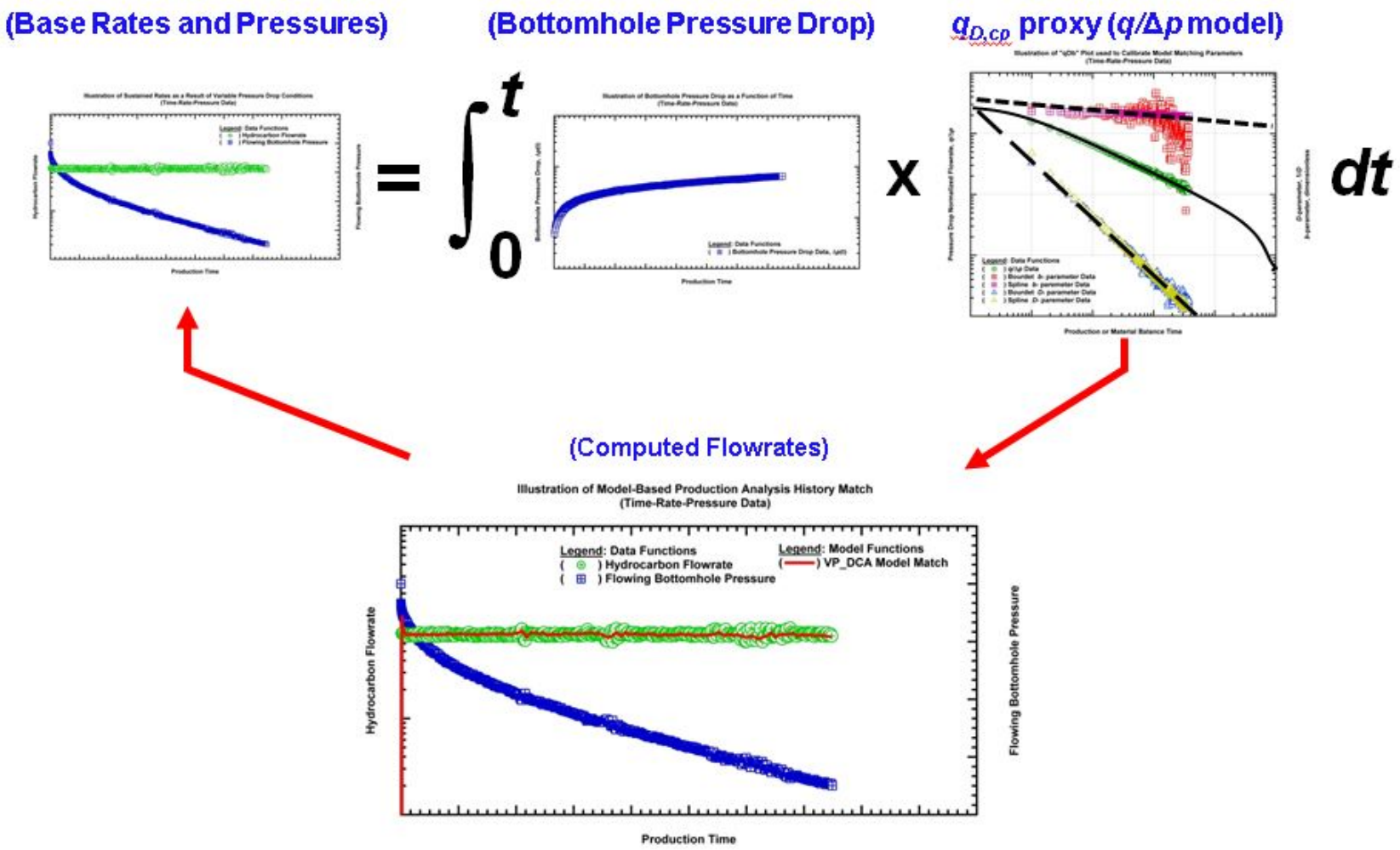

Figure 3.3 — Cartoon Schematic of the Developed Calibration and Superposition Process

Finally, we demonstrate the introduced process for the development case followed thus far in this chapter. Each of the introduced models is calibrated in turn in order to establish a simultaneously valid match of the data trends on the modified "qDb" diagnostic plot and the rate versus time data plot. The model parameters for each are provided below in **Table 3.1**.

Table 3.1 — Illustrative Development Case – Variable Pressure Decline Curve Model Parameter Results

Decline Model	$(q/\Delta p)_i$ *or* $(K/\Delta p)_i$ (STB/D/psi) or (STB/psi)	D_i *or* τ *or* a (1/D)	n or b *or* m (dim.less)	D_{lim} or D_∞ (percent/year) or (1/D)
M.HYP	0.187	0.025	1.700	10
PLE	0.375	0.520	0.250	0
SEM	0.375	13.68	0.250	-
DNG	0.220	1.100	1.110	-
LGM	77.00	250.0	0.800	-

Figures 3.4 and **3.5**, presented below, demonstrate that an adequate match was obtainable using all five of the models using the parameters listed above. As mentioned previously, some degree of iteration may be required in order to achieve an appropriate match across all plots and the exercise is likely to be non-unique.

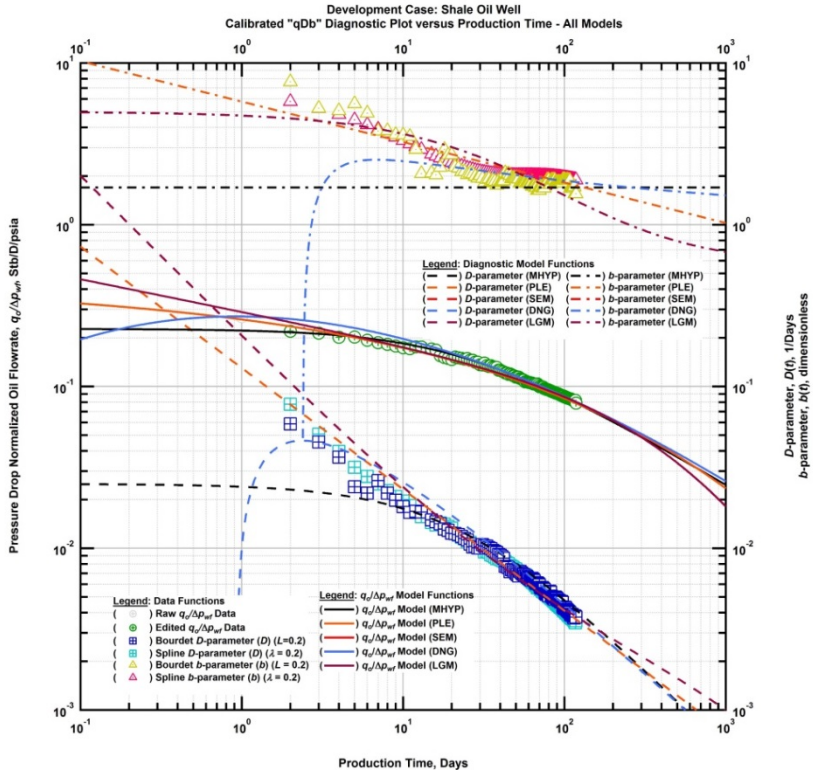

Figure 3.4 — Calibrated "qDb" Diagnostic Plot for Illustrative Development Case (All Models Shown)

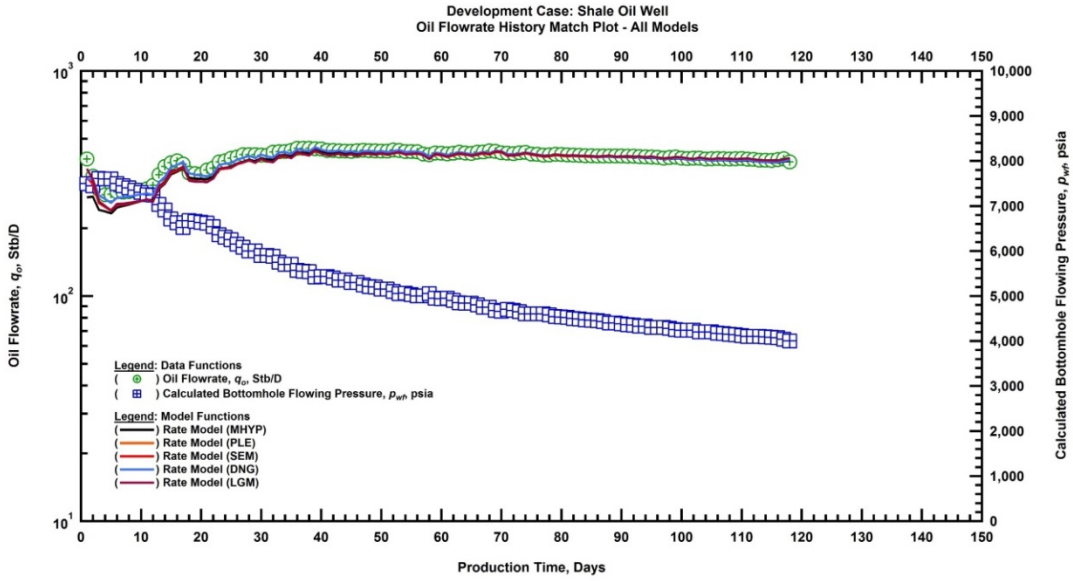

Figure 3.5 — History Match Plot Honoring Historical Rate Data (All Models Shown)

3.3 Production Forecasting

The final step of the workflow is to forecast the future production of the well in question. In order to do this, the concepts introduced in the last step are again used; however, the engineer must provide a pressure drawdown schedule based on the assumed operating conditions for the well into the future. This is identical in practice to the forecasting approach when performing model-based production analysis using analytical or numerical models. In fact, the ability to do so using empirical decline curves is a major advantage of the workflow over traditional decline curve techniques which assume a constant bottomhole pressure and more advanced model-based techniques which may require data that isn't readily available. This is especially useful when quick sensitivities investigating the effect of different pressure management practices into the future are desired early in the producing life of the well before a well has reached a constant drawdown and when a constrained and calibrated simulation model may not be feasible.

In practice, this is the simplest step in the workflow as no further analysis is required. In order to generate a time-rate forecast for the well in question the engineer simply provides a hypothetical pressure versus time profile after the last historic pressure point and the calibrated model, or models, are re-convolved with the new pressure data containing the historic pressure data and the projected pressure trend. **Figure 3.6** below depicts the forecasting results for the power-law exponential history match for the case analyzed throughout this chapter.

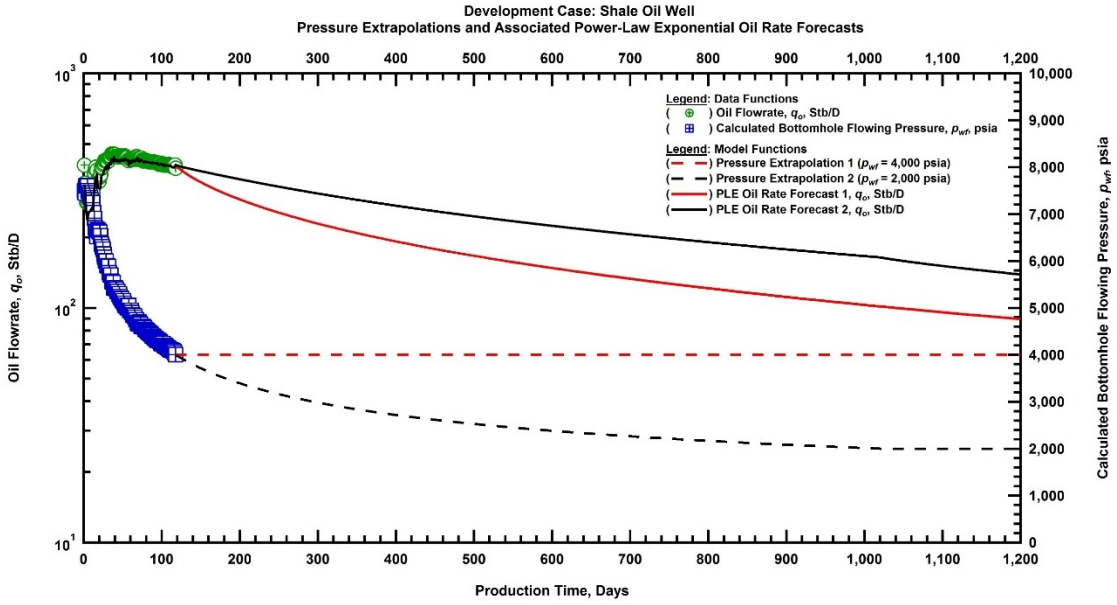

Figure 3.6 — Illustrative Development Case ─ Pressure Extrapolations and Power-Law Exponential Rate Forecasts

In the plot above, two different pressure drawdown assumptions were considered into the future where we clearly see differences in the resulting rate projections. The first drawdown case was a simple extrapolation of the last historic pressure until an abandonment limit where we can see that the projected rate trend immediately began falling off of the historical rate data which is being sustained by the variable pressure drawdown to date. The second drawdown assumption gradually reduces the flowing bottomhole pressure until a constant value of 2,000 psia is reached. The result of this pressure assumption is to maintain the rates for some time into the future. An additional point worthwhile point to note is that the history match depicted in **Figs. 3.4** and **3.5** has not been lost due to imposing pressure schedules into the future. Finally, the resulting parameters and EUR values are summarized in **Table 3.2** below.

Table 3.2 — Illustrative Development Case ─ All Models Forecasting Results

Decline Model	p_{wf} Forecast #1 EUR_{30yr} (Mstb)	p_{wf} Forecast #2 EUR_{30yr} (Mstb)
M.HYP	513	767
PLE	479	701
SEM	479	701
DNG	603	880
LGM	337	518

CHAPTER IV

VALIDATION OF THE METHODOLOGY

The aim of this chapter of the work is to provide a series of straightforward validation examples using the workflow developed in Chapter III. For each of the cases, synthetic pressure data was generated from an assumed near-constant rate trend using a finite element simulator with unstructured Voronoi gridding. The model parameter inputs, variable pressure decline results, and potential limitations are thoroughly discussed for each case in turn. The structure of the section is as follows.

- Black Oil Validation Example
- Gas Validation Example
- Gas Validation Example considering Pressure Dependent Permeability

4.1 Black Oil Validation Example

The first example is the simple case of a black oil producing at a near constant rate from an infinite acting system defined using the well and reservoir property inputs described in **Table 4.1**. The model inputs were chosen to mirror typical values determined when characterizing shale/tight-oil systems using model-based production analysis (*i.e.* inverse modeling). The pressure response to the near constant rate was limited to less than a year where the last historic flowing pressure remains high in order to demonstrate the history matching and forecasting capacity of the workflow for a case that has yet to reach a constant line pressure.

Table 4.1 — Validation Example #1 ─ Reservoir and Fluid Property Inputs for Simulated Data

Reservoir Properties:		
Net pay thickness, h	=	200 ft
Formation permeability, k	=	900 nD
Wellbore radius, r_w	=	0.3 ft
Formation compressibility, c_f	=	3 x 10^{-6} psi^{-1}
Porosity, ϕ	=	0.1 (fraction)
Initial reservoir pressure, p_i	=	9,000 psi
Oil saturation, S_o	=	1.0 (fraction)
Skin factor, s	=	0.00 (dimensionless)
Reservoir Temperature, T_r	=	212 °F
Fluid Properties:		
Oil specific gravity, γ_o	=	0.8 (water = 1)

Hydraulically Fractured Well Model Parameters:

Fracture half-length, x_f	=	250 ft
Number of fractures, n_f	=	25
Horizontal well length, L_w	=	5,000 ft

Production Parameters:

Last flowing pressure, psi	=	4,673 psi
Producing days, t	=	247 days

The simulated production data used for this example is depicted below in **Figure 4.1**. The rate and pressure trends are representative of what would be expected from an unconventional oil well flowing against managed drawdown conditions. The goal is to apply the variable pressure decline curve analysis workflow to this data for each of the five models outlined in chapter III and forecast the production into the future using two different pressure drawdown assumptions. The black oil scenario was chosen as a starting point due to a lack of significant non-linearities that would require pseudopressure transformations to utilize the superposition expression in Eq. 3.12.

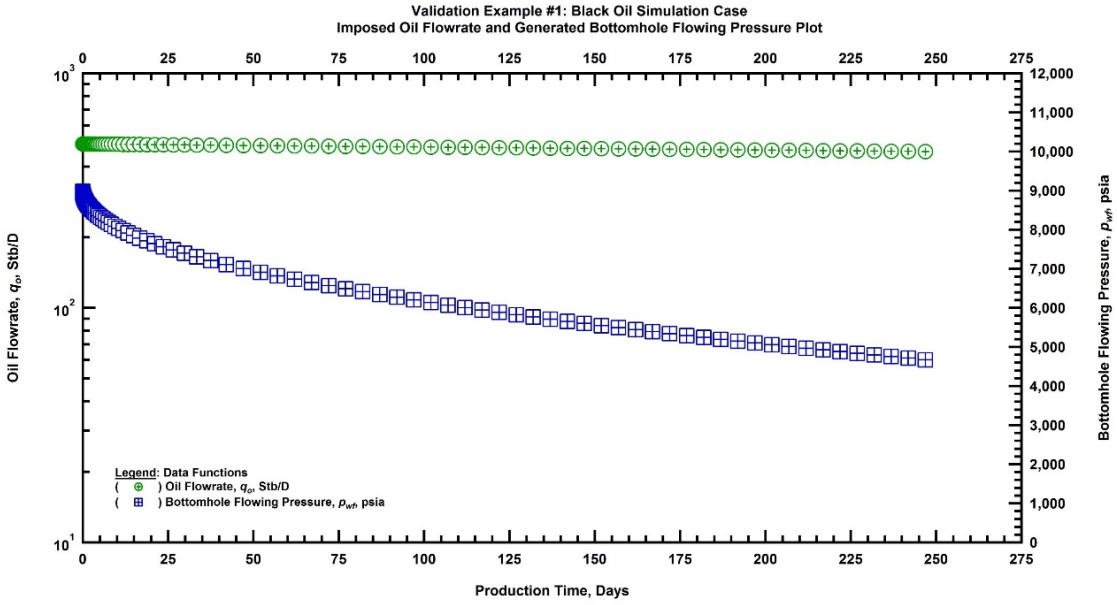

Figure 4.1 — Validation Example #1 ─ Simulated Black Oil Time-Rate-Pressure Production Data

Observation of the stand-alone rate and pressure measurement data is not enough to provide significant insight into the well performance for this case. The underlying assumption of the methodology relies upon the pressure drop normalized rate signature of the well providing an adequate approximation for the constant pressure rate response of the well in question. This assumption holding true, we are able to

identify prevailing flow regimes and calculate the diagnostic plotting functions, $D(t)$ and $b(t)$ which ultimately inform us about well performance and aid in model calibration. **Figure 4.2** below depicts the modified "qDb" plot which consists of the pressure drop normalized flowrate and calculated derivative diagnostics for this validation example.

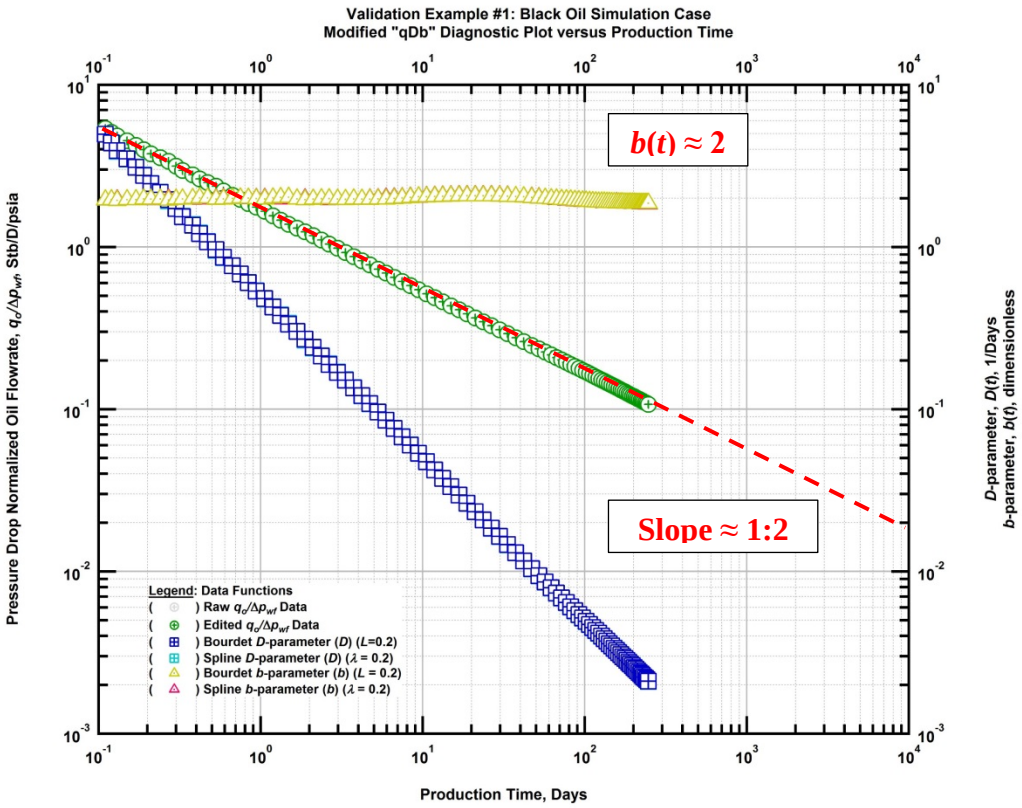

Figure 4.2 — Validation Example #1 ─ Modified "qDb" Diagnostic Plot

The pressure drop normalized rate trend and diagnostic responses in **Figure 4.2** are very consistent and well behaved which is to be expected from simulated data. Given the low permeability, infinitely conductive fractures, lack of reservoir boundaries and short time frame for the simulation history, the well should be exhibiting linear flow. This is indeed verified by the observation of a half-slope on the log cycles for the pressure drop normalized rate data and the corresponding stabilization of the loss-ratio derivative trend near a value of two. Departures from the linear flow regime, if present, are potentially indicative of a number of things including, but not limited to, fracture interference, phase changes, pressure dependent permeability, reservoir boundaries, or a combination of a number of factors.

Our knowledge of the well and reservoir properties of the system, which in this case is fully defined, and our diagnosis of the resulting production data are what allow us to validate or invalidate the keystone assumption that the pressure drop normalized rate data provides an accurate representation of the constant pressure rate solution of the well. Having validated this assumption for this example, the plotting functions in **Figure 4.2** are used to calibrate the model parameters for the empirical expressions in Eqs. 3.18 through 3.22 and Eqs. 3.28 through 3.37. The results of the diagnostic calibration are shown below in **Figure 4.3** for each of the five models focused on in this work.

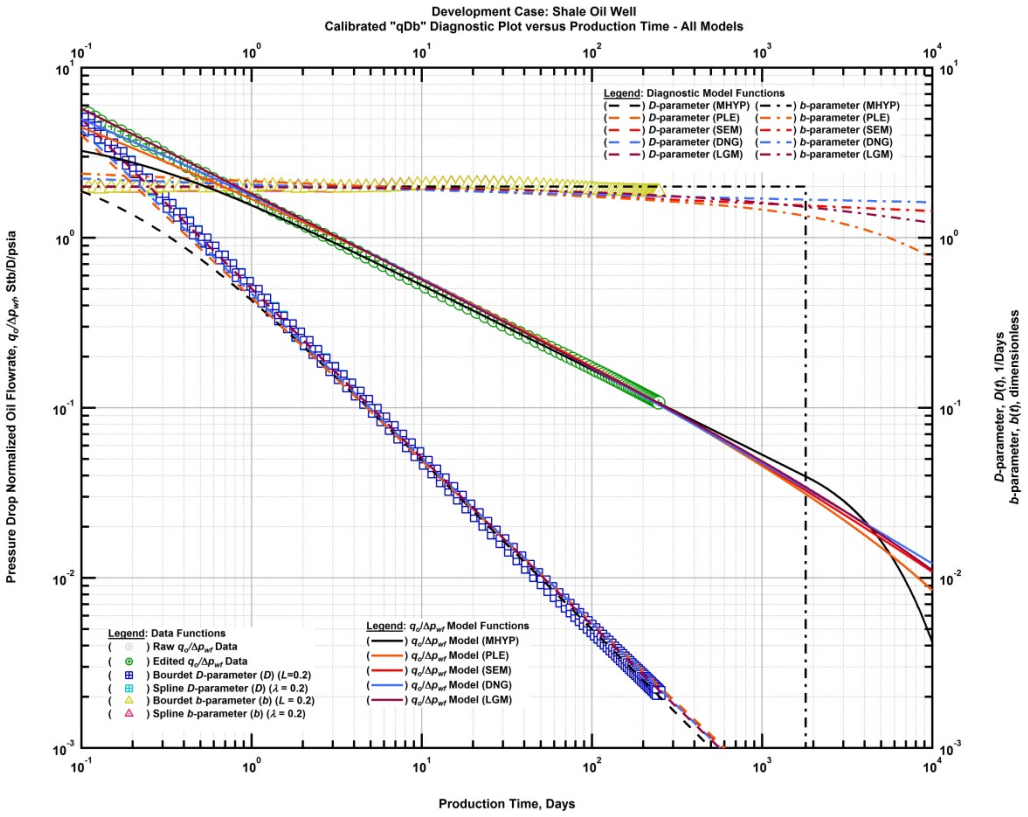

Figure 4.3 — Validation Example #1 ─ Calibrated "qDb" Diagnostic Plot (All Models Shown)

It is observed that each of the models adequately captures each of the diagnostic signatures in **Fig. 4.3**. Other than very early times, it is noted that each of the models nearly overlays the others for the historical period of the data. Deviations in the models only manifest themselves in the forecasts when the different mathematical characteristics begin to prevail. **Table 4.2** below summarizes the parameter results for each of the models where a small D_∞ value is imposed for the power-law exponential model to emphasis the only difference between it and the stretched exponential model. This term will only be included if the data signature justifies for the remainder of the cases in this work.

Table 4.2 — Validation Example #1 ─ Variable Pressure Decline Curve Model Parameter Results

Decline Model	$(q/\Delta p)_i$ *or* $(K/\Delta p)_i$ (STB/D/psi) or (STB/psi)	D_i *or* τ *or* a (1/D)	n or b *or* m (dim.less)	D_{lim} or D_∞ (percent/year) or (1/D)
M.HYP	2.95	3.000	2.000	10
PLE	28000	10.1	0.044	2.5e-5
SEM	28000	1.495e-23	0.044	-
DNG	1.2	0.56	1.03	-
LGM	900	355	0.5	-

While the model parameters are adjusted on the diagnostic calibration plot, the rate history is simultaneously matched by superposing a calibrated pressure drop normalized rate decline model with the actual pressure drop data. Eqs. 3.23 through 3.27 are the mathematical representations for this procedure and **Figure 4.4** below presents the final result for each of the calibrated models. It is reiterated that the history matching process is iterative and simultaneous across the three diagnostic trends, the rate data, and any other diagnostic trends that may be applicable for a particular case. This is a necessary measure to guide parameter selection and minimize non-uniqueness.

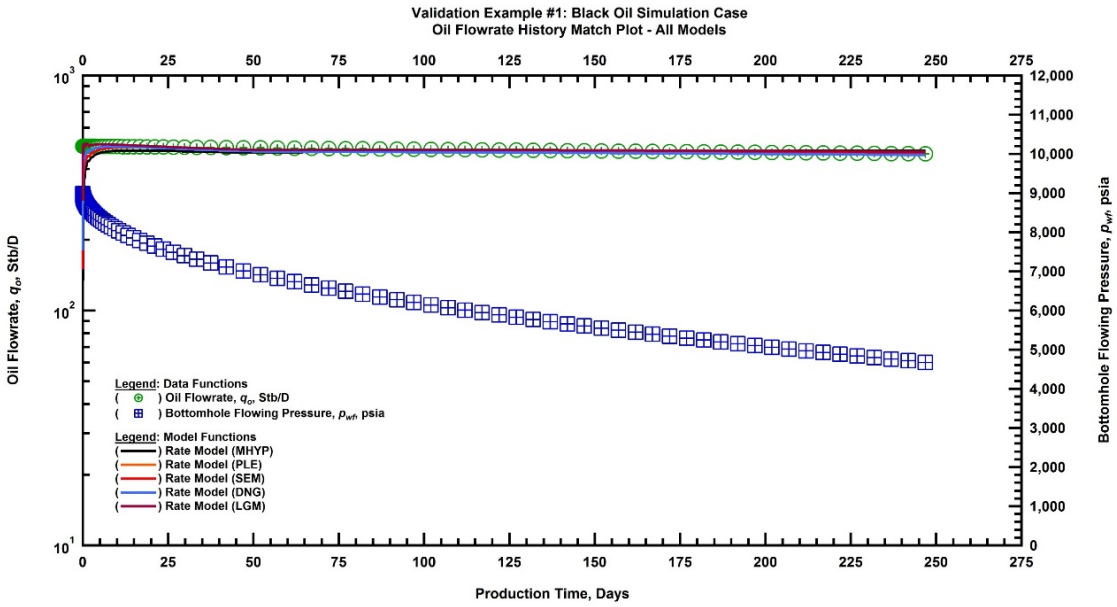

Figure 4.4 — Validation Example #1 ─ History Match Plot Honoring Historical Rate Data (All Models Shown)

Having calibrated each of the models and sufficiently history matching the rate versus time data, which we must always return to, we now turn to forecasting future production. The primary goal, and as a result one

of the main strengths, of the workflow presented is the incorporation of pressures into the decline curve analysis process. The result of this is the ability to impose any pressure drawdown schedule when forecasting future production of a well. For this example, the last historic pressure is high at nearly 5,000 psia which is far from what is typically expected when pressure stabilize for shale oil wells. For this example, we demonstrate that forecasting capability of the procedure by imposing two separate pressure drawdowns, namely one assuming the last historic pressure for the remainder of the life of the well and one where the pressure is driven down to 2,000 psia where the pressure is then maintained to 30 years of production time. **Figure 4.5** depicts the forecasting results for the power-law exponential model according to both pressure schemes and **Table 4.3** summarizes the estimated ultimate recovery (EUR) values for all models.

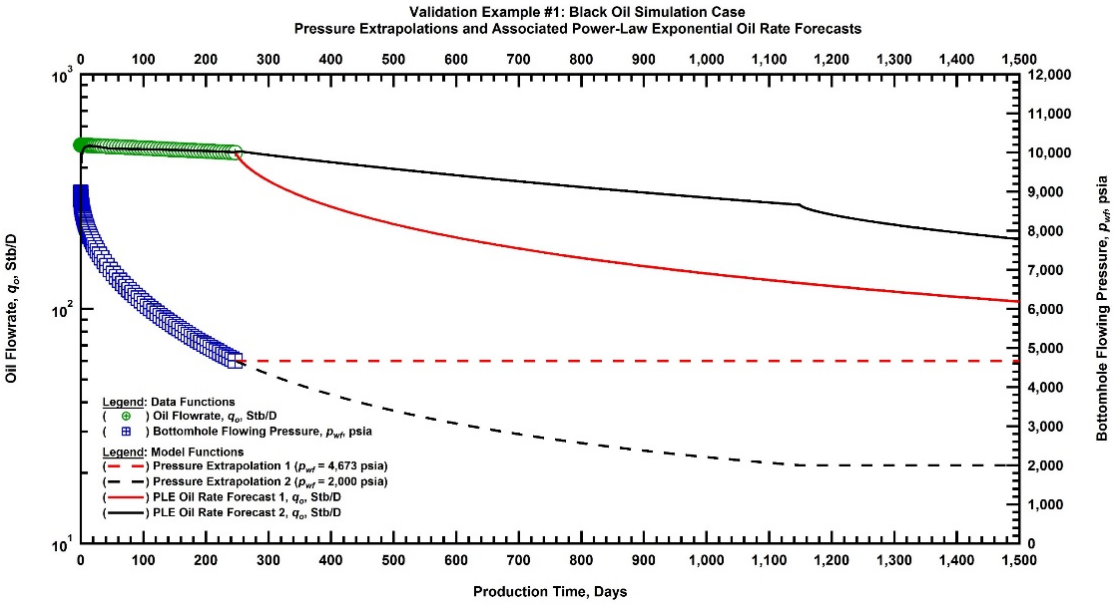

Figure 4.5 — Validation Example #1 ─ Pressure Extrapolations and Power-Law Exponential Rate Forecasts

Table 4.3 — Validation Example #1 ─ Forecasting Results for All Models

Decline Model	p_{wf} Forecast #1 EUR_{30yr} (Mstb)	p_{wf} Forecast #2 EUR_{30yr} (Mstb)
M.HYP	857	1,400
PLE	770	1,236
SEM	831	1,328
DNG	864	1,384
LGM	873	1,387

Clearly, the choice of drawdown schedule for this case has a significant impact on the 30 year estimated ultimate recovery (EUR). The forecasted rate departs from the historical sustained rate trend almost immediately if the last historic pressure is maintained throughout the remaining life of the well without any additional drawdown. The imposition of additional pressure drawdown over time creates an incremental wedge of increased production where the rate is projected to maintain the sustained trend.

While this is admittedly an extreme example to validate the methodology, the average increase from each of the models is high at approximately 60 percent. The ability to forecast pressure into the future allows the analyst to attempt to describe the shape and the magnitude of production differences due to operational changes to a well in the future. This type of analysis is something that is traditionally limited to more technically rigorous analytical or numerical methods as traditional decline curve analysis disregards pressure.

It is concluded here that the methodology is successfully validated for single phase oil production scenarios. The potential limitations for such scenarios are as follows.

- Inconsistent or poorly collected data will make analysis difficult or impossible.
- The analysis carries all of the limitations of the empirical models regarding their physical assumptions regarding flow regimes and their associated basis functions.
- The empirical models are described by three or four arbitrary parameters that do not contribute to reservoir characterization efforts.

4.2 Dry Gas Validation Example

For this example, pressures were simulated subject to imposed near constant gas rates. The goal is to validate the methodology for incompressible gas flow. As with analytical pressure transient analysis and model-based production analysis, appropriate pseudopressure transformations (Eq. 3.5) are required to

linearize, or partially linearize, the system to allow the application of superposition (Eq. 3.12). The system is fully defined and the simulation inputs are summarized in **Table 4.4**.

Table 4.4 — Validation Example #2 ─ Reservoir and Fluid Property Inputs for Simulated Data

Reservoir Properties:		
Net pay thickness, h	=	200 ft
Formation permeability, k	=	750 nD
Wellbore radius, r_w	=	0.3 ft
Formation compressibility, c_f	=	3 x 10^{-6} psi^{-1}
Porosity, ϕ	=	0.05 (fraction)
Initial reservoir pressure, p_i	=	8,000 psi
Gas saturation, S_g	=	1.0 (fraction)
Skin factor, s	=	0.01 (dimensionless)
Reservoir Temperature, T_r	=	212 °F
Fluid Properties:		
Gas specific gravity, γ_g	=	0.7 (air = 1)
Hydraulically Fractured Well Model Parameters:		
Fracture half-length, x_f	=	200 ft
Number of fractures, n_f	=	16
Horizontal well length, L_w	=	5,000 ft
Production Parameters:		
Last flowing pressure, psi	=	4,383 psi
Producing days, t	=	500 days

The simulated production data used for this example is depicted below in **Figure 4.6**. The rate and pressure trends approximate unconventional gas wells flowing against managed drawdown conditions. The production history is slightly longer that the black oil case presented previously at 500 days. As before, the last historic flowing bottomhole pressure is significantly higher than a typical line pressure value to demonstrate the forecasting capacity of the methodology.

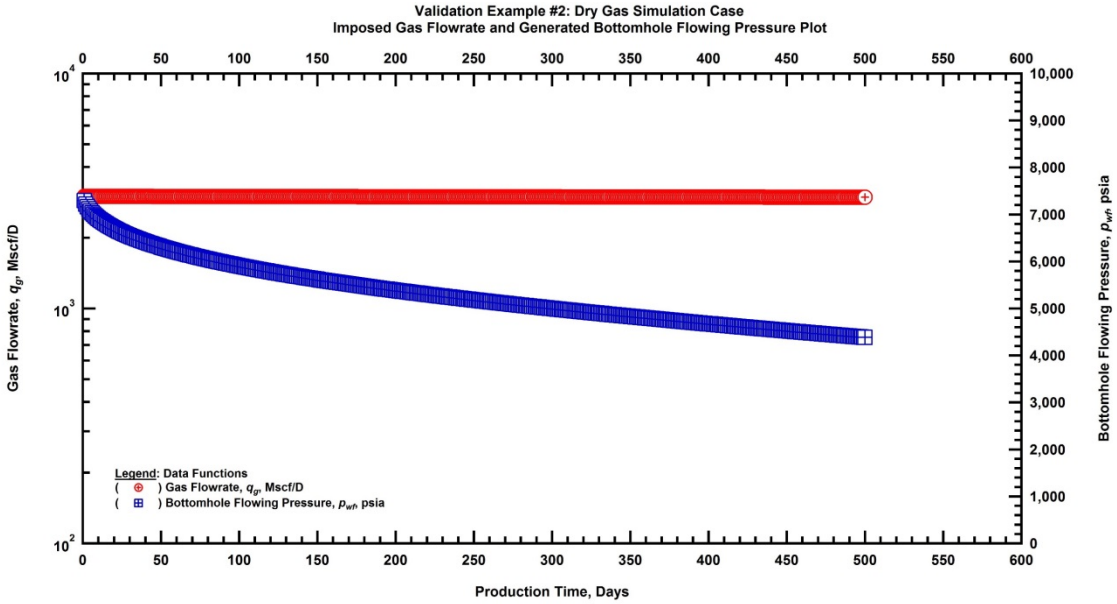

Figure 4.6 — Validation Example #2 ─ Simulated Dry Gas Time-Rate-Pressure Production Data

Continuing with our methodology, we must approximate the constant pressure rate signature of the well by normalizing by pressures, or in this case pseudopressures. The definition introduced by Al-Hussainy *et al.* (1966) and reproduced as Eq. 3.5 is used to calculate the initial and flowing pseudopressures from the flowing pressure trend knowing the PVT properties of the reservoir gas. Having performed these transformations, we now plot the pseudopressure drop normalized gas rates along with the $D(t)$ and $b(t)$ derivative trends calculated using both of the differentiation algorithms used throughout this work. **Figure 4.7** below depicts the modified "qDb" plot displaying each of the aforementioned plotting functions.

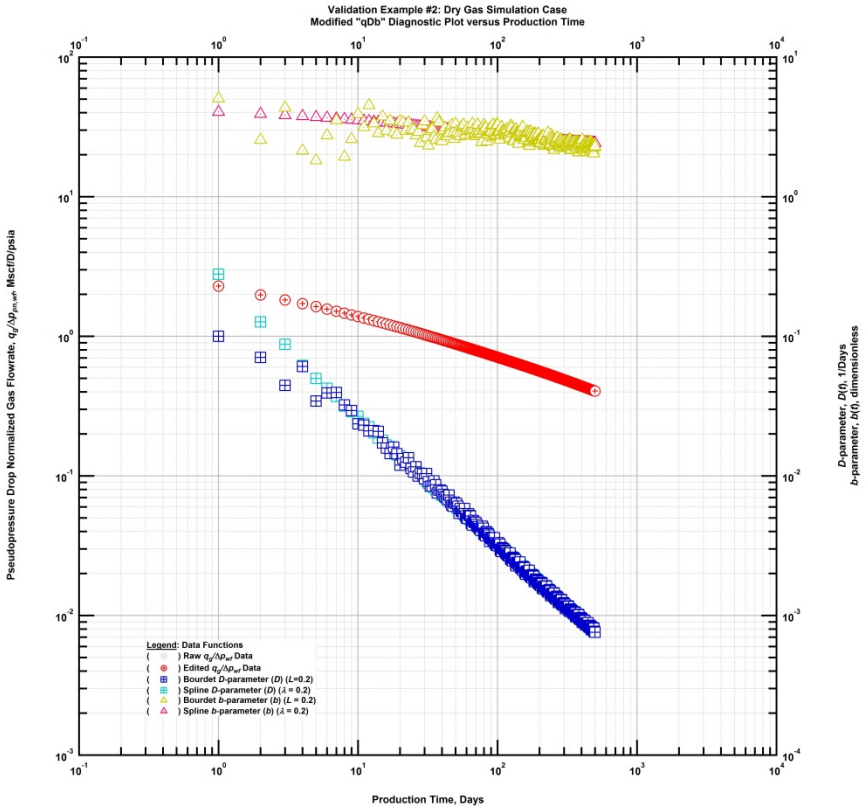

Figure 4.7 — Validation Example #2 ─ Modified "qDb" Diagnostic Plot

Consistency is again expected and observed as a result of the simulated data. The presence of the imposed skin effect is evident early time where the pseudopressure drop normalized rate trend is less that the half-slope expected by linear flow. It is also noted that the $b(t)$ trend is slightly declining as a function of time and the $D(t)$ trend is nearly a straight line on log-log coordinate suggesting power-law flow regimes are prevalent over the history of this well. This would suggest that the power-law exponential or stretched exponential may be more appropriate models that the modified hyperbolic which assumes a constant $b(t)$ behavior and boundary dominated flow. This information is critical when calibrating the decline models and their diagnostic functions which are depicted below in **Figure 4.8**.

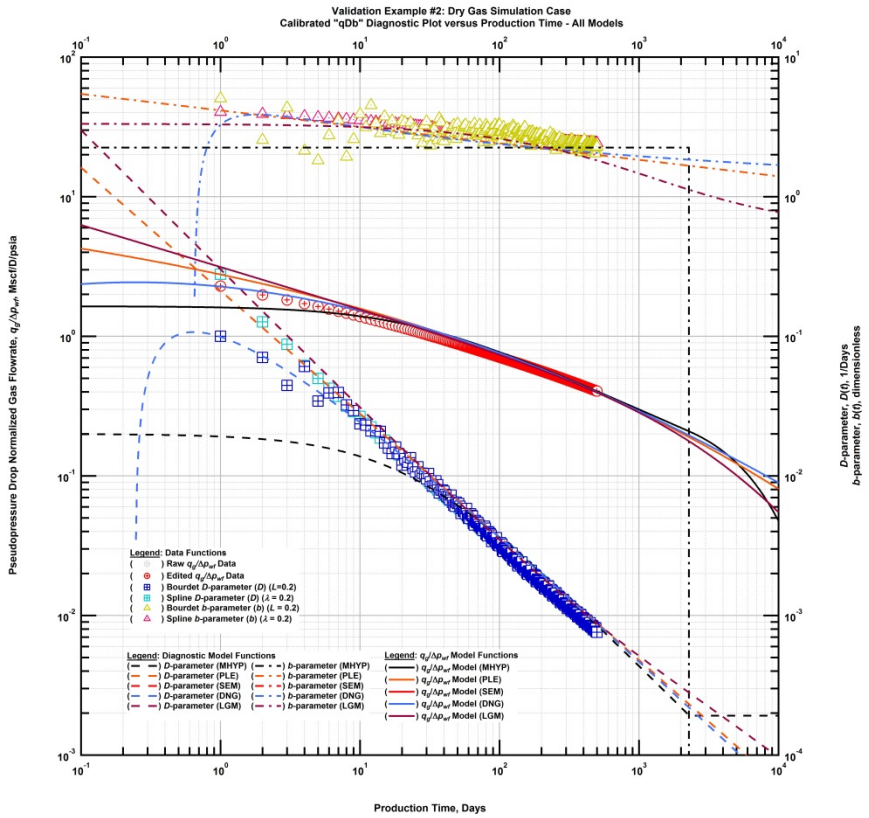

Figure 4.8 — Validation Example #2 ─ Calibrated "qDb" Diagnostic Plot (All Models Shown)

Each of the models is calibrated to honor the diagnostic signatures in **Fig. 4.8**. As before, the primary differences in the models do not appear until sometime after the historic production period of the well. The calibrated models are, in this case, convolved with the pseudopressure drop as opposed to the pressure drop in order to history match the gas rate as a function of time trend. This process is iterative and simultaneous across all diagnostic plots **Table 4.5** and **Figure 4.9** summarize the model parameters and depict the history match for each model respectively.

Table 4.5 — Validation Example #2 ─ Variable Pressure Decline Curve Model Parameter Results

Decline Model	$(q/\Delta p)_i$ *or* $(K/\Delta p)_i$ (MSCF/D/psi) or (MSCF/psi)	D_i *or* τ *or* a (1/D)	n or b *or* m (dim.less)	D_{lim} or D_∞ (percent/year) or (1/D)
M.HYP	1.3	0.020	2.25	7.0
PLE	13.5	1.800	0.118	-
SEM	13.5	6.87e-3	0.118	-
DNG	1.8	0.970	1.069	-
LGM	2500	700.0	0.70	-

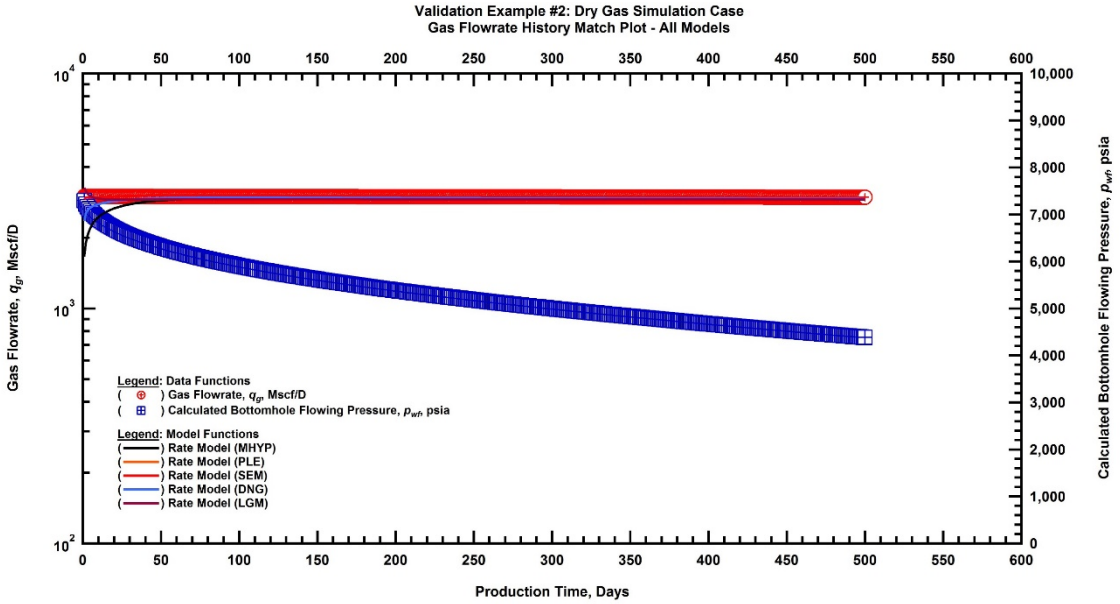

Figure 4.9 — Validation Example #2 ─ History Match Plot Honoring Historical Rate Data (All Models Shown)

The workflow continues to forecasting following the establishment of adequately calibrated models. Two separate pressure drawdown schedules are imposed for this example, one using the last historic flowing bottomhole pressure and one assuming additional pressure drawdown until a flowing bottomhole pressure of 1,500 psia is achieved. It is important to note that the imposed pressure drawdowns must be converted to pseudopressures just as the historical pressures. Once this is done, the calibrated models are re-run through the superposition equation using the imposed pressure schedules to calculate the rate forecast for each sensitivity. **Figure 4.10** depicts the forecast results for the power-law exponential decline model and **Table 4.6** summarizes the EUR results for each model and pressure sensitivity.

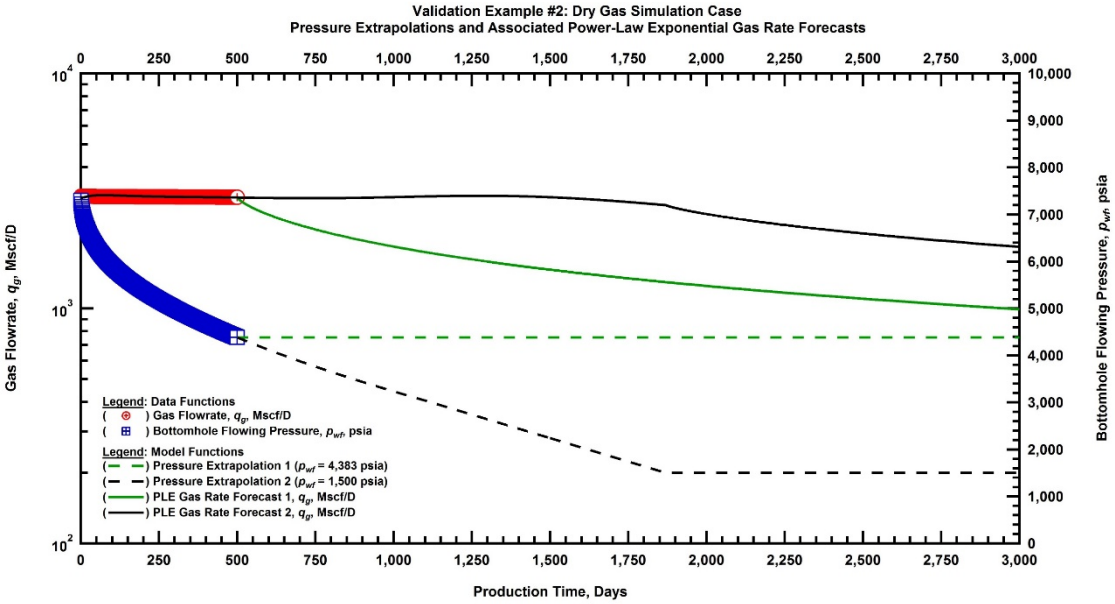

Figure 4.10 — Validation Example #2 ─ Pressure Extrapolations and Power-Law Exponential Rate Forecasts

Table 4.6 — Validation Example #2 ─ Forecasting Results for All Models

Decline Model	p_{wf} Forecast #1 EUR_{30yr} (Bscf)	p_{wf} Forecast #2 EUR_{30yr} (Bscf)
M.HYP	10.0	17.1
PLE	10.3	16.3
SEM	10.3	16.3
DNG	10.6	16.8
LGM	9.0	14.3

The imposition of additional pressure drawdown again has a significant effect on the rate forecast and recovery magnitude with the average uplift again at approximately 60 percent. It is concluded here that the methodology is successfully validated for single phase gas production scenarios. The potential limitations for such scenarios are as follows.

- Inconsistent or poorly collected data will make analysis difficult or impossible.
- The analysis carries all of the limitations of the empirical models regarding their physical assumptions regarding flow regimes and their associated basis functions.

- The empirical models are described by three or four arbitrary parameters that do not contribute to reservoir characterization efforts.
- Calculation of pseudopressures requires knowledge of the PVT characteristics of the system which should be available but often are not.
- Pseudopressures only partially linearize the system leaving some uncertainty surrounding the true constant pressure rate signature of the well.

4.3 Dry Gas Validation Example Considering Pressure Dependent Permeability

For this example, we again generate pressure as a result of an assumed near constant gas rate profile; however, in this example we include the effect of pressure dependent permeability to approximate a case where geomechanical effects influence the well performance. A numerical simulator with unstructured Voronoi gridding is again used and the permeability is solved for at each time step according to the functional relationship provided by Eq. 3.7. The simulation inputs are completely summarized in **Table 4.7** below.

Table 4.7 — Validation Example #3 ─ Reservoir and Fluid Property Inputs for Simulated Data

Reservoir Properties:		
Net pay thickness, h	=	200 ft
Formation permeability, k	=	900 nD
Wellbore radius, r_w	=	0.3 ft
Formation compressibility, c_f	=	3 x 10^{-6} psi^{-1}
Permeability Modulus, γ	=	4 x 10^{-4} psi^{-1}
Porosity, ϕ	=	0.05 (fraction)
Initial reservoir pressure, p_i	=	8,000 psi
Gas saturation, S_g	=	1.0 (fraction)
Skin factor, s	=	0.01 (dimensionless)
Reservoir Temperature, T_r	=	212 °F
Fluid Properties:		
Gas specific gravity, γ_g	=	0.7 (air = 1)
Hydraulically Fractured Well Model Parameters:		
Fracture half-length, x_f	=	250 ft
Number of fractures, n_f	=	16
Horizontal well length, L_w	=	5,000 ft
Production Parameters:		
Last flowing pressure, psi	=	5,545 psi
Producing days, t	=	500 days

The imposed rates and resulting pressures are depicted below in **Figure 4.11**. The rate and pressure trends are very similar to those seen in Validation Example #2 and support the reality that well performance cannot be assessed using standalone plots of rate and pressure versus time. The goal in this example is to

apply the variable pressure decline curve analysis workflow to this data for each of the five models outlined in chapter III and forecast the production into the future using two different pressure drawdown assumptions. Potential limitation from using pseudopressure transforms to linearize the effects of incompressible gas flow and pressure dependent permeability will be assessed.

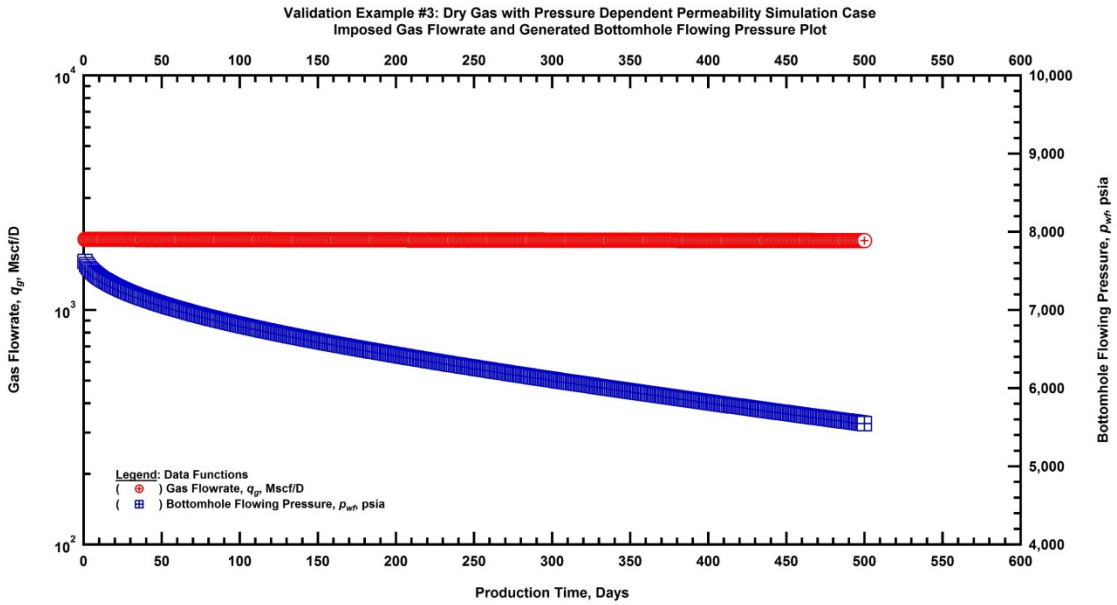

Figure 4.11 — Validation Example #3 ─ Simulated Dry Gas Time-Rate-Pressure Production Data

From a diagnostic standpoint, we know that the system was defined with pressure dependent permeability in place to produce dry gas. As a result, we must transform the raw flowing bottomhole pressure data and the initial static reservoir pressure to normalized pseudopressures using Eq. 3.6 as a first step towards diagnosing the approximate constant pressure rate signature of the well. It is noted that this expression is exactly the same as the pseudopressure definition proposed by Al-Hussainy *et al.* (1966) and defined in Eq. 3.5; however, the permeability is left inside the integral as a pressure dependent term as opposed to assuming constancy.

The evaluation of the pseudopressure integrals, namely Eqs. 3.5 and 3.6, require that each of the pressure dependent terms have a functional form either analytical or empirical. The fluid property terms, namely the gas viscosity and deviation factor, are defined either by laboratory tests of reservoir fluids (*i.e.* PVT reports) or well established correlations. To evaluate Eq. 3.6 for this example, a relationship describing permeability, a rock property, as a function of pressure must be imposed based on geomechanical lab tests or correlations. In this example, Eq. 3.7, which is an exponential correlation introduced by Yilmaz and

Nur (1991), was used to generate the pressures in the simulator and is thus used for the pseudopressure calculations.

Since the initial permeability and the permeability modulus, which describes the degree of pressure dependency for the permeability, are known for this synthetic system we use these as inputs. It is here noted that this is a potential limitation for field applications where these two parameters are typically not known *a priori*. Once these transformations are calculated, we again plot the pseudopressure drop normalized gas rates along with the $D(t)$ and $b(t)$ derivative trends calculated using both of the differentiation algorithms used throughout this work. **Figure 4.12** below depicts the modified "qDb" plot displaying each of the aforementioned plotting functions.

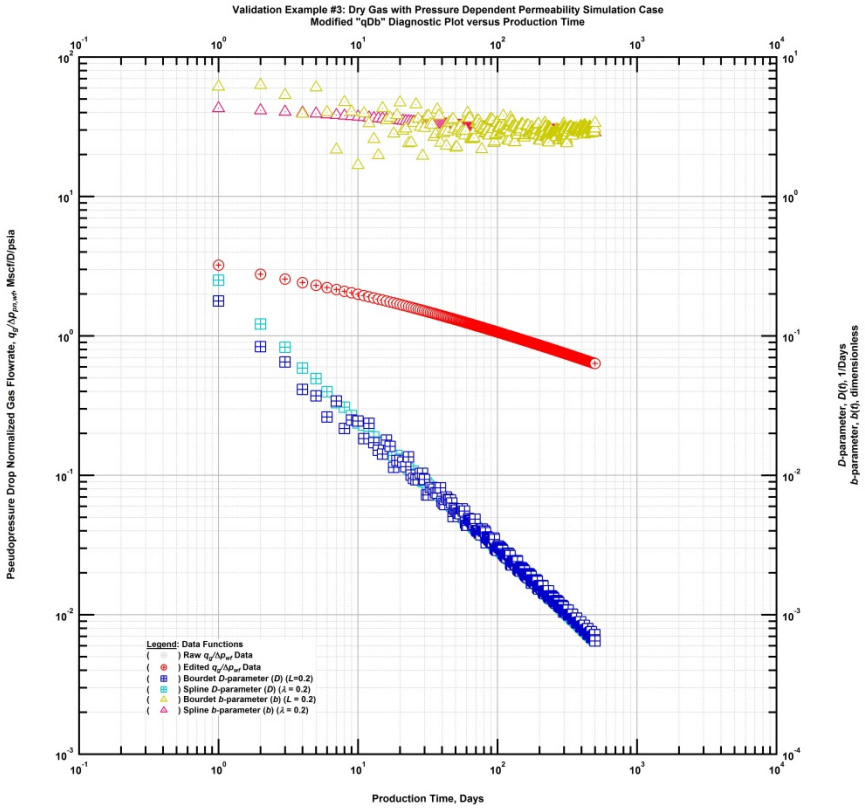

Figure 4.12 — Validation Example #3 ─ Modified "qDb" Diagnostic Plot

As with the other simulated validations examples, data consistency is observed. The slight skin effect is evident at early times where the slope is shallower than the half-slope indicating the expected linear flow signature. The reciprocal of the loss-ratio, $D(t)$, can be interpreted to be a straight line, or power-law, trend on the logarithmic scales. Similarly, the loss-ration derivative, $b(t)$, trend can again be interpreted to

be declining slightly as a function of time. The two different differentiation algorithms provide differing degrees of granularity that will aid in model calibration. The fully calibrated diagnostic functions for all five of the models are depicted below in **Figure 4.13**.

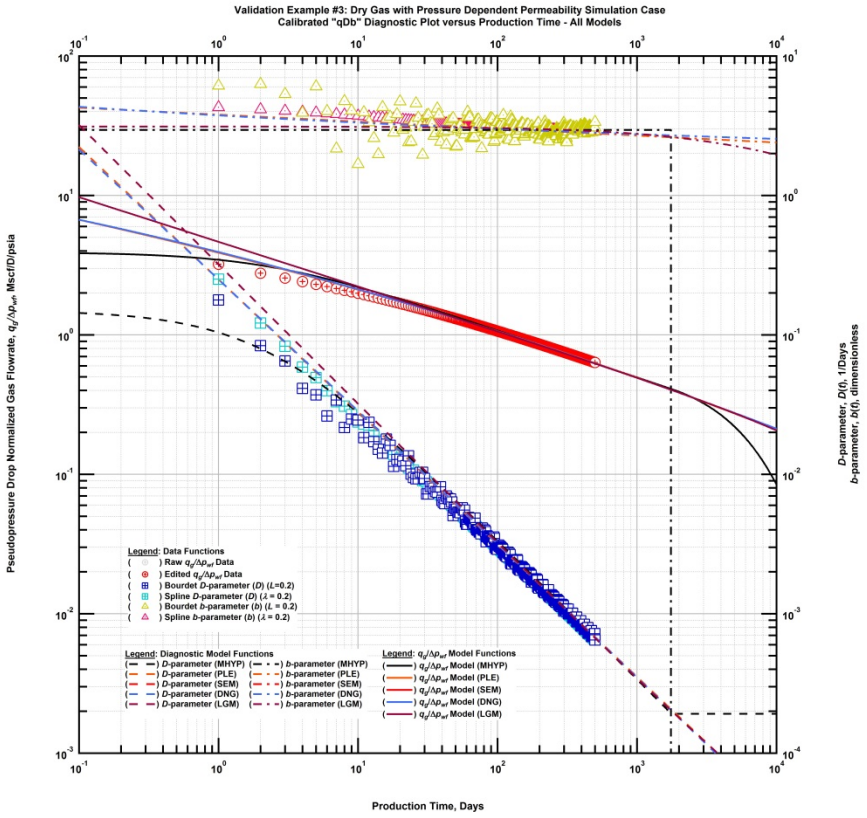

Figure 4.13 — Validation Example #3 ─ Calibrated "qDb" Diagnostic Plot (All Models Shown)

A match across each of the diagnostic signatures is achieved for all the decline models considered in this work. Interestingly, the only significant difference between the models is due to the terminal decline imposed after some time for the modified hyperbolic relation. The remainder of the models overlay each other throughout the historic portion of the future projected by the model. Having matched the diagnostic functions, the calibrated models are convolved with the pseudopressure drop data in order to history match the flowing gas rates as a function of time. **Table 4.8** and **Figure 4.14** summarize the model parameters and rate versus time history matches for all of the models.

Table 4.8 — Validation Example #3 ─ Variable Pressure Decline Curve Model Parameter Results

Decline Model	$(q/\Delta p)_i$ *or* $(K/\Delta p)_i$ (MSCF/D/psi) or (MSCF/psi)	D_i *or* τ *or* a (1/D)	n or b *or* m (dim.less)	D_{lim} or D_∞ (percent/year) or (1/D)
M.HYP	3.33	0.15	2.95	7.0
PLE	490	5.00	0.05	-
SEM	490	1.05e-14	0.05	-
DNG	3.35	0.77	1.02	-
LGM	35000	6000	0.68	-

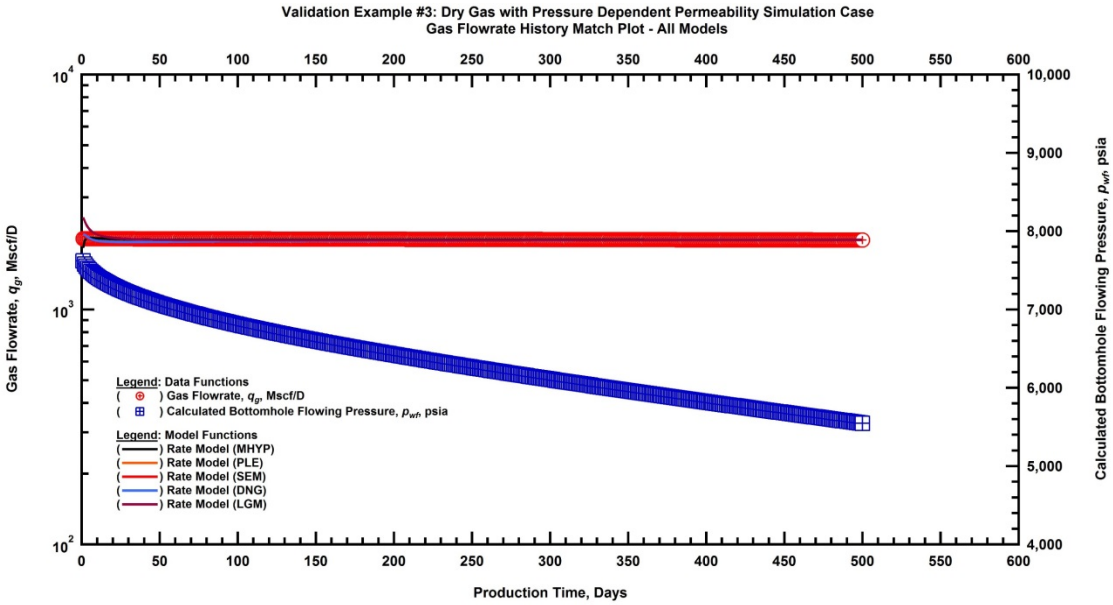

Figure 4.14 — Validation Example #3 ─ History Match Plot Honoring Historical Rate Data (All Models Shown)

Two separate pressure drawdown schedules are again used to forecast the future rates for each of the history matched decline models. The first forecasting scenario, illustrated in green in **Figure 4.15** represents the scenario where the last historic bottomhole pressure of 5,545 psia was assumed for the remainder of the 30 year assumed well life. The second pressure extrapolation scenario entails driving the bottomhole flowing pressure down to approximately 3,000 psia before stabilizing for the remainder of the 30 year production life of the well. These two pressure extrapolations are meant to illustrate two possible operational decisions for the well going further and the effect of each on the potential gas flowrate.

It is important to note that prior to utilizing superposition for the forecast, the pressure extrapolation needs to be converted to normalized pseudopressures just as the historical pressures were. Once the chosen pressure sensitivities are established and transformed, the calibrated pseudopressure drop normalized empirical models are superposed with the pseudopressure drop schedules. **Figure 4.15** depicts the forecast results for the power-law exponential decline model and **Table 4.9** summarizes the EUR results for each model and pressure sensitivity.

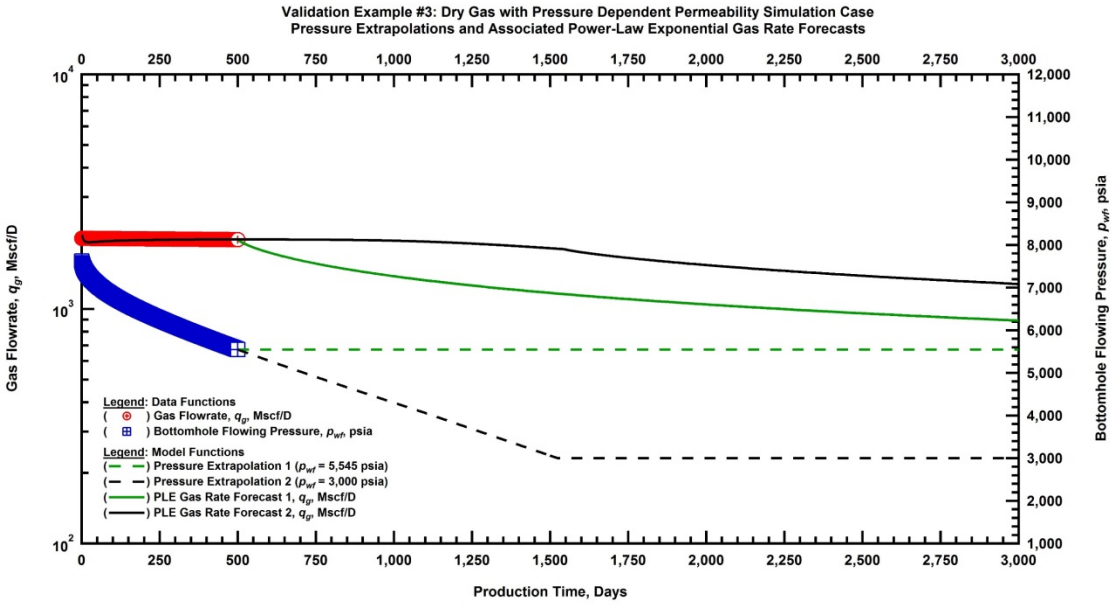

Figure 4.15 — Validation Example #3 ─ Pressure Extrapolations and Power-Law Exponential Rate Forecasts

Table 4.9 — Validation Example #3 ─ Forecasting Results for All Models

Decline Model	p_{wf} Forecast #1 EUR_{30yr} (Bscf)	p_{wf} Forecast #2 EUR_{30yr} (Bscf)
M.HYP	7.67	10.91
PLE	9.26	12.41
SEM	9.26	12.41
DNG	9.34	12.52
LGM	9.27	12.44

As with the other validation examples, the choice of pressure extrapolation schedule impacts the rate forecast; however, the magnitude EUR uplift at thirty years is less at an average of 36 percent across all models compared to the 60 percent for the first two validation cases. It is concluded here that the methodology is successfully validated for single phase gas production scenarios.

While not specifically addressed in a separate validation model, it is noted here that this example serves to validate the methodology for oil cases with pressure dependent permeability as well. The pseudopressure transformation necessary is indeed less complex than the gas production case presented here due to the lack high levels of pressure dependency for the reservoir fluid properties. The pressures are simply modified to include the effect of permeability degradation as a function of pressure. An oil scenario with pressure dependent permeability will be analyzed in the application examples in Chapter V.

The potential limitations for such scenarios are as follows.

- Inconsistent or poorly collected data will make analysis difficult or impossible.
- The analysis carries all of the limitations of the empirical models regarding their physical assumptions regarding flow regimes and their associated basis functions.
- The empirical models are described by three or four arbitrary parameters that do not contribute to reservoir characterization efforts.
- Calculation of pseudopressures requires knowledge of the PVT characteristics of the system which should be available but often are not.
- Pseudopressures only partially linearize the system leaving some uncertainty surrounding the true constant pressure rate signature of the well.
- The inclusion of pressure dependent permeability in the pseudopressure formulation requires *a priori* knowledge of the initial permeability of the system and the functional relationship describing the permeability loss with depletion both of which are typically unknowns for field application scenarios.

CHAPTER V

APPLICATION OF THE METHODOLOGY

The chapter seeks to apply the developed and validated variable pressure decline methodology to a number of practical application cases. The production data for the example cases comes from shale plays around the world and each case is unique in terms of reservoir properties, fluid type, and completion practices. Special attention is payed to frame each case in a practical sense that can aid in decision making from an operational or field development standpoint to highlight the strength of the workflow in everyday analysis. As important as the strengths, the limitations and weaknesses will be thoroughly addressed.

Each shale play is unique in terms of well performance and there are an endless number of reservoir engineering problems associated with each. The following list provides a summary of the structure of this chapter and the problems that will be addressed in each example.

- Shale Oil Well Near Constant Flowing Pressure
- Shale Oil Well with High Frequency Bottomhole Pressure Measurements
- High-Pressure/High-Temperature Shale Gas Well
- Type Curve Workflow Incorporating Multi-well Diagnostics

5.1 Shale Oil Well Near Constant Flowing Pressure

This first application example walks through the analysis of a shale well producing oil as the major phase. **Figure 5.1** below depicts the historical oil rate and calculated bottomhole flowing pressures as a function of time. The aim of this example is to follow the proposed workflow with the aim toward answering a question surrounding potential artificial lift uplift. The well in question is a horizontal well completed with multiple hydraulic fracture stages. There are no other producing wells expected to be influencing the performance of this well.

As noted above, the depicted consists of the primary oil phase production data along with the calculated bottomhole flowing pressure. Bottomhole pressures were calculated from surface pressure measurements using commonly flow correlations; however, it should be noted that this can be a problematic exercise and bottomhole gauges or nodal analysis are preferred if time, data, and budget permits. The benefits of high frequency bottomhole pressure measurements are well documented throughout the petroleum literature and this technique similarly benefits from such quality data.

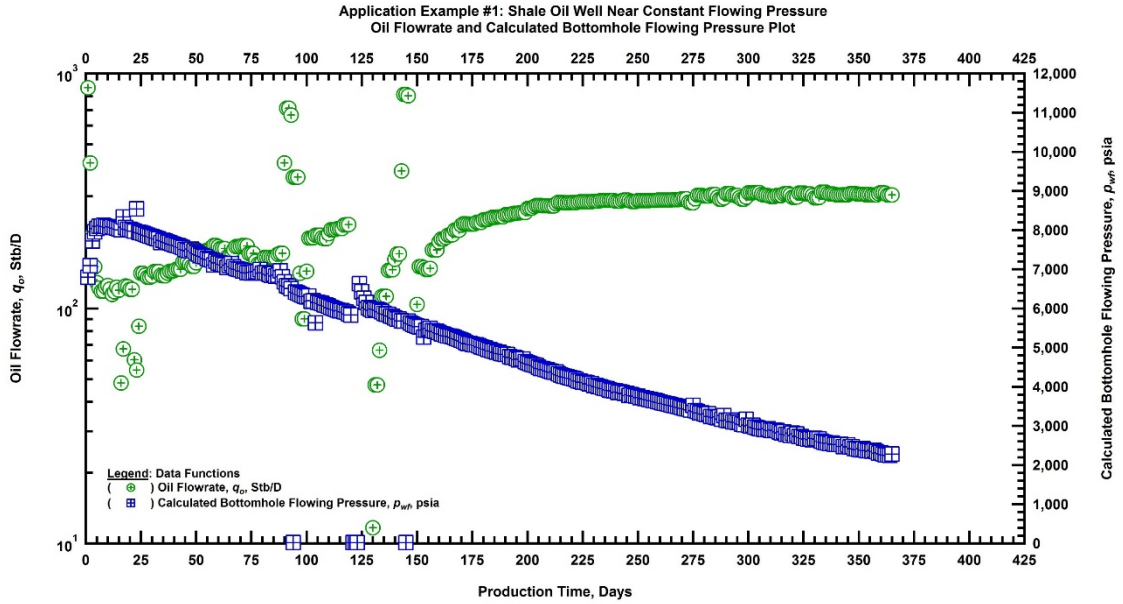

Figure 5.1 — Application Example #1 ─ Time-Rate-Pressure Production Data (Shale Oil Well)

The first step of this analysis process, and any well performance analysis technique utilizing flowing rate and pressure measurements (*e.g.* pressure transient analysis, rate-transient analyisis), is to assess data consistency. In particular, we are looking to ensure that changes in pressure result in a sensible change in rate (*i.e.* pressure drop corresponds to an increase or maintenance of rate). It is important to identify any periods of inconsistent data to avoid analyzing artifacts in the data that represent measurement, reporting, or instrumentation errors as opposed to the true reservoir signature. In **Figure 5.1** above, the data appears to be highly consistent across the historic period of the data and, as such, difficulties applying the superposition principle are not expected.

Moving forward with the diagnostic process, we must construct the pressure drop normalized rate signature to assess the prevailing flow regimes for this production case. This signature will help us to identify any non-linearities that may be present such as pressure dependent permeability caused by geomechanics. **Figure 5.2** depicts the modified "qDb" plot with the pressure drop normalized rate, reciprocal of the loss-ratio, and loss-ratio derivative plotted on logarithmic scales. Considerations when calculating the derivative diagnostic trends will be discussed in proceeding paragraphs.

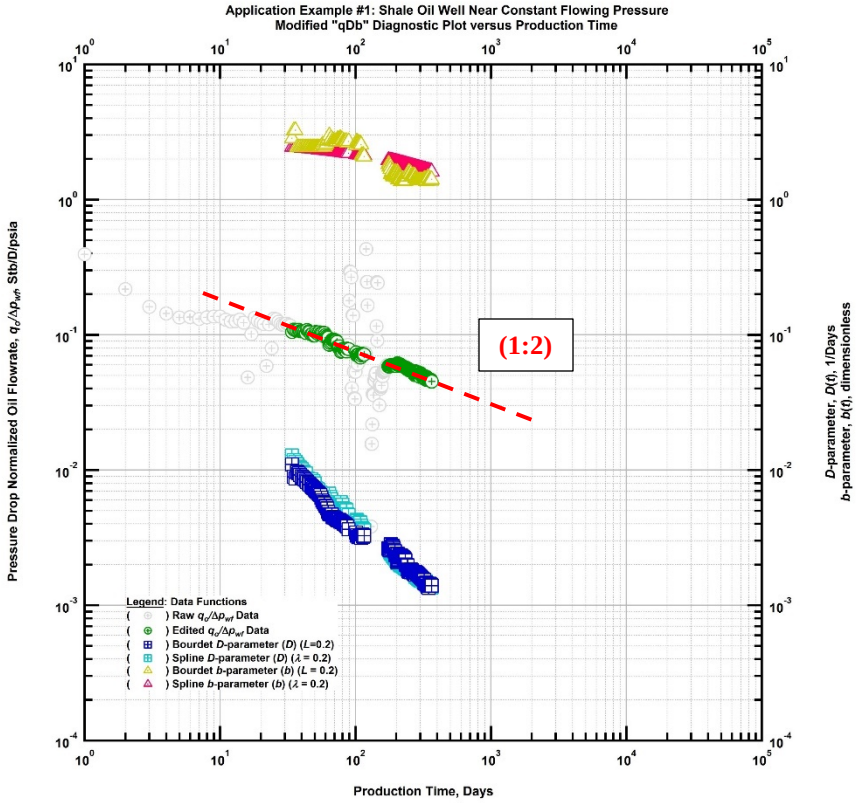

Figure 5.2 — Application Example #1 ─ Modified "qDb" Diagnostic Plot (Shale Oil Well)

Observing the raw pressure drop normalized flowrate data, represented by the gray points in **Figure 5.2**, it is apparent that there is a reasonable degree of noise in the data that is likely not representative of the true reservoir signature of the well. The primary goal of the diagnostic analysis for this workflow is to identify this trend and calculated the corresponding derivative diagnostics that will guide the model calibration process. It is imperative that the signature is filtered across a variety of plots prior to calculating the derivative trends using the Bourdet and Spline algorithms used in this work as numerical differentiation tends to propagate noise.

In this particular example, power-law flow regime trends (*e.g.* linear flow, bi-linear flow, etc.) are expected given the extremely low permeability of the matrix rock coupled with the hydraulic fracture treatment. The straight line trend imposed on **Figure 5.2** represents a power-law trend with a slope near one half. The half-slope trend indicates an infinite conductivity fracture signature and the slight departure at early times in the production history can be explained as a result of flow back after the fracture stimulation. The green points lying close to the identified flow-regime signature are filtered and used in the numerical differentiation algorithms to calculate $D(t)$ and $b(t)$.

Following the diagnostic stage of the workflow, we move to the model calibration process. To reiterate, Eqs. 3.18 through 3.22 and Eqs. 3.28 through 3.37 summarize the diagnostic model functions for each of the five decline models utilized in this work. **Figure 5.3** depicts the calibrated diagnostic functions for each of the empirical decline models.

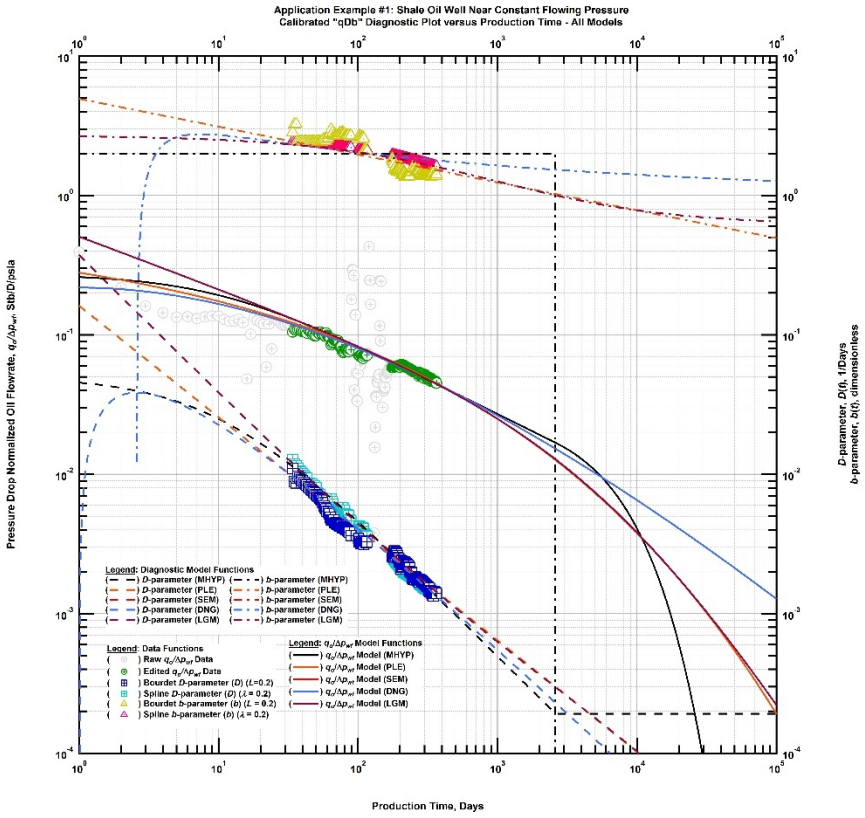

Figure 5.3 — Application Example #1 ─ Calibrated "qDb" Diagnostic Plot (Shale Oil Well)

At first glance, it is clear that each of the models provide an adequate match of the diagnostic plotting functions over the historical data period. It is worthwhile to note here that the power-law exponential (PLE), stretched exponential (SEM), and logistic growth (LGM) models all assume a continued degradation of the $b(t)$ trend seen in the data. The modified hyperbolic (M.HYP) and the Duong (DNG) model are more aggressive in their $b(t)$ assumptions due to the limitation in the former to a single constant b factor and the applicability of the later to long-term linear flow. The modified hyperbolic model is distinctive from the others due to its instantaneous switch to an exponential decline after approximately 2,700 days. Disregarding this switch to an exponential decline, it is clear that the PLE, SEM, and LGM models are more conservative in their flow-regime assumptions than the M.HYP and DNG models in this particular case.

After calibrating the diagnostic models, we superpose the calibrated pressure drop normalized rate versus time function for each model with the pressure drop data for the well. It is noted here that a few iterations may be required to adequately calibrate the diagnostic functions and the oil flowrate history. **Table 5.1** summarizes the model parameters for each model match while **Figure 5.4** depicts the final calibrated model match of the rate versus time data.

Table 5.1 — Application Example #1 ─ Variable Pressure Decline Curve Model Parameter Results

Decline Model	$(q/\Delta p)_i$ *or* $(K/\Delta p)_i$ (STB/D/psi) or (STB/psi)	D_i *or* τ *or* a (1/D)	n or b *or* m (dim.less)	D_{lim} or D_∞ (percent/year) or (1/D)
M.HYP	0.180	0.05	2	7
PLE	0.435	0.81	0.2	-`
SEM	0.435	2.868	0.2	-
DNG	0.150	1.1	1.1	-
LGM	160.0	300	0.63	-

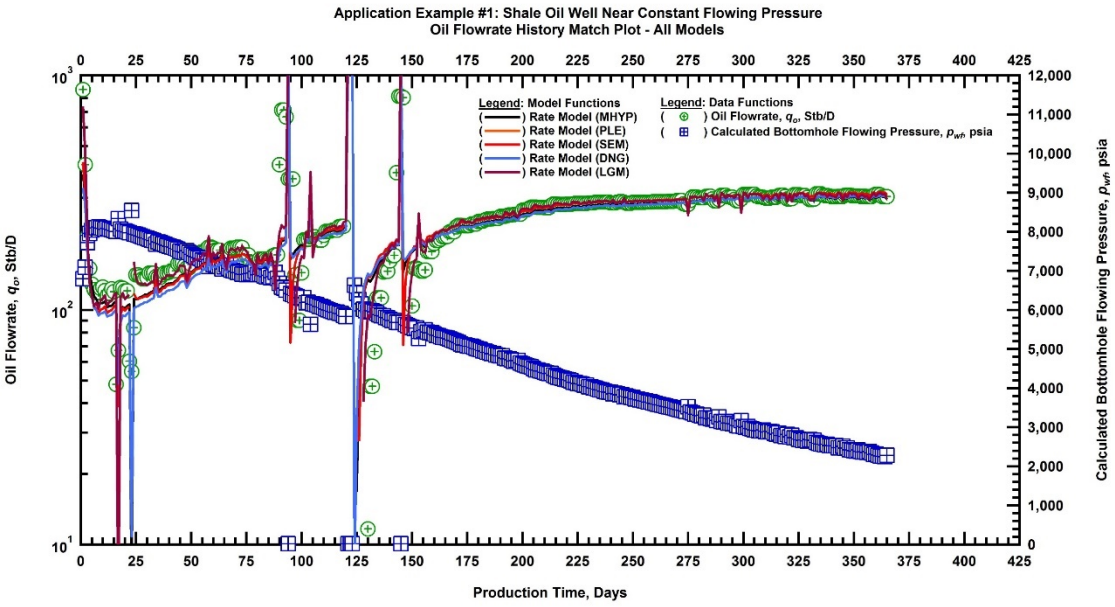

Figure 5.4 — Application Example #1 ─ History Match Plot Honoring Historical Rate Data (Shale Oil Well)

The final step for this application example involves forecasting future production considering two different bottomhole flowing pressure extrapolations. The first extrapolation considers extrapolation at the

last historic pressure of 2,275 psia which would reflect one artificial lift option, while the other option considers a system that is expected drive down the flowing pressure to a constant maintained value of approximately 560 psia. The incremental production differences between the two different options may be desired in order to justify the cost of installation of one system over the other. Each of the models was forecasted using the two different pressure extrapolations and the 30 year estimated ultimate recovery (EUR) values are summarized in **Table 5.2**. The power-law exponential forecasts for each pressure extrapolation case are shown in **Figure 5.5**.

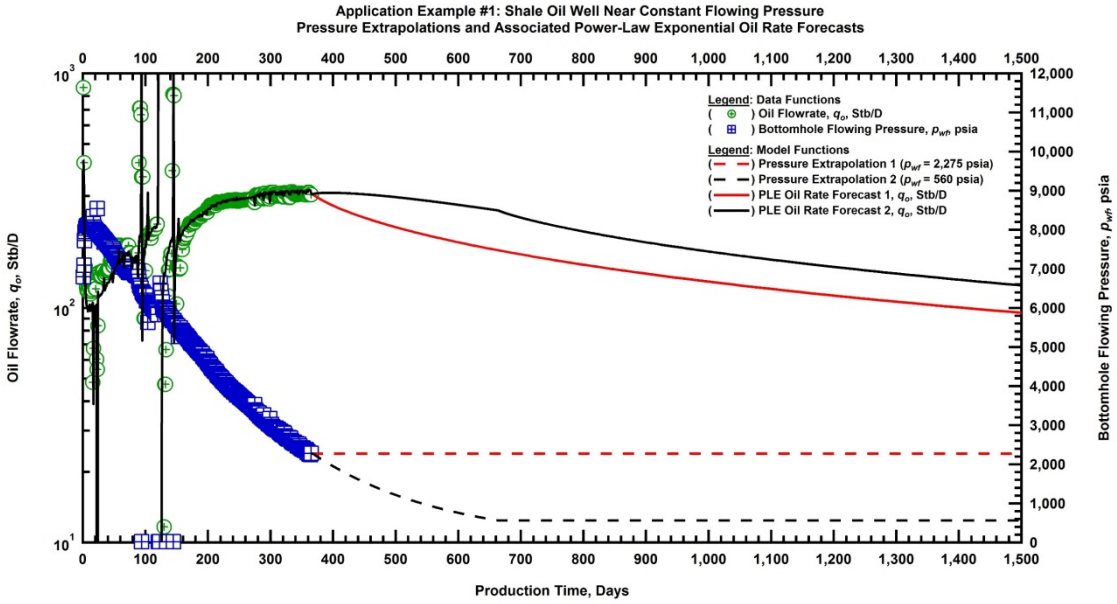

Figure 5.5 — Application Example #1 ─ Pressure Extrapolations and Power-Law Exponential Rate Forecasts

Table 5.2 — Application Example #1 ─ Forecasting Results for All Models

Decline Model	p_{wf} Forecast #1 EUR_{30yr} (Mstb)	p_{wf} Forecast #2 EUR_{30yr} (Mstb)
M.HYP	692	875
PLE	598	746
SEM	598	746
DNG	717	898
LGM	576	722

The scenario considering a pressure extrapolation to a flowing bottomhole pressure of 560 psia adds approximately 25 percent to the thirty year estimate ultimate recovery. It is clear from **Figure 5.5** that the pressure extrapolation resulted in an incremental wedge of production above the forecast generated using the last historic pressure. The two forecasts are nearly parallel after both cases reach a constant bottomhole flowing pressure. This case represents a simple example, absent of substantial non-linearities, where the variable pressure decline curve forecasting technique provides a framework to quickly and easily provide forecasts incorporating the effect of pressure which would otherwise require analytical or numerical modeling.

5.2 Shale Oil Well with High Frequency Bottomhole Pressure Measurements

The following example emphasizes the value of continuously measured flowing bottomhole pressure data. The well in question is a multi-fractured horizontal well producing oil from a shale play thought to exhibit geomechanical effects with depletion (*e.g.* pressure dependent permeability). This belief is justified by model based production analysis, pressure transient tests, and laboratory core testing. As a result of this belief, the example requires that pressures are transformed to pseudopressures in order to satisfy the linearity condition necessary for the application of superposition.

The field development in this particular shale field is in its early stages and the development decisions often require answers at a pace that may prohibit analytical and numerical techniques requiring significant data integration and carrying a significant deal of non-uniqueness due to the lack of production history. The variable-pressure decline curve workflow could provide a framework to make quick forecasts to make development decisions and justify operational practices. It is particularly valuable in this case as the flowing bottomhole pressure is significantly above the constant drawdown pressure reached in more mature wells after the installation of artificial lift. **Figure 5.6** presents the first 75 days of oil flowrate and measured bottomhole flowing pressure data.

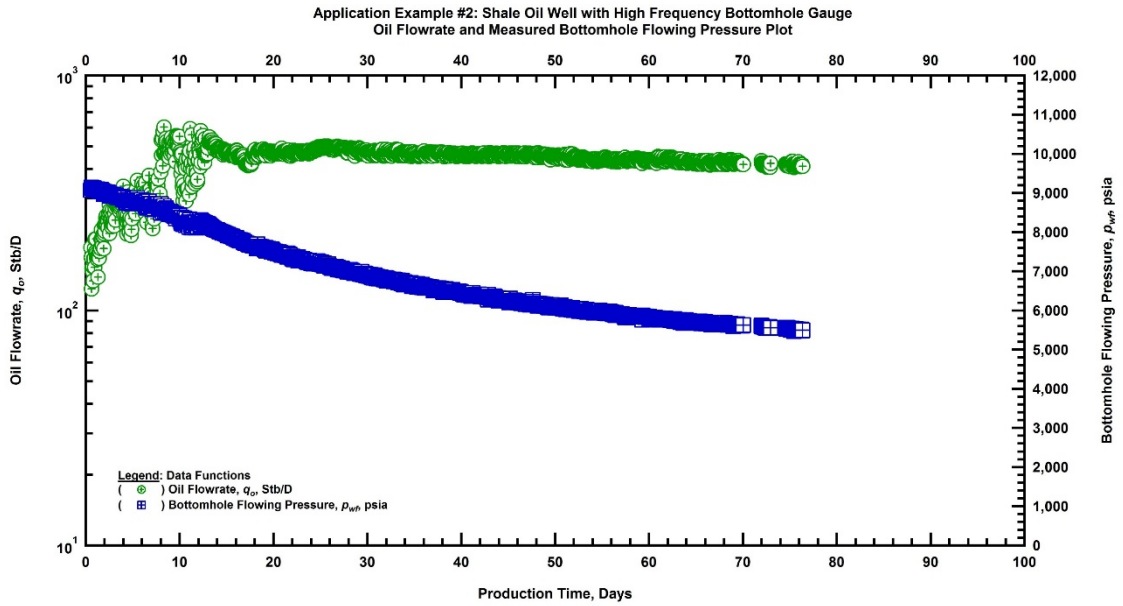

Figure 5.6 — Application Example #2 ─ Time-Rate-Pressure Production Data (Shale Oil Well)

Observing **Figure 5.6**, we see a clear period through approximately 15 days where the well is cleaning up following the fracture treatment. After the cleanup period, the oil rates are at a sustained level for the remainder of the 75 day production history. For a consistent data signature, this oil flowrate signature should correspond to a declining flowing pressure trend. Observing the pressure and rate trends, it appears that the data is highly consistent which is expected as a result of the high frequency bottomhole pressure gauge in this well.

From a data quality standpoint, this well meets the requirements for time-rate-pressure analysis techniques. Given the goal of this work, we will demonstrate the variable-pressure decline workflow but analytical and numerical production analysis could also be applied. Since geomechanical effects are highly suspected in this reservoir, we chose to incorporate pressure dependent permeability into the analysis. Since the superposition technique is relied upon, incorporating pressure dependent permeability requires linearization of the system using pseudopressures. Pseudopressures are calculated from the pressure data and the exponential function presented in Eq. 3.7 is used to describe the degradation of permeability with depletion. Unfortunately, this necessitates an *a priori* assignment of an initial permeability and the permeability modulus describing the severity of the exponential degradation function.

Through a combination of laboratory core measurements, diagnostic fracture injectivity test (DFIT) results, and model-based production analysis on more mature wells, an initial permeability and permeability modulus of 0.0055 md and 4.0e-4 psi^{-1} were assigned. Once the functional form of Eq. 3.7 is

defined we can perform the pseudopressure transformation by integrating said function with the measured bottomhole pressure data. This data is then used to plot the pseudopressure drop normalized rate trend and the $D(t)$ and $b(t)$ derivative signatures which are calculated using both the Bourdet and Spline differentiation algorithms. Each of these plotting functions is shown in **Figure 5.7**.

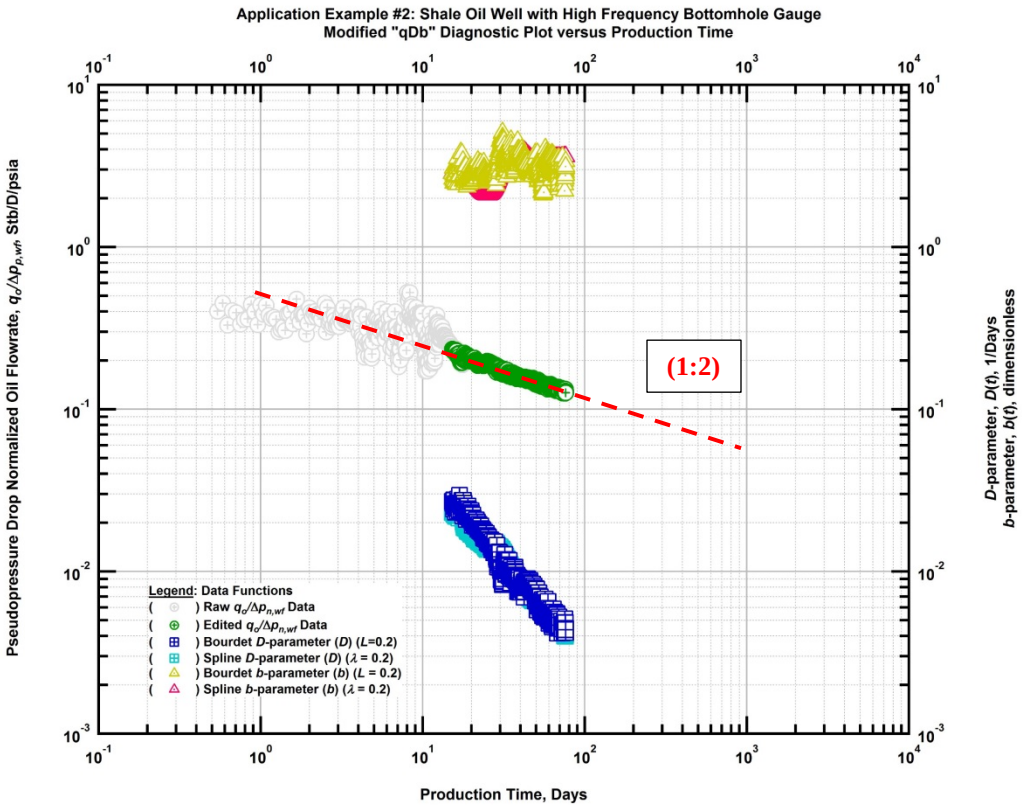

Figure 5.7 — Application Example #2 ─ Modified "qDb" Diagnostic Plot (Shale Oil Well)

Isolated in green are all of the pseudopressure drop normalized rate data points following the flowback period lasting approximately 15 days. These points where chosen as the portion of the data believed to be representative of the prevailing reservoir signature for this well absent any effects from the flowback of the water injected as part of the stimulation treatment. The signature observed is approximately equal to a one-third slope on the log cycles which has been suggested to be indicative of multi-fracture flow which may be caused by the intersection of multiple sets of vertical and horizontal fractures (Okouma *et al.* 2012). This isolated signature is the only portion of the data that is used to calculate the $D(t)$ and $b(t)$ derivative signatures using the Bourdet and Spline algorithms. An approximate trend around $b(t)$ equal to three is consistent with the third slope signature observed in the normalized production data.

Having assessed the consistency of the data and calculated the diagnostic plotting functions, we now aim to calibrate the various decline models used throughout this work. The diagnostic functions in **Figure 5.7** provide the guidance for calibrating the models by adding additional insight into the reservoir signature beyond a simple semi-log plot of rate versus time production data. **Figure 5.8**, below, shows the calibrated diagnostic matches for each of the five models focused on in this work.

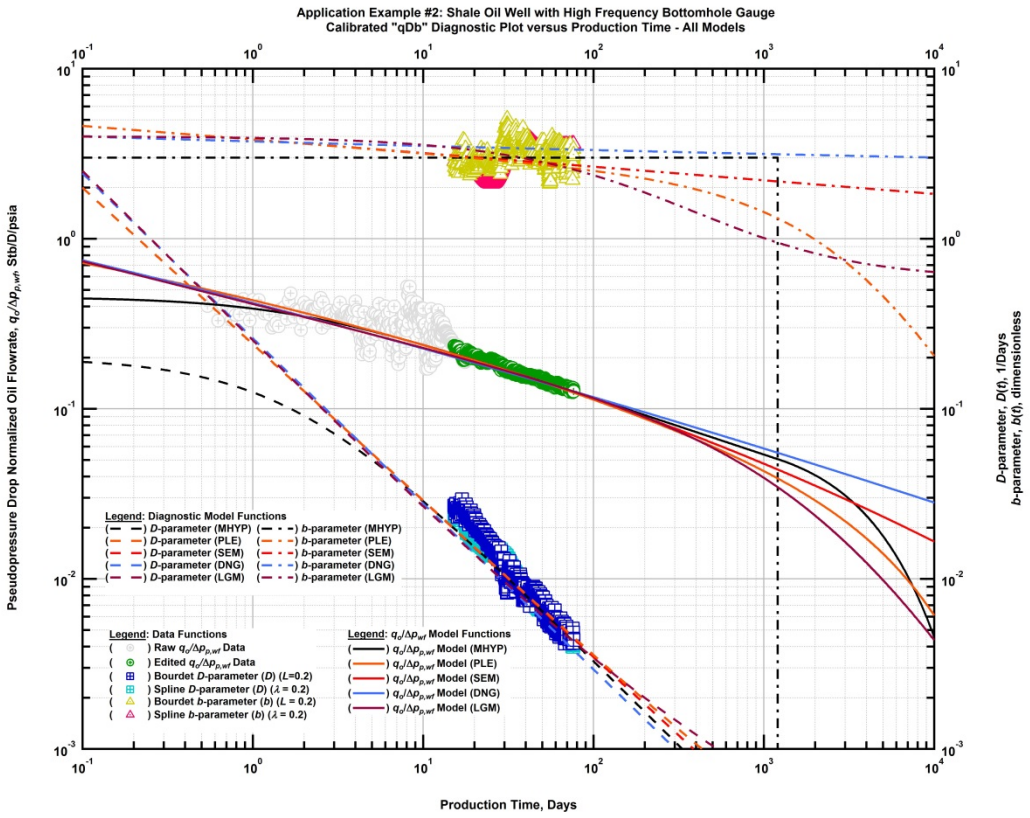

Figure 5.8 — Application Example #2 ─ Calibrated "qDb" Diagnostic Plot (Shale Oil Well)

Each of the five models provides an adequate match of each of the diagnostic functions. It is clear that each model honors the third slope trend throughout the production history of the well and into the future for varying lengths of time depending on the fundamental assumptions of the model in question. **Table 5.3** summarizes the final model parameters corresponding to the model matches depicted in **Figure 5.8**. It is worthwhile mentioning that the calibration process is non-unique and iterative. The ultimate goal is to establish a history match of the rate versus time production data by convolving the calibrated diagnostic models with the measured pressure drop data.

Table 5.3 — Application Example #2 ─ Variable Pressure Decline Curve Model Parameter Results

Decline Model	$(q/\Delta p)_i$ *or* $(K/\Delta p)_i$ (STB/D/psi) or (STB/psi)	D_i *or* τ *or* a (1/D)	n or b *or* m (dim.less)	D_{lim} or D_∞ (percent/year) or (1/D)
M.HYP	0.40	0.2	3	10
PLE	7.70	3.0	0.08	0.0001
SEM	7.70	1.086e-6	0.08	-
DNG	0.38	0.75	1.01	-
LGM	240	480	0.75	-

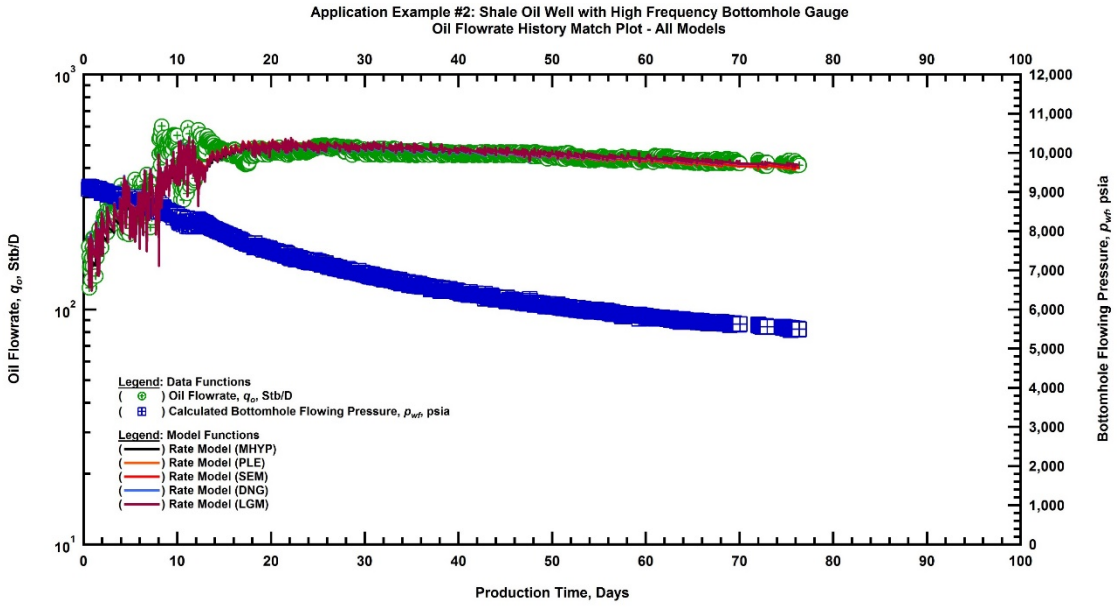

Figure 5.9 — Application Example #2 ─ History Match Plot Honoring Historical Rate Data (Shale Oil Well)

The model matches shown in **Figure 5.9** represent the fully calibrated rate versus time matches through the first 75 days of production history. The history match for each model is very good throughout both the flowback and established flow period after 15 days. This example is a wonderful illustration of the utility of measured bottomhole flowing pressures when performing any type of production analysis relying on pressure data. The quality of the rate and especially pressure data greatly facilitate the analysis process and leave open the possibility for more detailed techniques such as analytical and numerical modeling.

Given the short production history of this well, a constant flowing bottomhole pressure has yet to be established. It is common practice in this reservoir to manage the pressure drawdown as long as possible to mitigate proppant embedment, crushing, and fines migration that are detrimental to production. Forecasts of future well performance are, however, still required for reserves booking and field development planning. Forecasting using traditional decline curve analysis assumes that the flowing pressure is constant and the rate signature of the well may only be sustained for a limited time frame making forecasts prone to severe over or under estimates. As elaborated upon throughout this work, the variable pressure decline technique allows for any flowing pressure schedule to be assumed into the future and the resulting rate curves for a number of sensitivities may be compared.

The horizontal well in this particular case was one of the first drilled to test this particular field which to date had been exploited using primarily vertical fractured wells. The completion design was also slightly changed from a few previous horizontal wells and the data collection program was rigorous in order to facilitate characterization efforts. The variable pressure methodology was useful in providing a quick sensitivity analyzing the effect of increased pressure drawdown on the resulting rate projection in order to make quick decisions on whether to make further completion and/or field development changes in a rapid development environment. **Figure 5.10** shows the result of the power-law exponential projections assuming a constant flowing bottomhole pressure of 5,000 psia (*i.e.* last historic flowing pressure) and continued drawdown to a constant flowing bottomhole pressure of 2,000 psia. **Table 5.4** summarizes the EUR results for each of the five decline models.

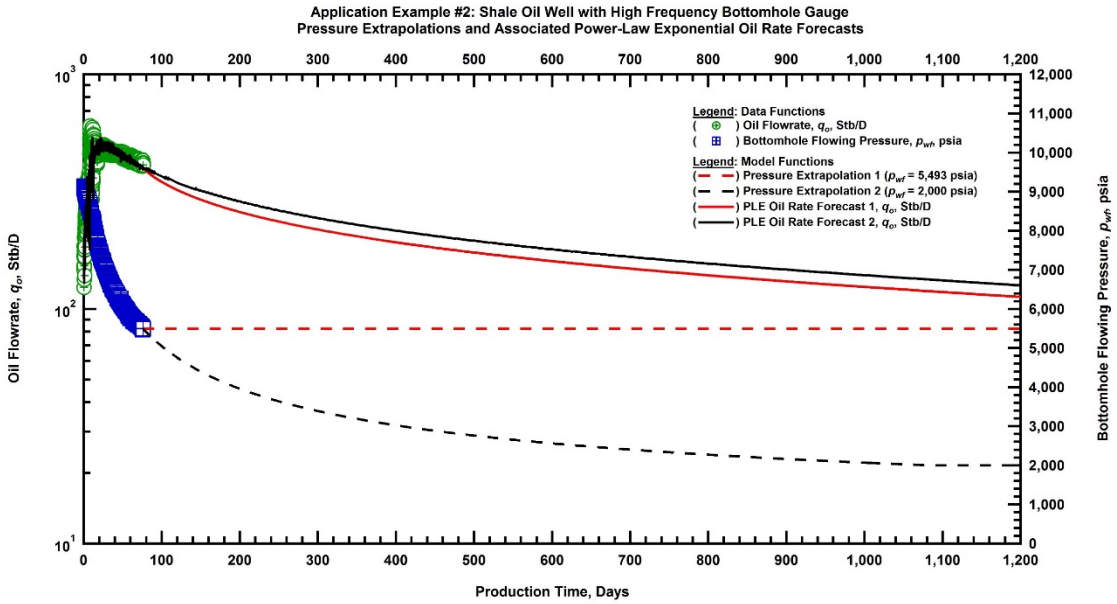

Figure 5.10 — Application Example #2 ─ Pressure Extrapolations and Power-Law Exponential Rate Forecasts

Table 5.4 — Application Example #2 ─ Forecasting Results for All Models

Decline Model	p_{wf} Forecast #1 EUR_{30yr} (Mstb)	p_{wf} Forecast #2 EUR_{30yr} (Mstb)
M.HYP	754	922
PLE	631	806
SEM	896	1,085
DNG	1,289	1,480
LGM	538	702

It is clear from the production forecast that only a slight increase in future performance is modeled as a result of quite a bit of additional pressure drawdown through time. This is a result of the imposition of pressure dependent permeability in the pseudopressure calculation and will be elaborated upon completely in Application Example #3 in the following section. For this particular case, the variable pressure forecasting methodology provided a quick justification and forecast that provided backing for continuing horizontal well development in this particular field. It was done in conjunction with more detailed modeling and provided a quick and valuable look into future production performance while honoring flow regimes and well performance diagnostics under a variable pressure operating environment.

5.3 High-Pressure/High-Temperature Shale Gas Well

The application example worked through in this section details an analysis case producing from a high-pressure/high-temperature shale gas reservoir. The high reservoir pressures and nanodarcy matrix permeabilities necessitate high producing pressure drawdowns for commercial flowrates. As a result of this reality, geomechanical effects are known to prevail in this reservoir which results in degradation in well productivity over time. To mitigate these geomechanical effects, it is common practice for operators to choke wells for as long as possible in order to minimize fracture closure, proppant crushing, pressure dependent permeability changes, and to meet facilities constraints. **Figure 5.11** below depicts nearly a year of production history for the well in question.

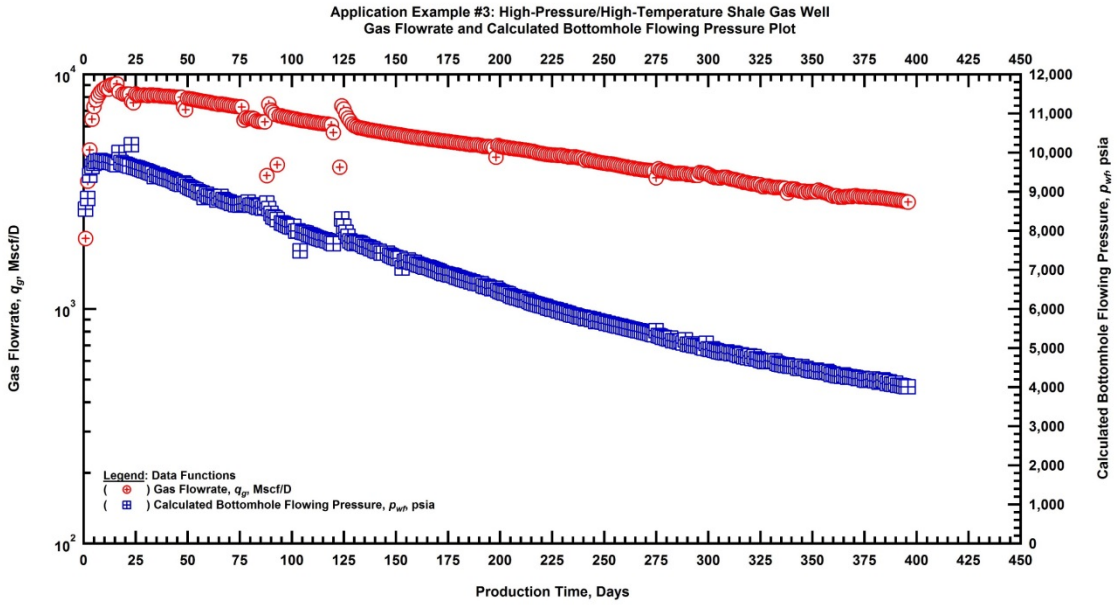

Figure 5.11 — Application Example #3 ─ Time-Rate-Pressure Production Data (Shale Gas Well)

It is clear that the pressure drawdown is being highly regulated when observing the calculated flowing bottomhole pressures in **Figure 5.11**. Another point to note is that the drawdown is approaching 6,100 psia from an initial reservoir pressure of 10,730 psia which is already quite a bit higher than the other two application examples discussed so far. The pressure management has so far led to a highly sustained rate signature which could be mistaken as an exponential decline if observed solely on a semi-log rate versus time plot.

As mentioned before, it is a commonly held belief that this reservoir experiences changes in effective permeability with pressure as a result of the high drawdown management. This introduces a non-linearity

into the system which necessitates linearization using pseudopressure transformations for analytical solutions (relied upon in this example) or nonlinear simulation models. Equations 3.6 and 3.7 are used to calculate the normalized pseudopressure values for this example where the initial permeability, k_i, and the permeability modulus, γ, must be known or estimated *a priori* to any analysis. In effect they become additional history match parameters without some sort of constraining laboratory data and their incorporation is not without limitation which will be discussed as this example develops.

Continuing with the workflow presented throughout this work, we now calculate the pseudopressure drop normalized rate plotting functions, quality control the data to determine the true reservoir signature, and differentiate using the Bourdet and smoothing spline routines to establish the $D(t)$ and $b(t)$ diagnostic signatures for the well. For calculating the pseudopressures, an initial permeability, k_i, of 900 nanodarcy and a permeability modulus, γ, of 5.25 x 10^{-4} $psia^{-1}$ were assumed based on model based production analysis results for other wells in this area. **Figure 5.12** below represents the modified "qDb" plot which has served as the final diagnostic step throughout the work.

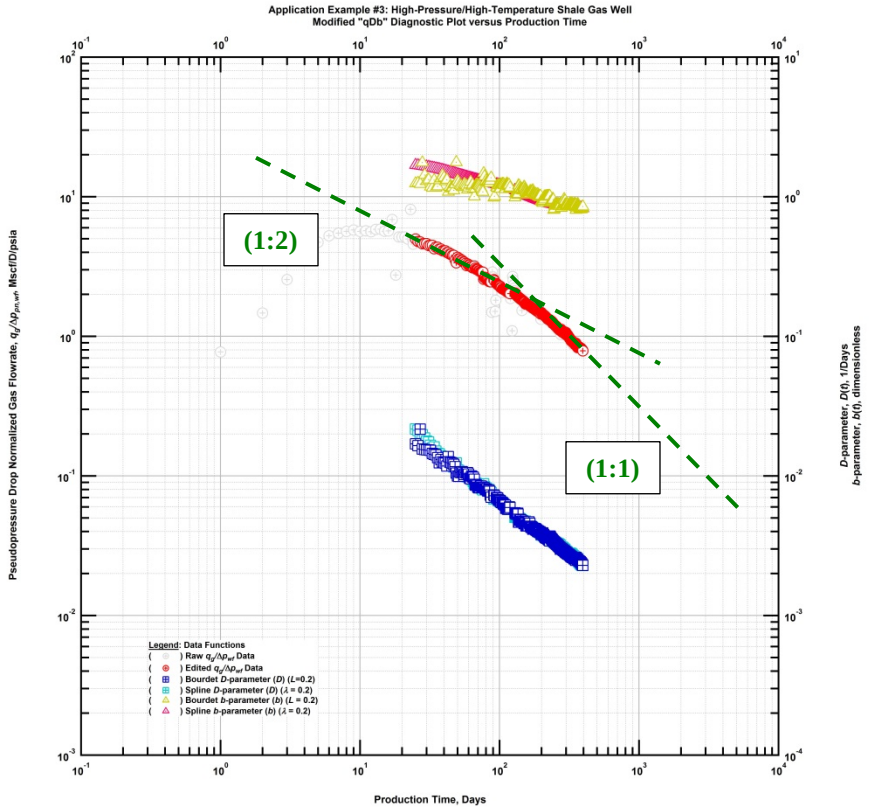

Figure 5.12 — Application Example #3 ─ Modified "qDb" Diagnostic Plot (Shale Gas Well)

The first thing that stands out from the diagnostic signatures presented in **Fig. 5.12** are the clear power-law (straight-line) signatures of both the $D(t)$ and $b(t)$ plotting functions. Furthermore, it is noted that the pseudopressure drop normalized rate trend is highly consistent with minimal data points excluded from the differentiation calculations. The dashed green lines on the plot represent one-half and unit slope trends indicative of changing flow regimes through time with the half-slope indicative of an infinite conductivity fracture signature and the departure away from the half-slop represents a continuous loss of productivity as a result of interfracture interference, pressure dependent permeability, well interference, or reservoir boundaries to name a few. It is important to note that this degradation in productivity corresponds with a continuous decline in the $b(t)$ trend.

Having completed a base level diagnostic analysis, we move forward with the calibration phase of the variable pressure decline curve analysis workflow. The calibration process is again guided by the diagnostic model functions which are summarized by Eqs. 3.28 through 3.37. Ultimately, this is again an iterative process where simultaneous matches of the diagnostic plotting functions and the rate versus time production data are achieved. **Figure 5.13** and **Table 5.5** represent the final calibrated model matches and their associated model parameters.

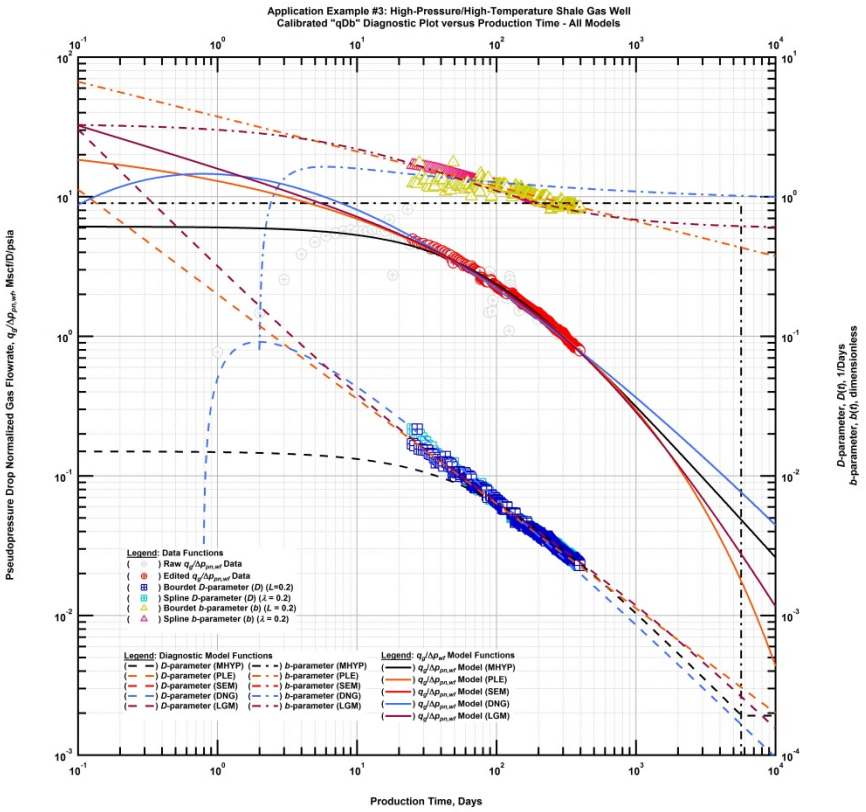

Figure 5.13 — Application Example #3 ─ Calibrated "qDb" Diagnostic Plot (Shale Gas Well)

Table 5.5 — Application Example #3 ─ Variable Pressure Decline Curve Model Parameter Results

Decline Model	$(q/\Delta p)_i$ *or* $(K/\Delta p)_i$ (MSCF/D/psi) or (MSCF/psi)	D_i *or* τ *or* a (1/D)	n or b *or* m (dim.less)	D_{lim} or D_∞ (percent/year) or (1/D)
M.HYP	4.80	0.015	0.9	7
PLE	22.0	0.80	0.25	-
SEM	22.0	2.44	0.25	-
DNG	11.5	1.18	1.13	-
LGM	1340	0.7	75	-

The model matches achieved across the diagnostic plotting functions are adequate in capturing the history of the well to date with the exception of the modified hyperbolic function at early time. This is to be expected given that we clearly see a declining $b(t)$ trend where the hyperbolic model assumes a constant b factor with time. After achieving the calibrated diagnostic matches, the pressure drop normalize rate

functions, represented by Eqs. 3.13 to 3.17, are convolved with the pressure drop data to match the gas flowrate history. This is the final step prior to forecasting production. The matches are represented visually in **Figure 5.14**.

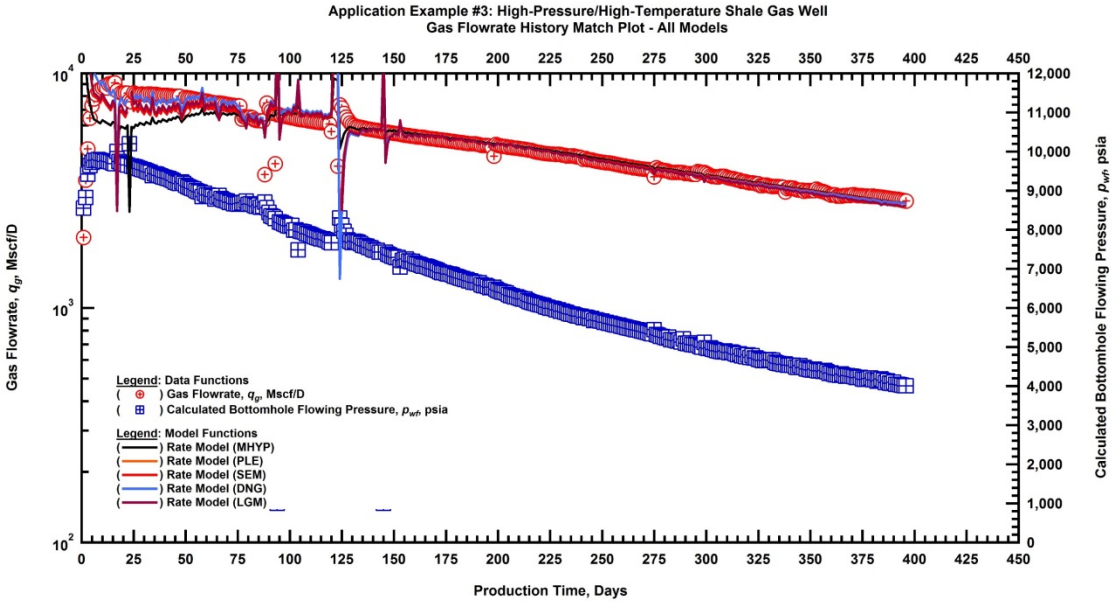

Figure 5.14 — Application Example #3 ─ History Match Plot Honoring Historical Rate Data (Shale Gas Well)

Just as with the "qDb" plot in **Figure 5.13**, adequate matches are achieved across the flowrate history for each of the five models. The modified hyperbolic model was unable to match all portions of the production history which again is a result of the assumption of a single *b* factor trend. This result agrees with the diagnostic trends and matches shown in **Figure 5.13**. Having achieved adequate history matches, the final step is to forecast gas rates into the future. **Figure 5.15** presents the forecasting results for four sensitivities.

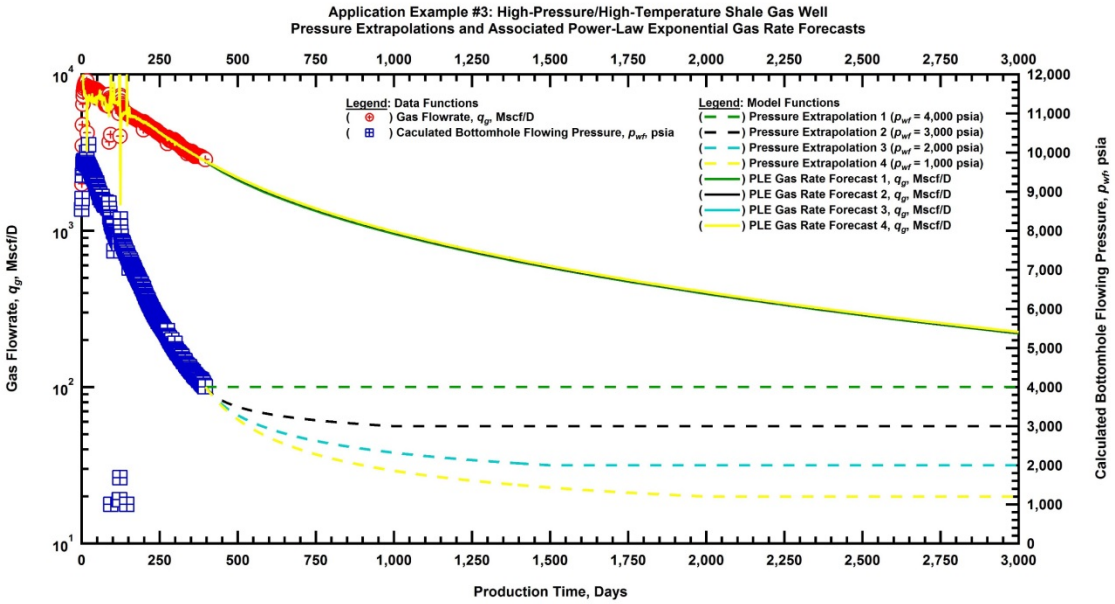

Figure 5.15 — Application Example #3 ─ Pressure Extrapolations and Power-Law Exponential Rate Forecasts

A surprising result of this particular analysis exercise was the minimal influence on the projected gas flowrates as a result of substantial additional pressure drawdown with time. The dashed lines in **Figure 5.15** depict the imposed pressure drawdown schedules for each of the four forecast sensitivities for this application example. The corresponding solid colored lines are the rate forecasts for each pressure sensitivity. Clearly there is minimal difference between the rate forecast profiles. **Table 5.6** tabulates the thirty year ultimate recoveries which also confirm the minimal difference in forecast behavior.

Table 5.6 — Application Example #3 ─ Forecasting Results for All Models

Decline Model	p_{wf} Forecast #1 EUR_{30yr} (Bscf)	p_{wf} Forecast #2 EUR_{30yr} (Bscf)	p_{wf} Forecast #3 EUR_{30yr} (Bscf)	p_{wf} Forecast #4 EUR_{30yr} (Bscf)
M.HYP	4.95	4.99	5.01	5.02
PLE	4.45	4.49	4.51	4.52
SEM	4.45	4.49	4.51	4.52
DNG	5.92	5.98	6.00	6.01
LGM	4.28	4.32	4.34	4.34

The lack of impact on the rate projection as a result of almost 3000 psia of additional drawdown came as a surprise during this analysis and further investigation was warranted to determine the limitation. The initial hypothesis was that the incorporation of pressure dependent permeability with a fairly high permeability modulus (γ = 5.25 x 10^{-4} $psia^{-1}$) was minimizing the effect of the additional pressure drop when the pressure and scheduled pressure forecast were converted to normalized pseudopressures. In order to investigate this, a plot of pressure drop versus pseudopressure drop for varying permeability modulus values was created and is shown below in **Figure 5.16**.

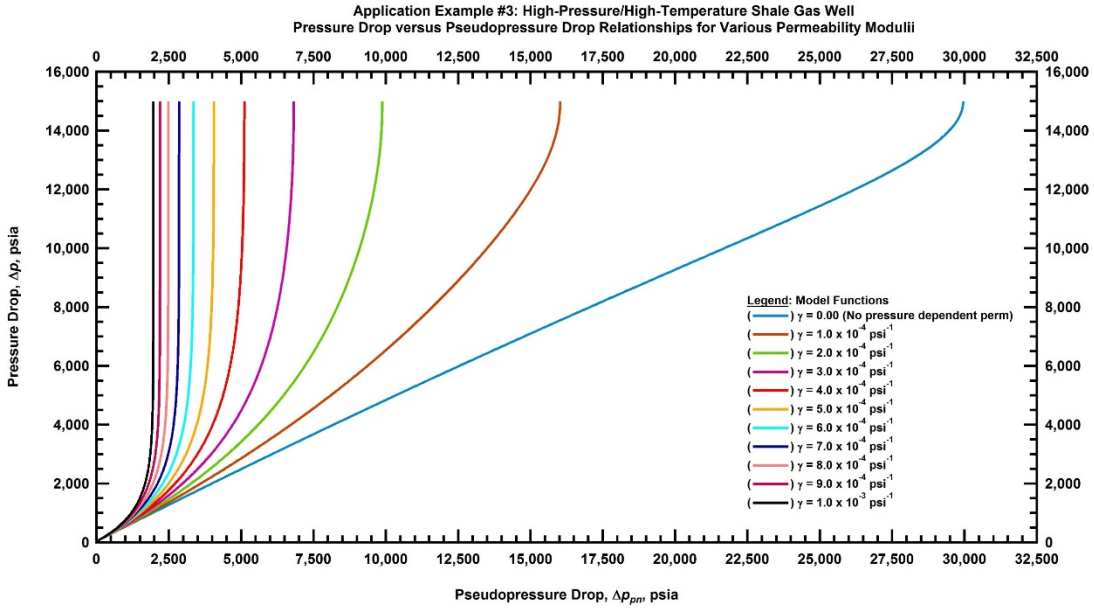

Figure 5.16 — Application Example #3 – Pressure Drop Versus Pseudopressure Drop Incorporating Pressure Dependent Permeability

Observing **Figure 5.16** our hypothesis begins to move towards a conclusion. It is noted that as the permeability modulus governing the pressure dependent permeability function increases in magnitude, the relationship between pressure drop and pseudopressure drop loses a good deal of linearity compared to the standard pseudopressure represented by the γ = 0.00 $psia^{-1}$ case. As a matter of fact, aside from very low pressure drop values and correspondingly low permeability moduli, the pseudopressure formulation does not linearize the system completely at all. Furthermore, after a certain point in time, the curvature of the relationship is so severe that significant additions in pressure drop correspond to unsubstantial additions in pseudopressure drop which explains the forecasting phenomena discussed previously and illustrated in **Figure 5.15** (*e.g.* 3000 psia pressure drop increase corresponds to approximately 75 psia increase in pseudopressure drop).

The use of pseudopressure transformations including pressure dependent permeability is clearly a limitation for the variable pressure decline curve methodology for cases with significant pressure drawdown and pronounced geomechanical effects. In fact, it is noted here that this is a limitation that is not limited solely to the variable pressure decline curve methodology but any relying upon the superposition equation (*e.g.* analytical models). Further linearization using pseudotime, direct formulizations, semi-analytical solutions, and/or numerical (*i.e.* non-linear) model based analysis are all potentially viable solutions for handling situations such as the one described above.

5.4 Type Curve Workflow Incorporating Multi-well Diagnostics

The final application example in this work is different in that it utilizes production data diagnostics for a group of producing wells along with variable pressure decline methodology to assign potential type well profiles for undeveloped locations in a field development plan. This is admittedly a complex problem and the identification of analogous wells, normalizations for sometimes dramatic changes in completions practices, and changes in development well spacing are all topics that influence the ultimate shape of the production profile and the number of potential well locations across a particular acreage position. This example aims to demonstrate a potential application workflow using a small group of wells where a change in pressure management policy from the former policy of producing against a constant bottomhole pressure is being evaluated for economic benefit. In depth discussion on the complex topics listed above is beyond the scope of this work and they will thus be addressed sparingly.

As before with our single well analysis examples, production diagnostics forms the foundation of all analysis steps to be performed later. The most critical aspect of production diagnostics in this particular case is to gain an understanding of the characteristic behavior(s) of the wells included in the dataset in order to make an informed decision regarding the most likely well performance signature for a new well drilled and completed in an analogous manner. The benefit of using the variable-pressure decline curve techniques presented throughout this work coupled with multi-well diagnostics is the ability to incorporate a number of potential drawdown regimes to allow for more realistic rate profiles with time and to facilitate economic analysis to justify specific drawdown practices.

The first step toward developing a type curve is to identify an analogous well group to allow for meaningful investigation into the characteristic performance signature through time. These analogous well groups are often subsets of a larger group of wells across an operator's acreage position or across a regional setting. It is here stated that these subsets are established by like fluid type, completion practices, completion horizon, start of production, geologic similarity or any other division required by the problem at hand. **Figures 5.17** and **5.18** below depict the gas flowrate and calculated bottomhole flowing pressure for the eight well analogous group used for this example.

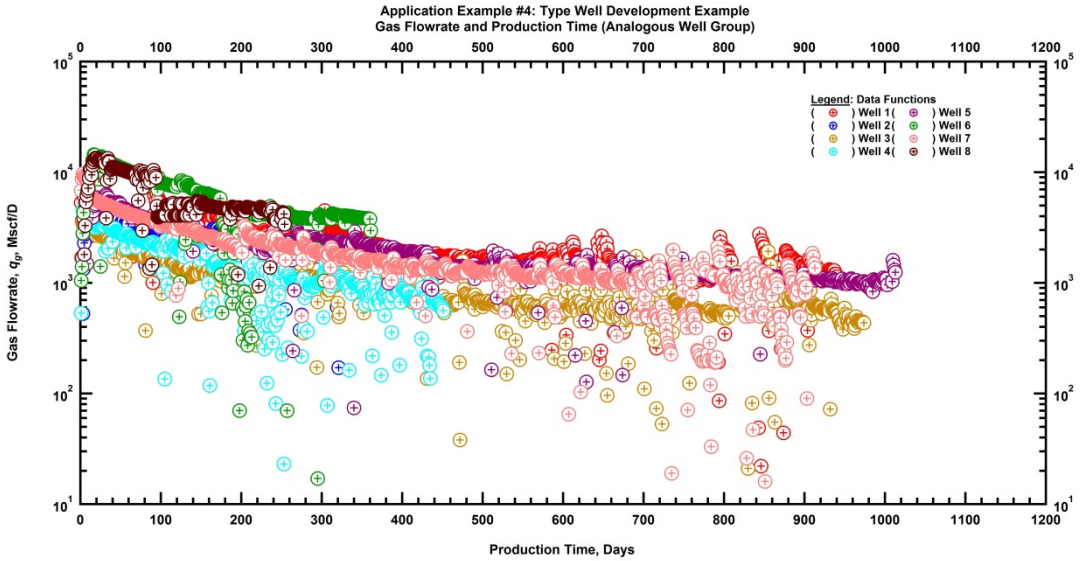

Figure 5.17 — Application Example #4 ─ Gas Flowrate Versus Production Time (Analogous Well Group)

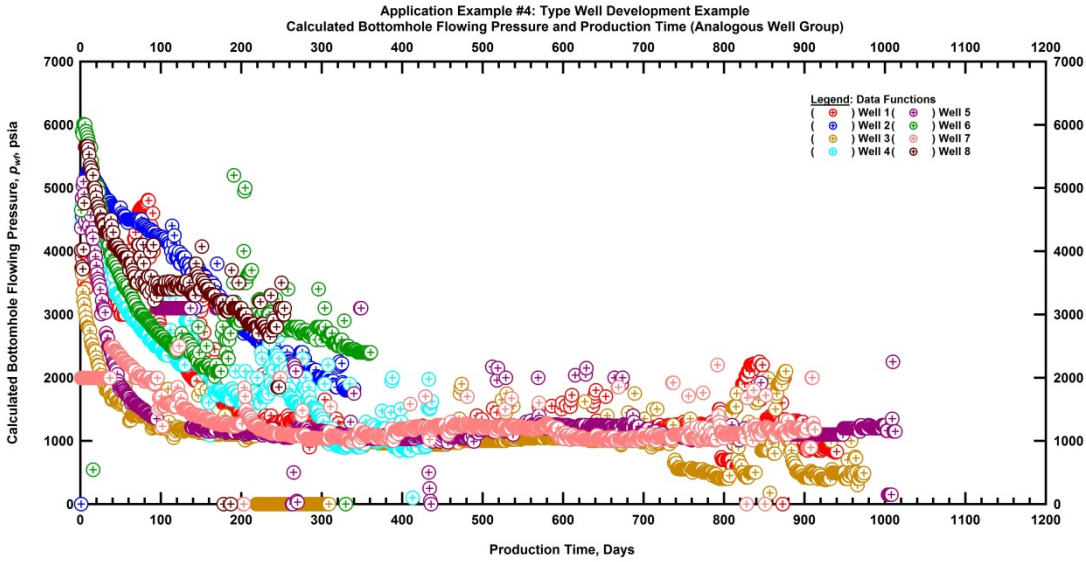

Figure 5.18 — Application Example #4 ─ Calculated Bottomhole Pressure Versus Production Time (Analogous Well Group)

As described above, the analogous group chosen for this example was established primarily due to geographic proximity in a pervasive regional geological setting, nearly identical fluid properties, and

nearly identical completion practices. Rate differences between the wells are clear when observing **Figure 5.17** and are likely due to differences local rock quality, completion execution efficiency, slight differences in lateral lengths, and differences in flowing bottomhole pressure management through time. Observing **Figure 5.18**, it is also clear that there are indeed variances in bottomhole flowing pressure management practices with the older wells arriving at the approximate 1,000 psia constant line pressure fairly quickly while the drawdown for the newer wells is being managed to maintain the gas flowrates at a shallower decline trend.

It is important to investigate the characteristic well performance trend for the analogous group of wells by observing the data signatures across a range of specialized diagnostic plots. In this particular example, we are particularly interested in the flow regimes exhibited and the timing associated with any changes. In order to achieve this goal we create logarithmic plots of pseudopressure drop normalized gas flowrate versus production time and material balance time which are presented below on the left and right hand side of **Figure 5.19**. It is important in this particular example to plot pseudopressure normalized rates in this particular case in order to directly compare wells produced against differing bottomhole flowing pressures to wells produced against a constant bottomhole flowing pressure. The two separate time plotting functions provide different degrees of resolution with the latter specifically meant to interpret boundary dominated flow which is indicated by a unit slope in the data.

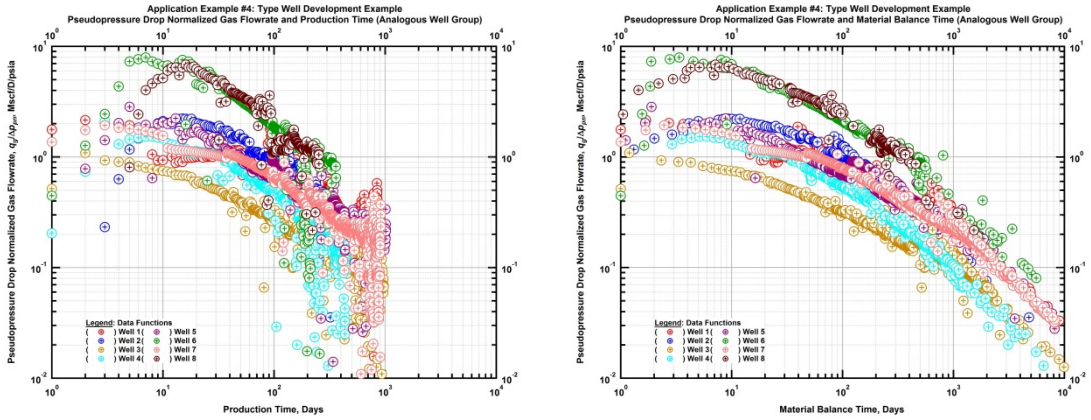

Figure 5.19 — Application Example #4 ─ Pseudopressure Drop Normalized Gas Flowrate Versus Production Time (left) and Material Balance Time (right)

Based on the above plots our story and strategy for defining the shape of our type curve profile begins to gain some clarity. While we still observe differences in productivity between the individual well signatures, it is clear that there are similarities in the flow regime signatures through time. After a brief cleanup period following fracture stimulation, each well exhibits a power-law (*e.g.* linear flow) flow

regime followed by a gradual departure after some period of time. While this generality can be made by observing the plots in **Figure 5.19**, we still have yet to explain the differences in performance. A common practice to attempt to identify performance drivers between otherwise analogous wells is to normalize the production data by specific metrics. **Figure 5.20** below is one such plot.

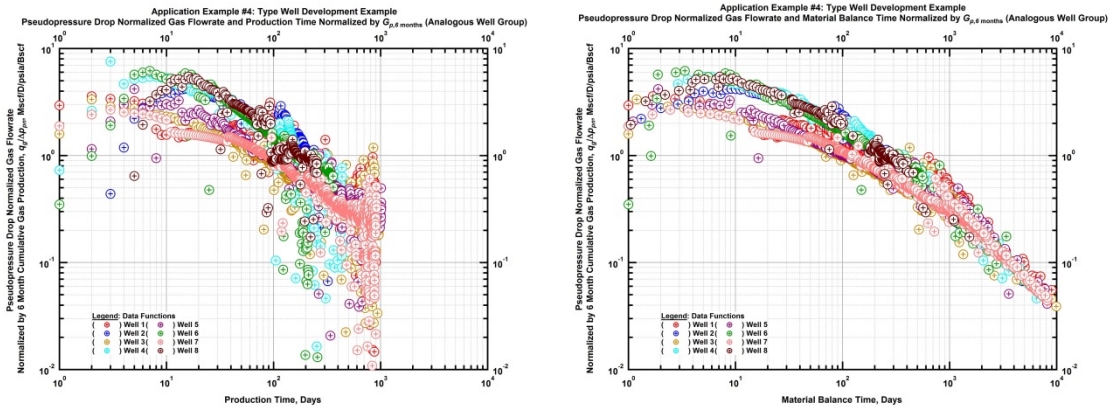

Figure 5.20 — Application Example #4 ─ Pseudopressure Drop Normalized Gas Flowrate Versus Production Time (left) and Material Balance Time (right) ─ Normalized by $G_{p,6\ \text{months}}$

Figure 5.20 is identical to **Figure 5.19** with the exception that the data signatures for each well have been normalized by their respective 6 month cumulative production value. While an in depth discussion of the limitless number of normalizations possibilities is beyond the scope of this work, we must still try and address the rationale behind choosing 6 month cumulative production as a normalization parameter beyond it producing a convenient result. For the purposes of this work it is put forth that the cumulative production normalization is simply a "lump parameter" that serves as a proxy for localized reservoir heterogeneity, slight fluid property differences, differences in lateral length, etc., all of which would drive the 6 month cumulative production for a particular well. It is noted that this practice somewhat "collapses" the data signatures that we observed in **Figure 5.19** into two unique groups. These two groups, while somewhat difficult to see in **Figure 5.20**, are further clarified below in **Figure 5.21**.

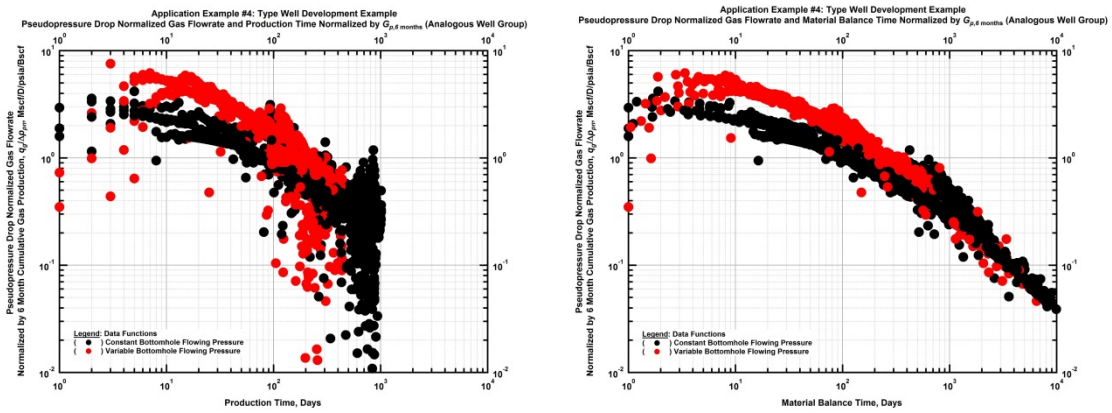

Figure 5.21 — Application Example #4 ─ Comparison Between Pressure Drop Normalized Gas Flowrate Signatures

One group, colored black, consists of the older wells producing at or near a constant bottomhole flowing pressure from inception while the other, colored red, is composed of those producing against a variable bottomhole flowing pressure. Based on **Figure 5.21**, it is clear that the wells being drawdown managed have a slightly different performance signature from the wells producing against a constant bottomhole pressure. Given that the goal of this exercise is to develop type curves for various potential pressure drawdown schedules for future wells, we would like to focus on the well group identified in red in **Figure 5.21**. The variable bottomhole pressure subset consists of four of the eight wells all of which are isolated in **Figure 5.22**.

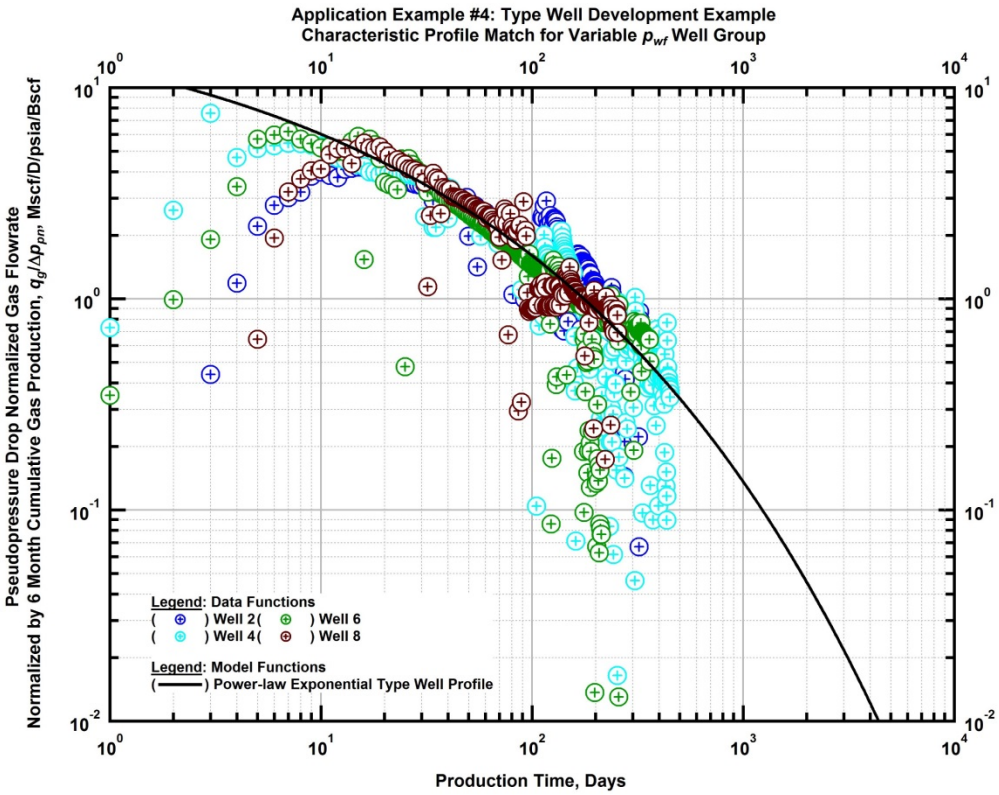

Figure 5.22 — Application Example #4 ─ Power-law Exponential Characteristic Profile Match for Variable p_{wf} Well Group

After identifying the subset of wells that are representative of the problem at hand, we proceed to defining a general type curve shape using the logarithmic plot of pseudopressure normalized gas flowrate normalized by 6 month cumulative production versus production time shown above. For this example the power-law exponential rate profile was chosen due to its characteristic basis function that models a declining *b*-factor with time which is a widely documented phenomena in unconventional oil and gas reservoirs. It must be emphasized that any model could be substituted in place of the power-law exponential relation. **Figure 5.22** above depicts the power-law exponential type well profile and the parameters are summarized below in **Table 5.7**.

Table 5.7 — Application Example #4 ─ Variable Pressure Type Curve Model Parameter Results

Decline Model	$(q/\Delta p)_i$ (MSCF/D/psi)	D_i (1/D)	n (dim.less)	D_∞ (1/D)
PLE	15.4	0.825	0.27	-

As with the single well analysis examples, the final step of the variable pressure decline curve workflow is to forecast production according to a specified pressure schedule. For the individual well scenarios, we were observing the pressure drawdown behavior to-date and speculating on potential changes into the future to generate a corresponding rate profile. For this exercise, the aim is to generate potential rate profiles reflective of different drawdown practices implemented from inception. In **Figure 5.23** seven different pressure extrapolation scenarios are depicted ranging from a constant bottomhole pressure the second the well comes on-line to a managed drawdown of only an average of 2.5 psia/D. This range was chosen to reasonably reflect the range exhibited by the analogous well dataset shown in **Figure 5.18**.

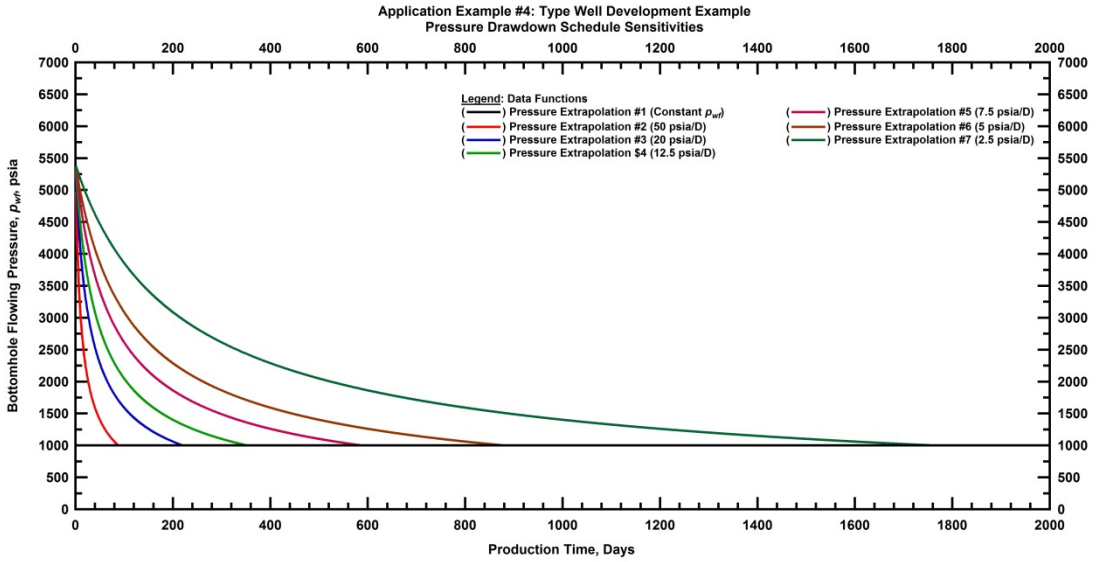

Figure 5.23 — Application Example #4 ─ Pressure Drawdown Schedule Sensitivities

Having defined the pressure drawdown sensitivity scenarios, the final step is to convolve the pressure drop data streams (p_i = 5,400 psia) with the general type well profile shown in **Figure 5.22**. The result of this exercise is seven different rate versus time production profiles with differences resulting from the various pressure assumptions. The results are displayed graphically in **Figure 5.24** and the thirty year estimated ultimate recoveries are tabulated in **Table 5.8**.

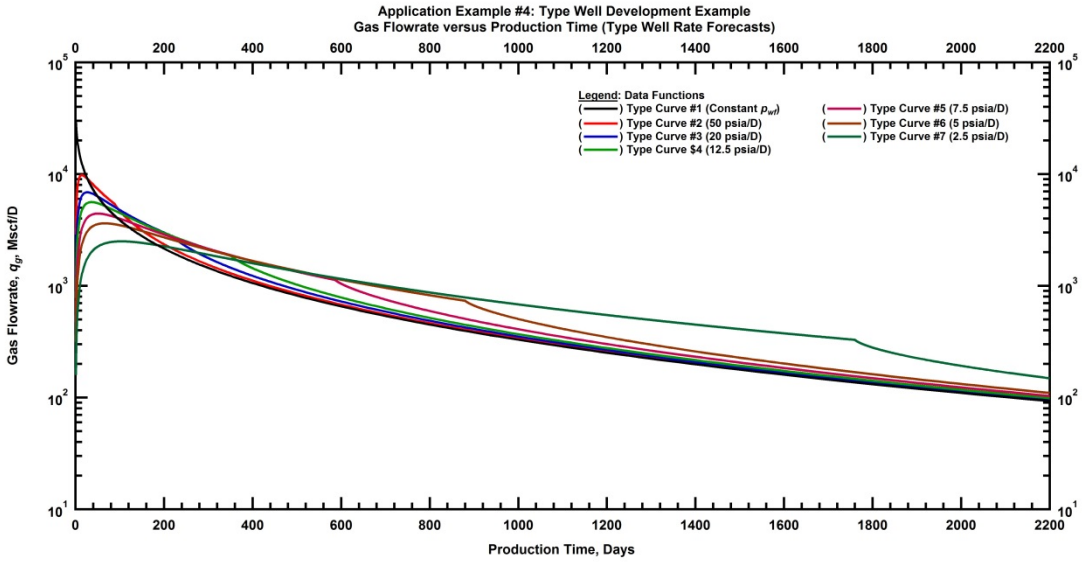

Figure 5.24 — Application Example #4 ─ Gas Flowrate Versus Production Time (Type Well Rate Forecasts)

Table 5.8 — Application Example #4 ─ Variable Pressure Type Curve Forecasting Results

Pressure Forecast Sensitivity	PLE EUR_{30yr} (Bscf)
p_{wf} Forecast #1 (constant)	2.12
p_{wf} Forecast #2 (50 psia/D)	2.11
p_{wf} Forecast #3 (20 psia/D)	2.11
p_{wf} Forecast #4 (12.5 psia/D)	2.11
p_{wf} Forecast #5 (7.5 psia/D)	2.11
p_{wf} Forecast #6 (5 psia/D)	2.11
p_{wf} Forecast #7 (2.5 psia/D)	2.11

The first thing to note from the results presented above is the constancy in thirty-year recovery values regardless of the pressure drawdown assumption. This is an interesting result that is expected when it is realized that regardless of how the pressure drawdown is managed, a maximum drawdown of 4,400 psia is eventually achieved and maintained for a fairly extended period of time. While this scenario arrives at the same ultimate recovery for our simple scenario, which assumes dry gas, it is noted that we ignore realities such as fluid property changes, field development changes, or major operational changes that may be

present in more complex reservoir settings all of which may impact the EUR achievable as a result of different pressure drawdowns.

The second point to note is the behavior of the rate versus time profiles in **Figure 5.24** resulting from the superposition calculations. It is clear that the more aggressive drawdown scenarios achieve higher initial rates quicker while the more conservative pressure drawdown scenarios sacrifice higher initial rates for a sustained period of moderate rates. At later times, after a constant bottomhole flowing pressure of 1,000 psia is achieved, all of the rate profiles converge onto a fairly unified decline trend. This result is interesting as it provides a specific input for the economic question posed in the problem statement of this example. Based on the specific corporate objectives of the operator in question, the pros and cons of the different potential profile shapes can be analyzed quantitatively without resorting to more detailed forward modeling approaches. The strength of the methodology ultimately lies in its foundation being based on observed well performance signatures during the production diagnostics stage of the workflow.

CHAPTER VI

SUMMARY AND CONCLUSIONS

6.1 Summary

The author believes that the developed variable-pressure decline curve technique is a valuable tool for quickly evaluating and forecasting wells where operating conditions preclude the use of traditional decline curve analysis and data or time constraints limit more advanced modeling measures. Reserves estimation, field development decision making, and operational sensitivities are all practical problems where the methodology fills a needed void left by other analysis techniques.

The methodology was fully validated using synthetic data generated using a commercial reservoir signature for oil and gas cases with and without pressure dependent permeability effects. The simulated systems were constrained to mimic the authors experience from analyzing unconventional wells using model based production analysis. The synthetic exercises provided validation for the type of field production scenarios that the technique could comfortably be applied to.

Application examples sought to address a few of the potential operational and field development problems that the methodology applies to (*e.g.* artificial lift, undeveloped type curves, early time high-frequency data, etc.). The techniques adequately captured the prevailing well performance behavior for each of the four application examples and strengths and weaknesses were outlined for each. Special emphasis is placed on the importance of adequate diagnostic investigation, consistent data with a preference for high resolution bottomhole pressure measurements, and caution when analyzing systems with a significant degree of non-linearity.

6.2 Conclusions

The following section summarizes the conclusions are made based on the results of this work. The conclusions are organized based on the methodology, validation, and application aspects of the work.

The methodology was presented in a three step approach that is broadly applicable across a range of application scenarios. Five pressure drop normalized empirical decline models were used as proxies for traditional analytical constant pressure rate solutions in the convolution integral. It is concluded that the applicability and effectiveness of the analysis technique is reliant upon thorough production diagnostics and data consistency. The analysis procedure itself is somewhat non-unique but model calibration and

forecasting are achievable with a reasonable degree of confidence by relying upon the presented "qDb" diagnostic plot along with traditional semi-log data representations.

The examples considered relied upon synthetic data generate from a "known" system where the goal was to bracket the applicable bounds of the techniques proposed. Single phase oil and gas cases with and without pressure dependent permeability were considered with the systems exhibiting non-linearities using traditionally applied pseudopressure transformations to linearize the system as is required for superposition. For each of the synthetic cases tested an adequate match and forecast was achieved; however, some limitations were noted as additional non-linearities increased system complexity. It is concluded that the methodology is applicable for a wide range of scenarios observed in unconventional reservoirs.

Field production cases were selected to represent practical scenarios where the techniques proposed facilitate a solution. Artificial lift decision making, early time monitoring of high-frequency rate and pressure measurements, high-pressure/high-temperature gas production, and field development planning were all addressed as individual examples. It is here that a *key limitation* for high-drawdown wells exhibiting pressure dependent permeability established.

6.3 Recommendations for Future Work

The following is a list of recommendations for continuing this research:

- Extend the methodology to enabled monitoring of variable rate pressure responses using the same, or similar, empirical proxy models. Equating the constant pressure rate response proxies to a constant rate pressure response in the Laplace domain is a starting point.
- Defend the "physical" meaning of the empirical proxies by correlating model parameters with well and reservoir information. This may not to lead to a global solution defining any given relationship but is likely to lead to localized insight.
- Extend the methodology to address additional non-linearities such as multi-phase flow, reservoir boundaries, well-interference, etc.

NOMENCLATURE

a_{Dng}	Model coefficient for the Duong time-rate model, D^{-1}
a_{LGM}	Model coefficient for the Logistic Growth time-rate model, D^{-1}
b	Arps' decline exponent (hyperbolic time-rate relation), dimensionless
c_f	Reservoir compressibility, psi^{-1}
c_t	Total system compressibility, psi^{-1}
D	Reciprocal of the loss ratio, D^{-1}
D_{lim}	Terminal decline constant for the exponential time-rate relation, D^{-1}
D_i	Initial decline constant for the exponential and hyperbolic time-rate relations, D^{-1}
$\hat{D}_i$	Decline coefficient for the Power-Law Exponential time-rate model, D^{-1}
D_∞	Terminal decline coefficient for the Power- Law Exponential time-rate model, D^{-1}
EUR	Estimated ultimate recovery, Bscf or Mstb
h	Net formation thickness, ft
γ_g	Specific gas gravity, dimensionless (air 1)
γ_o	Specific oil gravity, dimensionless (water 1)
γ	Permeability Modulus, psi^{-1}
k	Formation permeability, md
k_i	Initial Formation permeability, md
K	Carrying Capacity for the Logistic Growth time-rate model, Bscf or Mstb
$(K/\Delta p)_i$	Initial rate coefficient for the variable pressure logistic growth model (time-rate-pressure), Mscf/D/psi or Stb/D/psi
L_w	Horizontal Well length, ft
m_{Dng}	Time exponent for the Duong time-rate model, dimensionless
n	Time exponent for the Power-Law and Stretched Exponential time-rate models, dimensionless
n_f	Number of hydraulic fractures, dimensionless
n_{LGM}	Time exponent for the Logistic Growth time-rate model, dimensionless
ϕ	Porosity, fraction
p	Pressure, psia
Δp_{wf}	Bottomhole pressure drop, psi
p_{cr}	Constant-rate pressure solution, psia/Stb/D or psia/Mscf/D
p_i	Initial pressure, psia
p_{tf}	Surface pressure, psia
q	Production rate, Mscf/D or Stb/D
q_{cp}	Constant-pressure rate solution, Mscf/D/psia or Stb/D/psia

q_i	Initial rate for the exponential and hyperbolic time-rate models, Mscf/D or Stb/D
$\hat{q}_i$	Initial rate coefficient for the Power-Law and Stretched Exponential time-rate models, Mscf/D or Stb/D
q_1	Initial rate coefficient for the Duong time-rate model, Mscf/D or Stb/D
$(q/\Delta p)_i$	Initial rate coefficient for the variable pressure decline model (time-rate-pressure), Mscf/D/psi or Stb/D/psi
r	Distance in radial coordinates, ft
r_w	Wellbore radius, ft
S_g	Oil saturation, fraction
S_o	Oil saturation, fraction
S	skin factore, dimensionless
T_r	Reservoir Temperature, °F
t	Production time, days
τ	Time coefficient for the Stretched Exponential time-rate model, D^{-1}
μ_g	Viscosity, cp
x_f	Effective fracture half length, ft
z	gas-law deviation factore, dimensionless

REFERENCES

Agarwal, R.G. 1979. Real Gas Pseudotime – A New Function for Pressure Buildup Analysis of MHF Gas Wells. Paper SPE 8279 presented at the SPE Annual Technical Conference and Exhibition, Las Vegas, NV, 23-26 September 1979.

Agarwal, R.G., Gardner, D.C., Kleinstieber, S.W., and Fussell, D.D. 1999. Analyzing Well Production Data Using Combined Type Curve and Decline Curve Analysis Concepts. *SPEREE* **2** (5): 478-486.

Al-Hussainy, R., Ramey, H.J. Jr., and Crawford, P.B. 1966. The Flow of Real Gas Through Porous Media. *JPT* (May 1966) 637; *Trans*., AIME, **237**.

Amini, S., Ilk, D., and Blasingame, T.A. 2007. Evaluation of the Elliptical Flow Period for Hydraulically-Fractured Wells in Tight Gas Sands – Theoretical Aspects and Practical Considerations. Paper SPE 106308 presented at the SPE Hydraulic Fracturing Technology Conference, College Station, TX, 29-31 January 2007.

Arps, J.J. 1945. Analysis of Decline Curves. *Trans*. AIME **160**: 228-247.

Arps, J.J. 1956. Estimation of Primary Oil Reserves. *Trans.* AIME **207**: 182-191.

Blasingame, T.A. and Lee, W.J. 1986. Properties of Homogeneous Reservoirs, Naturally Fractured Reservoirs, and Hydraulically Fractured Reservoirs From Decline Curve Analysis. Paper SPE 15018 presented at the Permian Basin Oil & Gas Recovery Conference, Midland, TX, 13-14 March 1986.

Blasingame, T.A. and Lee, W.J. 1986. Variable-Rate Reservoir Limits Testing. Paper SPE 15028 presented at the Permian Basin Oil & Gas Recovery Conference, Midland, TX, 13-14 March 1986.

Blasingame, T.A. and Lee, W.J. 1988. The Variable-Rate Reservoir Limits Testing of Gas Wells. Paper SPE 17708 presented at the SPE Gas Technology Symposium, Dallas, TX, 13-15 June 1988.

Blasingame, T.A and Lee, W.J. 1989. Type-Curve Analysis Using the Pressure Integral Method. Paper SPE 18799 presented at the SPE California Regional Meeting, Bakersfield, CA, 5-7 April 1989.

Blasingame, T.A., Johnston, J.L., Rushing, J.A., Thrasher, T.S., Lee, W.J, and Raghavan, R. 1990. Paper SPE 20535 presented at the SPE Annual Technical Conference and Exhibition, New Orleans, LA, 23-25 September 1990.

Blasingame, T.A., McCray, T.L., and Lee, W.J. 1991. Decline Curve Analysis for Variable Pressure Drop/Variable Flowrate Systems. Paper SPE 21513 presented at the SPE Gas Technology Symposium, Houston, TX, 23-24 January 1991.

Blumberg, A.A. 1968. Logistic Growth Rate Functions. *Journal of Theoretical Biology* **21**: 42-44.

Bourdet, D., Ayoub, J.A., and Pirard, Y.M. 1989. Use of Pressure Derivative in Well Test Interpretation. *SPEFE* (June 1989) 293, *Trans.*, AIME, **287**.

Camacho-Velazquiez, R.G. and Raghavan, R. 1989. Boundary-Dominated Flow in Solution-Gas-Drive Reservoirs. *SPERE* **4** (4): 503-512.

Carter, R.D. 1985. Type Curves for Finite Radial and Linear Gas-Flow Systems: Constant-Terminal-Pressure Case. *SPEJ* **25** (5): 719-728.

Chen, C.C. and Raghavan, R. 1997. A Multiply-Fractured Horizontal Well in a Rectangular Drainage Region. *SPEJ* **2** (4): 455-465.

Clark, A.J., Lake, L.W., and Patzek, T.W. 2011. Production Forecasting with Logistic Growth Models. Paper SPE 144790 presented at the SPE Annual Technical Conference and Exhibition, Denver, CO, 30 October – 02 November 2011.

Collins, P.W., Ilk, D., and Blasingame, T.A. 2014. Practical Considerations for Forecasting Production Data in Unconventional Reservoirs - Variable Pressure Drop Case. Paper SPE 170945 presented at the SPE Annual Technical Conference and Exhibition, Amsterdam, The Netherlands, 17-29 October 2014.

Cutler, W.W. 1924. Estimation of Underground Oil Reserves by Oil-Well Production Curves. *Bull*. USBM 228 (1).

Doublet, L.E. and Blasingame, T.A. 1995. Decline Curve Analysis Using Type Curves: Water Influx/Waterflood Cases. Paper SPE 30774 presented at the SPE Annual Technical Conference and Exhibition, Dallas, TX, 22-25 October 1995.

Doublet, L.E., Pande, P.K., McCollum, T.J., and Blasingame, T.A. 1994. Decline Curve Analysis Using Type Curves – Analysis of Oil Well Production Data Using Material Balance Time: Application to Field Cases. Paper SPE 28688 presented at the Petroleum Conference and Exhibition of Mexico, Veracruz, Mexico, 10-13 October 1994.

Duhamel, J.M.C.: Mémoire sur la methode générale relative au mouvement de la chaleur dans les corps solides plongés dans les milieux dont la temperature varie avec le temps. *J. de Ec. Polyt.* (Paris) 14 (1833) 20-77.

Duong, A.N. 2011. Rate-Decline Analysis for Fracture-Dominated Shale Reservoirs. SPE *Reservoir Evaluation and Engineering* **14** (3): 337-387.

El-Banbi, A.H. and Wattenbarger, R.A. 1998. Analysis of Linear Flow in Gas Well Production. Paper SPE 39972 presented at the SPE Gas Technology Symposium, Calgary, Alberta, Canada, 15-18 March 1998.

Fetkovich, M.J. 1980. Decline Curve Analysis Using Type Curves. *JPT* **32** (6): 1065 1077.

Fetkovich, M.J., Vienot, M.E., Bradley, M.D., and Kiesow, U.G. 1987. Decline Curve Analysis Using Type Curves: Case Histories. *SPEFE* **2** (4): 637-656.

Fraim, M.L. and Wattenbarger, R.A. 1987. Gas Reservoir Decline-Curve Analysis Using Type Curves With Real Gas Pseudopressure and Normalized Time. Paper SPE 14238 presented at the SPE Annual Technical Conference and Exhibition, Las Vegas, NV, 22-25 September 1987.

Guo, G. and Evans, R.D. 1993. Pressure-Transient Behavior and Inflow Performance of Horizontal Wells Intersecting Discrete Fractures. Paper SPE 26446 presented at the Annual Technical Conference and Exhibition, Houston, TX, 3-6 October 1993.

Horne, R.N. and Temeng, K.O. 1995. Relative Productivities and Pressure Transient Modeling of Horizontal Wells with Multiple Fractures. Paper SPE 29891 presented at the Middle East Oil Show, Bahrain, 11-14 March 1995.

Ilk, D. 2010. Well Performance Analysis for Low to Ultra-Low Permeability Reservoir Systems. PhD dissertation. Texas A&M University, College Station, TX.

Ilk, D., Perego, A.D., Rushing, J.A., and Blasingame, T.A. 2008. Exponential vs. Hyperbolic Decline in Tight Gas Sands – Understanding the Origin and Implications for Reserve Estimates Using Arps' Decline Curves. Paper SPE 116731 presented at the SPE Annual Technical Conference and Exhibition, Denver, CO, 21–24 September 2008.

Ilk, D., Rushing, J.A., Sullivan, R.B., and Blasingame, T.A. 2007. Evaluating the Impact of Waterfrac Technologies on Gas Recovery Efficiency: Case Studies Using Elliptical Flow Production Data Analysis. Paper SPE 110187 presented at the SPE Annual Technical Conference and Exhibition, Anaheim, CA, 11-14 November 2007.

Ilk, D., Rushing, J.A., and Blasingame, T.A. 2009. Decline Curve Analysis for HP/HT Gas Wells: Theory and Applications. Paper SPE 125031 presented at the SPE Annual Technical Conference and Exhibition, New Orleans, LA, 04–07 October 2009.

Ilk, D. and Blasingame, T.A. 2013. Decline Curve Analysis for Unconventional Reservoir Systems - Variable Pressure Drop Case. Paper SPE 167253 presented at the SPE Unconventional Resources Conference-Canada, Calgary, Alberta, Canada, 05-07 November 2013.

Johnson, R.H. and Bollens, A.L. 1927. The Loss Ratio Method of Extrapolating Oil Well Decline Curves. *Trans*. AIME **77**: 771.

Kisslinger, C. 1993. The Stretched Exponential Function as an Alternative Model for Aftershock Decay Rate. *Journal of Geophysical Research* **98** (2): 1913-1921.

Kohlrausch, R. 1854. Theorie des elektrischen Rückstandes in der Leidner Flasche. *Paggendorff* **91**: 56-82.

Lacayo, J. and Lee, J. 2014. Pressure Normalization of Production Rates Improves Forecasting Results. Paper SPE 168974 presented at the SPE Unconventional Resources Conference, The Woodlands, TX, 1-3 April 2014.

Larsen, L. and Hegre, T.M. 1991. Pressure Transient Behavior of Horizontal Wells with Finite-Conductivity Vertical Fractures. Paper SPE 22076 presented at the SPE International Arctic Technology Conference and Exhibition, Anchorage, AK, 29-31 May 1991.

Larsen, L. and Hegre, T.M. 1994. Pressure Transient Analysis of Multifractured Horizontal Wells. Paper SPE 28389 presented at the SPE Annual Technical Conference and Exhibition, New Orleans, LA, 25-28 September 1994.

Lee, W.J. and Holditch, S.A. 1982. Application of Pseudotime to Buildup Test Analysis of Low-Permeability Gas Wells With Long-Duration Wellbore Storage Distortion. SPE 9888 presented at the SPE Low-Permeability Symposium, Denver, CO, 27-29, 1982.

Lee, W.J. and Sidle, R.E. 2010. Gas Reserves Estimation in Resource Plays. Paper SPE 130102 presented at the 2010 SPE Unconventional Reservoirs Conference, Pittsburgh, PA 23-25 February 2010.

Lee, J. and Wattenbarger, R.A. 1996. *Gas Reservoir* Engineering, Vol. 5, 215. Richardson, Texas. Textbook Series, SPE.

Lewis, J.O. and Beal, C.H. 1918. Some New Methods for Estimating the Future Production of Oil Wells. *Trans*. AIME **59**: 492-525.

Maley, S. 1985. The Use of Conventional Decline Curve Analysis in Tight Gas Well Applications. Paper SPE 13898 presented at the Low Permeability Gas Reservoirs Conference, Denver, CO, 19-22 May 1985.

Marhaendrajana, T. and Blasingame, T.A. 2001. Decline Curve Analysis Using Type Curves - Evaluation of Well Performance Behavior in a Multiwell Reservoir System. Paper SPE 71517 presented at the SPE Annual Technical Conference and Exhibition, New Orleans, LA, 30 September- 3 October 2001.

McCray, T.L. 1990. Reservoir Analysis Using Production Data and Adjusted Time. MS thesis, Texas A&M University, College Station, TX.

Nelson, P.H. 2009. Pore-throat Sizes in Sandstones, Tight Sandstones, and Shales. *Bull.* AAPG **93** (3): 1071-1098.

Okouma, V., Symmons, D., Hosseinpour-Zonoozi, N., Ilk, D., and Blasingame, T.A. 2012. Practical Considerations for Decline Curve Analysis in Unconventional Reservoirs-Application of Recently Developed Time-Rate Relations. Paper SPE 162910 presented at the SPE Hydrocarbon, Economics, and Evaluation Symposium, Calgary, Alberta, Canada, 24-25 September 2012.

Ozkan, E., Brown, M., Raghavan, R., and Kazemi, H. 2009. Comparison of Fractured Horizontal-Well Performance in Conventional and Unconventional Reservoirs. Paper SPE 121290 presented at the SPE Western Regional Meeting, San Jose, CA, 24-26 March 2009.

Palacio, J.C. and Blasingame, T.A. 1993. Decline-Curve Analysis Using Type Curves - Analysis of Gas Well Production Data. Paper SPE 25909 presented at the SPE Joint Rocky Mountain Regional and Low Permeability Reservoirs Symposium, Denver, CO, 26-28 April 1993.

Pollock, D.S.G. Smoothing with Cubic Splines. Available from the Department of Economics, Queen Mary College, University of London, Mile End Road, London E1 4 NS.

Pratikno, H., Rushing, J.A., and Blasingame, T.A. 2003. Decline Curve Analysis Using Type Curves – Fractured Wells. Paper SPE 84287 presented at the SPE Annual Technical Conference and Exhibition Denver, CO, 5-8 October 2003.

Raghavan, R.S., Chen, C.C., and Agarwal, B. 1997. An Analysis of Horizontal Wells Intercepted by Multiple Fractures. *SPEJ* **2** (3): 235-245.

Robertson, S. 1988. Generalized Hyperbolic Equation. Paper SPE 18731 available from SPE, Richardson, TX.

Rushing, J.A., Perego, A.D., Sullivan, R.B., and Blasingame, T.A. 2007. Estimating Reserves in Tight Gas Sands at HP/HT Reservoir Conditions: Use and Misuse of an Arps Decline Curve Methodology. Paper SPE 109625 presented at the SPE Annual Technical Conference and Exhibition, Anaheim, CA, 11-14 November 2007.

Shih, M.Y. and Blasinagme, T.A. 1995. Decline Curve Analysis Using Type Curves: Horizontal Wells. Paper SPE 29572 presented at the SPE Joint Rocky Mountain Regional and Low Permeability Reservoirs Symposium, Denver, CO, 19-22 March 1995.

Soliman, M.Y., Hunt, J.L., and El Rabaa, A.M. 1990. Fracturing Aspects of Horizontal Wells. *JPT* **42** (8): 966-973.

Valkó, P.P. 2009. Assigning Value to Stimulation in the Barnett Shale: A Simultaneous Analysis of 7000 Plus Production Histories and Well Completion Records. Paper SPE 119369 presented at the SPE Hydraulic Fracturing Technology Conference, College Station, TX, 19-21 January 2009.

van Everdingen, A.F. and Hurst, W. 1949. Application of the Laplace Transformation to Flow Problems in Reservoirs. *Trans*. AIME **186**: 305-324.

van Kruysdijk, C.P.J.W. and Dullaert, G.M. 1989. A Boundary Element Solution of the Transient Pressure Response of Multiply Fracture Horizontal Wells. Paper presented at the 2nd European Conference on the Mathematics of Oil Recovery, Cambridge, England.

Wattenbarger, R.A. and Ramey, H.J. 1968. Gas Well Testing With Turbulence, Damage and Wellbore Storage. *Trans*. AIME **243**: 877-888.

Wattenbarger, R.A. El-Banbi, A.H., Villegas, M.E., and Maggard, J.B. 1998. Production Analysis of Linear Flow Into Fractured Tight Gas Wells. Paper SPE 39931 presented at the SPE Rocky Mountain Regional/Low Permeability Reservoirs Symposium and Exhibition, Denver, CO, 5 8 April 1998.

APPENDIX A

ARPS' DECLINE CURVE RELATIONS

This section aims to fully derive the base Arps' (1945) exponential and hyperbolic decline relations. Additionally, the modified hyperbolic proposed by Robertson (1988) is outlined. A schematic "qDb plot" and a brief time-rate application example is included demonstrating the rate and derivative behavior of each model.

For orientation, it is noted that the derivations of both the exponential and hyperbolic decline relations were based on empirical observations of the loss-ratio and loss-ratio derivative originally proposed by Johnson and Bollens (1927). The mathematical definitions pertaining to both are provided below. Numerical procedures for calculating the derivative of noisy production data are necessary and the Bourdet (1989) technique and a smoothing spline technique are relied upon in this work.

$$\frac{1}{D(t)} = -\frac{q(t)}{dq(t)/dt} \quad \text{.....(A.1)}$$

$$b(t) = \frac{d}{dt}\left[\frac{1}{D(t)}\right] = -\frac{d}{dt}\left[\frac{q(t)}{dq(t)/dt}\right] \quad \text{.....(A.2)}$$

where q is flowrate in volume per unit time t, $D(t)$ is the decline rate as a function of time expressed as a percentage decline per unit time, and $b(t)$ is the dimensionless loss ratio derivative as a function of time.

Prior to deriving and applying any decline relation it is crucial to understand all of the limitations from both a theoretical and practical standpoint. First, it must be understood that Arps' hyperbolic decline is an empirical relation meaning it was derived based on an observed data behavior. The exponential decline was originally derived based on empiricism; however, it can be derived rigorously for the case of pseudo-steady state production of a slightly compressible fluid against a constant sandface pressure. With this in mind, Arps' provided the following practical criteria when applying the exponential or hyperbolic decline relations.

- The extrapolation of a curve (*i.e.* rate-time model) through the historic production data is an adequate representation of future production trends.
- Current operating conditions and field development will continue without substantial changes which may affect the model extrapolation into the future.

- The well is producing from an unchanging drainage area with no-flow boundaries (*i.e.* boundary dominated flow).
- The well is producing against a constant bottomhole flowing pressure.

A.1 Derivation of Arps' Exponential Decline Relation

Arps provided a mathematical derivation of the constant percentage decline, or exponential decline based on observations of the loss ratio defined as Eq. A.1. He used a simple finite difference calculation in order to calculate the derivative term resulting in a behavior similar to that observed in **Fig. A.1** where the $D(t)$ was assumed to be approximately constant.

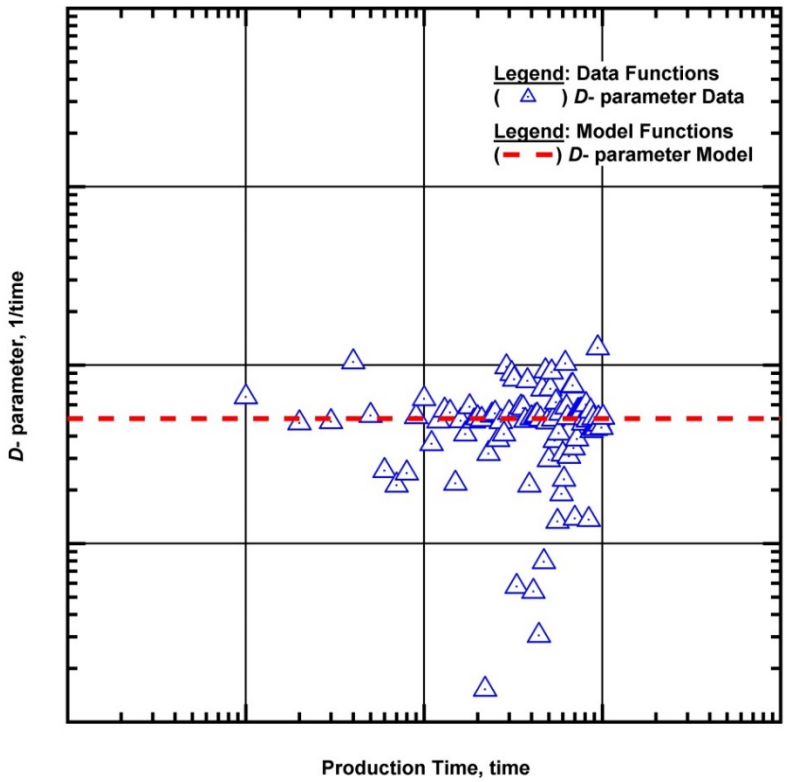

Figure A.1 — Schematic of the Constant Behavior of the Loss-Ratio Characterizing Arps' Exponential Decline

Rearranging Eq. A.1, we obtain a mathematical relationship describing $D(t)$ as:

$$D(t) = -\frac{1}{q(t)}\frac{dq(t)}{dt} \quad \text{.....(A.3)}$$

Based on the observed constant behavior of $D(t)$ similar to that shown in **Fig. A.1**, Eq. A.3 can be rearranged and the $D(t)$ term replaced by a constant as shown below:

$$\frac{1}{q}\frac{dq}{dt} = -D_i \quad \text{.....(A.4)}$$

where D_i is the initial decline expressed as a percentage decline per unit time. For simplicity in derivation the (t) notation was dropped. Separating the variables in Eq. A.4 we obtain:

$$\frac{dq}{q} = -D_i dt \quad \text{.....(A.5)}$$

Integrating both sides of Eq. A.5 as follows:

$$\int_{q_i}^{q(t)} \frac{dq}{q} = -D_i \int_0^t dt \quad \text{.....(A.6)}$$

where q_i refers to the initial rate at time zero in volume per unit time. In order to complete the integral on the left hand side (LHS) of Eq. A.6 the definition of a natural logarithm is recalled:

$$\ln[x] = \int_1^x \frac{dx}{x} \quad \text{.....(A.7)}$$

where x serves as a generic placeholder variable. Utilizing the definition in Eq. A.7 the integration is completed as follows:

$$\ln[q]\Big|_{q_i}^{q(t)} = -D_i t\Big|_0^t \quad \text{.....(A.8)}$$

Substitution of the limits of integration yields:

$$\ln[q(t)] - \ln[q_i] = -D_i(t-0) \quad \text{.....(A.9)}$$

We again recall a logarithmic identity before proceeding in our derivation:

$$\ln[x] - \ln[y] = \ln\left[\frac{x}{y}\right] \quad \text{.....(A.10)}$$

where y serves as an additional generic placeholder variable. Using Eq. A.10, the LHS of Eq. A.9 simplifies to arrive at the following form:

$$\ln\left[\frac{q(t)}{q_i}\right] = -D_i t \quad \text{.....(A.11)}$$

Exponentiation both sides of Eq. A.11 yields:

$$\frac{q(t)}{q_i} = \exp\left[-D_i t\right] \quad \text{.....(A.12)}$$

The final time-rate form of Arps' exponential decline is obtained by a simple rearrangement of Eq. A.12:

$$q(t) = q_i \exp\left[-D_i t\right] \quad \text{.....(A.13)}$$

Eq. A.13 is now differentiated to obtain the model behavior of $D(t)$ and $b(t)$. The model and data behavior of these trends can be calibrated against each other in order to obtain a time-rate match between Eq. A.13 and a particular data series. We will use Eq. A.1 to calculate $D(t)$ the definition of which is as follows:

$$\frac{1}{D(t)} = -\frac{q(t)}{dq(t)/dt} \quad \text{.....(A.1)}$$

Rearranging Eq. A.1 and substituting Eq. A.13 for the rate terms we obtain:

$$D(t) = -\frac{1}{q_i \exp\left[-D_i t\right]} \frac{d}{dt}\left\{q_i \exp\left[-D_i t\right]\right\} \quad \text{.....(A.14)}$$

Performing the derivation yields the following:

$$D(t) = \frac{D_i\, q_i \exp\left[-D_i t\right]}{q_i \exp\left[-D_i t\right]} \quad \text{.....(A.15)}$$

Cancelling like terms yields the relation for the decline as a function of time. As expected, the equation below is in agreement with the observation shown in **Fig. A.1**.

$$D(t) = D_i \quad \text{.....(A.16)}$$

In order to calculate the loss ratio derivative, or $b(t)$, Eq. A.2 is used.

$$b(t) = \frac{d}{dt}\left[\frac{1}{D(t)}\right] \quad \text{.....(A.2)}$$

Combining Eq. A.16 and Eq. A.2 yields:

$$b = \frac{d}{dt}\left[\frac{1}{D_i}\right] \quad \text{.....(A.17)}$$

Completing the derivative of the constant term on the right hand side (RHS) we obtain the following relationship for $b(t)$:

$$b(t) = 0 \quad \text{.....(A.18)}$$

All of the equations up until this point in the derivation are concerned with the modeling of time-rate data based on the assumption of a constant bottomhole flowing pressure. In keeping with the aim of this work, namely incorporating pressure data into decline curve analysis, the variable pressure form of the exponential decline is provided below.

The discrete form of the convolution integral is used to account for variations in bottomhole flowing pressure as a function of time. A complete development of the superposition equation is included in Appendix F. The final mathematical form is provided below:

$$q(t) = \sum_{k=1}^{u} (\Delta p_{wf,k} - \Delta p_{wf,k-1})(q_{cp}(t_u - t_{k-1})) \quad \text{.....(A.19)}$$

where Δp_{wf} is the bottomhole pressure drop in units of pressure at a specific point in time and q_{cp} denotes a constant pressure rate solution which is traditionally obtained by solving the diffusivity equation for a particular well and reservoir configuration. This work makes the assumption that the constant pressure rate signature of a well is accurately represented by the pressure drop normalized rate behavior of that well. If this assumption holds, it is proposed that this data trend can be modeled using a pressure drop normalized form of an empirical time-rate decline relation serving as the unknown constant pressure rate solution in Eq. A.19. The pressure drop normalized form of the exponential decline is provided below:

$$q_{cp}(t) \approx \frac{q(t)}{\Delta p(t)} = \left(\frac{q}{\Delta p}\right)_i \exp\left[-D_i t\right] \quad \text{.....(A.20)}$$

Finally, combining Eq. A.19 and Eq. A.20 the superposition form of the exponential decline is obtained:

$$q(t)=\left(\frac{q}{\Delta p}\right)_i \sum_{k=1}^{u}(\Delta p_{wf,k}-\Delta p_{wf,k-1})\exp\left[-D_i(t_u-t_{k-1})\right] \quad \text{.....(A.21)}$$

As before, the characteristic behaviors of $D(t)$ and $b(t)$ are desired. The definition of the loss-ratio in Eq. A.1 assumes that production is against a constant bottomhole flowing pressure. When variable pressure drop conditions prevail, pressure drop normalized rates should be differentiated as opposed to rates. Performing this modification yields:

$$\frac{1}{D(t)}=-\frac{q(t)/\Delta p(t)}{d(q(t)/\Delta p(t))/dt} \quad \text{.....(A.22)}$$

Substituting Eq. A.20 into Eq. A.22:

$$D(t)=-\frac{1}{(q/\Delta p)_i\exp\left[-D_i t\right]}\frac{d}{dt}\left\{(q/\Delta p)_i\exp\left[-D_i t\right]\right\} \quad \text{.....(A.23)}$$

Evaluating the derivative term:

$$D(t)=\frac{D_i(q/\Delta p)_i\exp\left[-D_i t\right]}{(q/\Delta p)_i\exp\left[-D_i t\right]} \quad \text{.....(A.24)}$$

Finally, cancelling like terms yields:

$$D(t)=D_i \quad \text{.....(A.16)}$$

Similarly modifying Eq. A.2 for pressure drop normalized rates yields the following form of the loss-ratio derivative:

$$b(t)=\frac{d}{dt}\left[\frac{1}{D(t)}\right]=-\frac{d}{dt}\left[\frac{q(t)/\Delta p(t)}{d(q(t)/\Delta p(t))/dt}\right] \quad \text{.....(A.25)}$$

Combining Eqs. A.16 and A.25 yields

$$b(t)=\frac{d}{dt}\left[\frac{1}{D_i}\right] \quad \text{.....(A.17)}$$

Finally, the $b(t)$ expression is defined as follows:

$$b(t)=0 \quad \text{.....(A.18)}$$

It is important to note that the derivative terms arrived at using the pressure drop normalized rate form and the time-rate form are identical. This is a result of the assumption that pressure drop normalization of rate data adequately transforms the variable pressure signature of the well to the equivalent constant pressure signature. This has important implications from a diagnostic standpoint and allows the derivative trends to guide calibration regardless of whether time-rate or time-rate-pressure decline methods are utilized.

A.2 Derivation of Arps' Hyperbolic Decline Relation

Arps observed that the loss-ratio (*i.e.* $D(t)$) was not always constant. To investigate, he differentiated the loss-ratio again using a simple finite difference calculation where he observed near constant loss-ratio derivative trends similar to that seen in **Fig. A.2**. This observation forms the empirical foundation of Arps' hyperbolic decline.

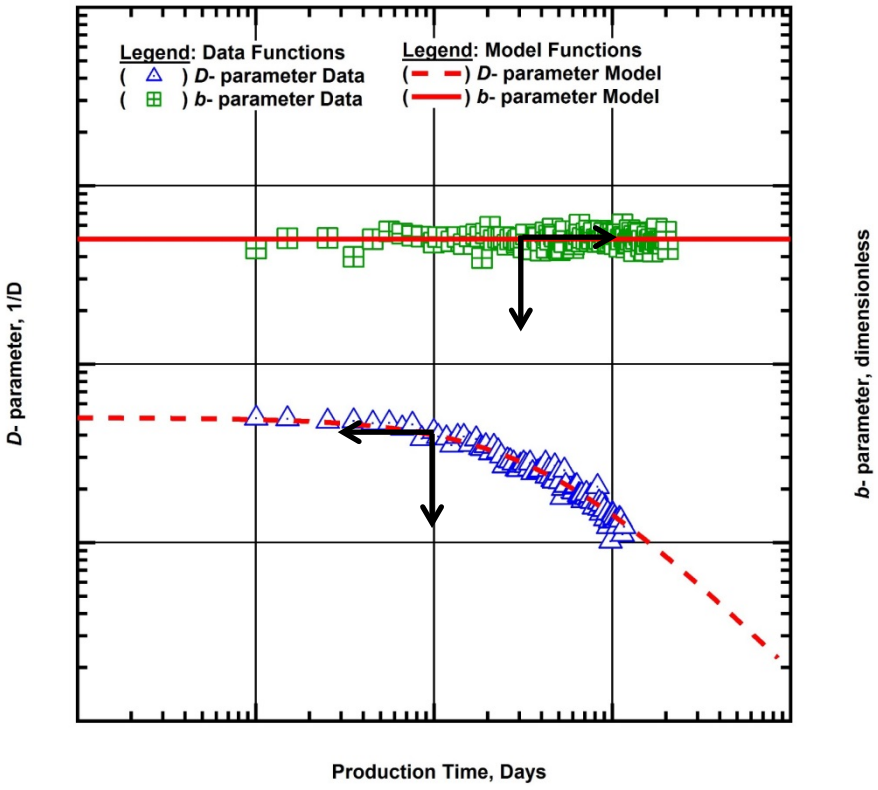

Figure A.2 — Schematic of the Constant Behavior of the Loss-Ratio Derivative Characterizing Arps' Hyperbolic Decline.

In order to obtain a mathematical definition of the hyperbolic decline we begin with the definition of the loss-ratio derivative:

$$b(t) = -\frac{d}{dt}\left[\frac{q(t)}{dq(t)/dt}\right] \quad \text{.....(A.2)}$$

Dropping the function of time notation and assuming a constant $b(t)$ as shown in **Fig. A.2**:

$$\frac{d}{dt}\left[\frac{q}{dq/dt}\right] = -b \quad \text{.....(A.26)}$$

Separating variable and taking the indefinite integral of both sides:

$$\int d\left[\frac{q}{dq/dt}\right] = -b\int dt \quad \text{.....(A.27)}$$

Evaluating the integral on the LHS and RHS we arrive at the following:

$$\frac{q}{dq/dt} = -bt - C \quad \text{.....(A.28)}$$

where C is a constant of integration. Recalling our definition of the loss ratio provided by Eq. A.1 and substituting into Eq. A.28 yields:

$$\frac{1}{D} = bt + C \quad \text{.....(A.29)}$$

Assuming a boundary condition where $D(t=0) = D_i$ and solving Eq. A.29 for the constant of integration:

$$\frac{1}{D_i} = C \quad \text{.....(A.30)}$$

Substituting Eq. A.30 into Eq. A.29:

$$\frac{q}{dq/dt} = -bt - \frac{1}{D_i} \quad \text{.....(A.31)}$$

Rearranging yields:

$$\frac{1}{q}\frac{dq}{dt} = -\frac{D_i}{1+bD_it} \quad \text{.....(A.32)}$$

If we again separate variables we obtain:

$$\frac{dq}{q} = -\frac{D_i}{1+bD_it}dt \quad \text{.....(A.33)}$$

Taking the definite integral of both sides gives:

$$\int_{q_i}^{q(t)} \frac{dq}{q} = -D_i \int_0^t \frac{1}{1+bD_it}dt \quad \text{.....(A.34)}$$

In order to complete the integration on the RHS we introduce the following variable of integration:

$$z = 1+bD_it \quad \text{.....(A.35)}$$

where z is a variable of substitution. Additionally, we calculate the derivative of the variable of substitution as follows:

$$\frac{dz}{dt} = bD_i \quad \text{.....(A.36)}$$

Rearranging yields:

$$dt = \frac{1}{bD_i}dz \quad \text{.....(A.37)}$$

In order to correctly integrate using the variable of substitution we need to transform the limits of integration as follows:

$$z(t=0) = 1 \quad \text{.....(A.38)}$$

$$z(t=t) = 1+bD_it \quad \text{.....(A.39)}$$

Substituting Eqs. A.35, A.37, A.38, and A.39 into Eq. A.34 we obtain the following expression:

$$\int_{q_i}^{q(t)} \frac{dq}{q} = -D_i \int_1^{1+bD_it} \left[\frac{1}{z}\right]\left[\frac{1}{bD_i}\right]dz \quad \text{.....(A.40)}$$

Removing the constant terms from the integral and cancelling we obtain:

$$\int_{q_i}^{q(t)} \frac{dq}{q} = -\frac{1}{b}\int_{1}^{1+bD_i t} \frac{dz}{z} \quad \text{.....(A.41)}$$

In order to complete the integral terms we again recall the definition of a natural logarithm:

$$\ln[x] = \int_{1}^{x} \frac{dx}{x} \quad \text{.....(A.7)}$$

Completing the integration yields the following:

$$\ln[q]\Big|_{q_i}^{q(t)} = -\frac{1}{b}\ln[1+bD_i t] \quad \text{.....(A.42)}$$

Prior to substitution the limits of integration we recall the following properties of logarithms:

$$\ln[x] - \ln[y] = \ln\left[\frac{x}{y}\right] \quad \text{.....(A.10)}$$

$$y\ln[x] = \ln\left[x^y\right] \quad \text{.....(A.43)}$$

Using the identities in Eqs. A.10 and A.43, Eq. A.42 simplifies as follows:

$$\ln\left[\frac{q(t)}{q_i}\right] = \ln\left[\left(1+bD_i t\right)^{-\frac{1}{b}}\right] \quad \text{.....(A.44)}$$

Exponentiating both sides yields:

$$\frac{q(t)}{q_i} = \frac{1}{\left(1+bD_i t\right)^{1/b}} \quad \text{.....(A.45)}$$

Finally, rearranging Eq. A.45 yields the time-rate formulation of Arps' hyperbolic relation.

$$q(t) = \frac{q_i}{\left(1+bD_i t\right)^{1/b}} \quad \text{.....(A.46)}$$

The forms of $D(t)$ and $b(t)$ are again desired in order to aid in model calibration. In order to calculate $D(t)$ we begin with the equation of the loss-ratio provided below:

$$\frac{1}{D(t)} = -\frac{q(t)}{dq(t)/dt} \quad \text{.....(A.1)}$$

Rearranging and substituting Eq. A.46 into Eq. A.1:

$$D(t) = -\frac{(1+bD_i t)^{1/b}}{q_i}\frac{d}{dt}\left\{\frac{q_i}{(1+bD_i t)^{1/b}}\right\} \quad \text{.....(A.47)}$$

Again recalling our variable of substitution and its derivative:

$$z = 1 + bD_i t \quad \text{.....(A.35)}$$

$$\frac{dz}{dt} = bD_i \quad \text{.....(A.36)}$$

For the moment we substitute Eq. A.35 into Eq. A.47:

$$D(t) = -z^{\frac{1}{b}}\frac{d}{dt}\left\{z^{-\frac{1}{b}}\right\} \quad \text{.....(A.48)}$$

In order to carry out the derivation we utilize the chain rule defined as:

$$\frac{dq}{dt} = \frac{dq}{dz}\frac{dz}{dt} \quad \text{.....(A.49)}$$

Applying the chain rule to the RHS of Eq. A.48:

$$D(t) = -z^{\frac{1}{b}}\frac{d\left\{z^{-\frac{1}{b}}\right\}}{dz}\frac{dz}{dt} \quad \text{.....(A.50)}$$

Substituting the derivative of the variable of substitution shown in Eq. A.36 yields:

$$D(t) = -bD_i z^{\frac{1}{b}}\frac{d\left\{z^{-\frac{1}{b}}\right\}}{dz} \quad \text{.....(A.51)}$$

Evaluating the derivative term:

$$D(t) = \frac{bD_i}{b} z^{\frac{1}{b}} z^{-\frac{1}{b}-1} \quad \text{.....(A.52)}$$

In order to proceed we define the following identity:

$$z^x z^y = z^{x+y} \quad \text{.....(A.53)}$$

Utilizing the above identity we obtain:

$$D(t) = D_i z^{\frac{1}{b}} z^{-\frac{1}{b}} z^{-1} \quad \text{.....(A.54)}$$

Rearranging and substituting the z variable defined in Eq. A.35:

$$D(t) = \frac{D_i (1+bD_i t)^{\frac{1}{b}}}{(1+bD_i t)^{\frac{1}{b}} (1+bD_i t)} \quad \text{.....(A.55)}$$

Finally, cancelling like terms yields the decline parameter as a function of a time relation for Arps' hyperbolic relation.

$$D(t) = \frac{D_i}{(1+bD_i t)} \quad \text{.....(A.56)}$$

The definition of the loss-ratio derivative is the basis for the $b(t)$ relation:

$$b(t) = \frac{d}{dt}\left[\frac{1}{D(t)}\right] \quad \text{.....(A.2)}$$

Combining Eq. A.56 and Eq. A.2 we arrive at:

$$b(t) = \frac{d}{dt}\left[\frac{1+bD_i t}{D_i}\right] \quad \text{.....(A.57)}$$

Rearranging the derivative term:

$$b(t) = \frac{d}{dt}\left[\frac{1}{D_i}\right] + \frac{d}{dt}\left[\frac{bD_i t}{D_i}\right] \quad \text{.....(A.58)}$$

Evaluating the derivatives on the RHS yields the expected constant $b(t)$ relation forming the foundation of the hyperbolic relation.

$$b(t) = b \quad \text{.....(A.59)}$$

In order to develop a time-rate-pressure form of Arps' hyperbolic decline we again begin with the discrete form of the convolution integral as follows:

$$q(t) = \sum_{k=1}^{u} (\Delta p_{wf,k} - \Delta p_{wf,k-1})(q_{cp}(t_u - t_{k-1})) \quad \text{.....(A.19)}$$

The assumption for the development of the variable pressure decline curve analysis form is that pressure drop normalization of rates provides a proxy for the constant pressure decline behavior of a well. Accordingly, pressure drop normalization of the hyperbolic decline, provided below, is assumed to be an adequate equivalent constant pressure decline model for substitution into Eq. A.19.

$$q_{cp}(t) \approx \frac{q(t)}{\Delta p_{wf}(t)} = \left(\frac{q}{\Delta p}\right)_i \frac{1}{(1+bD_i t)^{1/b}} \quad \text{.....(A.60)}$$

Substituting Eq. A.60 into Eq. A.19 yields the variable pressure decline relation presented in this work.

$$q(t) = \left(\frac{q}{\Delta p}\right)_i \sum_{k=1}^{u} (\Delta p_{wf,k} - \Delta p_{wf,k-1}) \frac{1}{(1+bD_i(t_u - t_{k-1}))^{1/b}} \quad \text{.....(A.61)}$$

In the interest of space the mechanics of the $D(t)$ and $b(t)$ differentiation will not be shown for the variable pressure decline relation. As shown for the exponential decline it works out that the derivative behavior is identical to that of the time-rate form of the hyperbolic relation provided by Eq. A.56 and Eq. A.59.

A final point of practical importance is the unbounded nature of the hyperbolic equation when the b parameter is greater than unity. It is well documented that production from low-permeability formations tends to exhibit decline trends indicative of higher b values thus opening up the risk of overestimating the ultimate recover from these reservoirs. Numerous alternative time-rate models (presented in the following appendices) have been developed to address this challenge; however, the most common approach is the so called modified hyperbolic introduced by Robertson (1988). The modified hyperbolic is a practice based approach in which the exponential decline is spliced as a tail after an initial hyperbolic segment at a specified switch time. The piecewise time-rate and pressure drop normalized rate expressions are provide below.

$$q(t)=\begin{Bmatrix}\dfrac{q_i}{(1+bD_it)^{1/b}} & (t<t^*)\\ q_i\exp[-D_it] & (t>t^*)\end{Bmatrix} \quad \text{.....(A.62)}$$

$$q(t)=\begin{Bmatrix}\left(\dfrac{q}{\Delta p}\right)_i\sum_{k=1}^{u}(\Delta p_{wf,k}-\Delta p_{wf,k-1})\dfrac{1}{(1+bD_i(t_u-t_{k-1}))^{1/b}} & (t<t^*)\\ \left(\dfrac{q}{\Delta p}\right)_i\sum_{k=1}^{u}(\Delta p_{wf,k}-\Delta p_{wf,k-1})\exp\left[-D_i(t_u-t_{k-1})\right] & (t>t^*)\end{Bmatrix} \quad \text{.....(A.63)}$$

The modified hyperbolic decline is a useful practical tool to avoid overestimating reserves in low-permeability formations; however, the timing and magnitude of the exponential tail is generally an ambiguous decision. As a result of this reality, the modified hyperbolic has the potential for both under and overestimates if particular care is not taken in its application.

A.3 Hyperbolic Type Plots and Application Example

The aim of this section is to provide a cartoon schematic showing the diagnostic behavior of Arps' hyperbolic decline and to demonstrate a simple application example using a variety of plots to aid in model calibration. The first objective is addressed in this appendix, as well as the remaining time-rate model appendices, by using a type plot of the "qDb" behavior. This plot for Arps' hyperbolic and modified hyperbolic models is provided below as **Fig. A.3**.

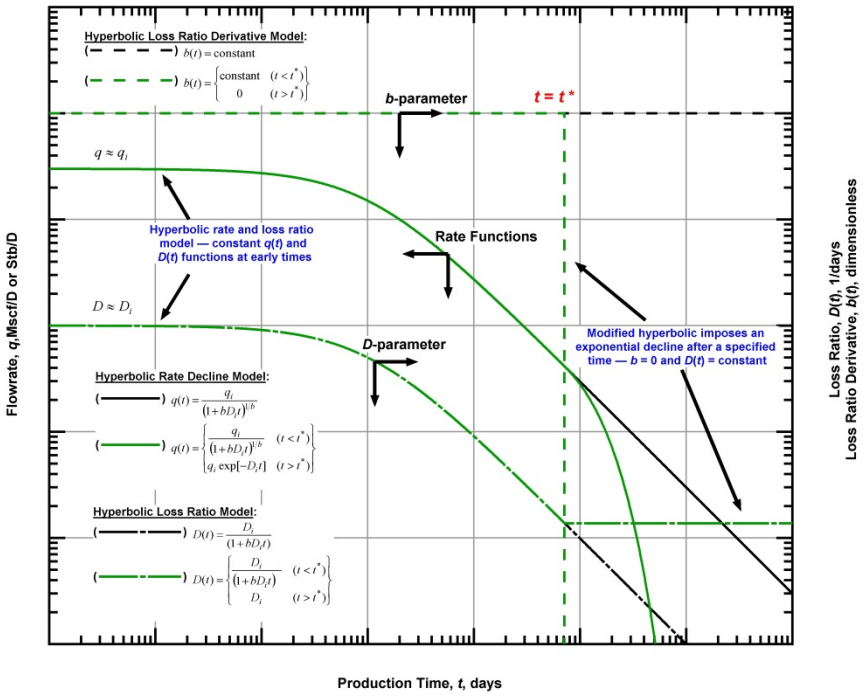

Figure A.3 — Schematic Type Plot of "qDb" Model Behavior for Arps' Hyperbolic and Modified Hyperbolic Decline

The model parameters governing the shape of Arps' decline models need to be calibrated in order to generate a forecast of future production performance. Unfortunately non-uniqueness in match calibration is an unfortunately reality for all production analysis techniques and decline curve analysis is no exception. In order to mitigate this issue, it is recommended that a suite of diagnostic plots is used as opposed to solely rate versus time analysis. These additional plots provide further match confirmation and help to ensure that the calibrated model honors well performance characteristics such as prevailing flow regime(s). Included below in **Fig. A.4** is an example of such an approach applied to a field production scenario where the hyperbolic model is calibrated across a suite of plots. The corresponding rate-time and rate-cumulative matches are shown in **Fig. A.5** and **A.6**.

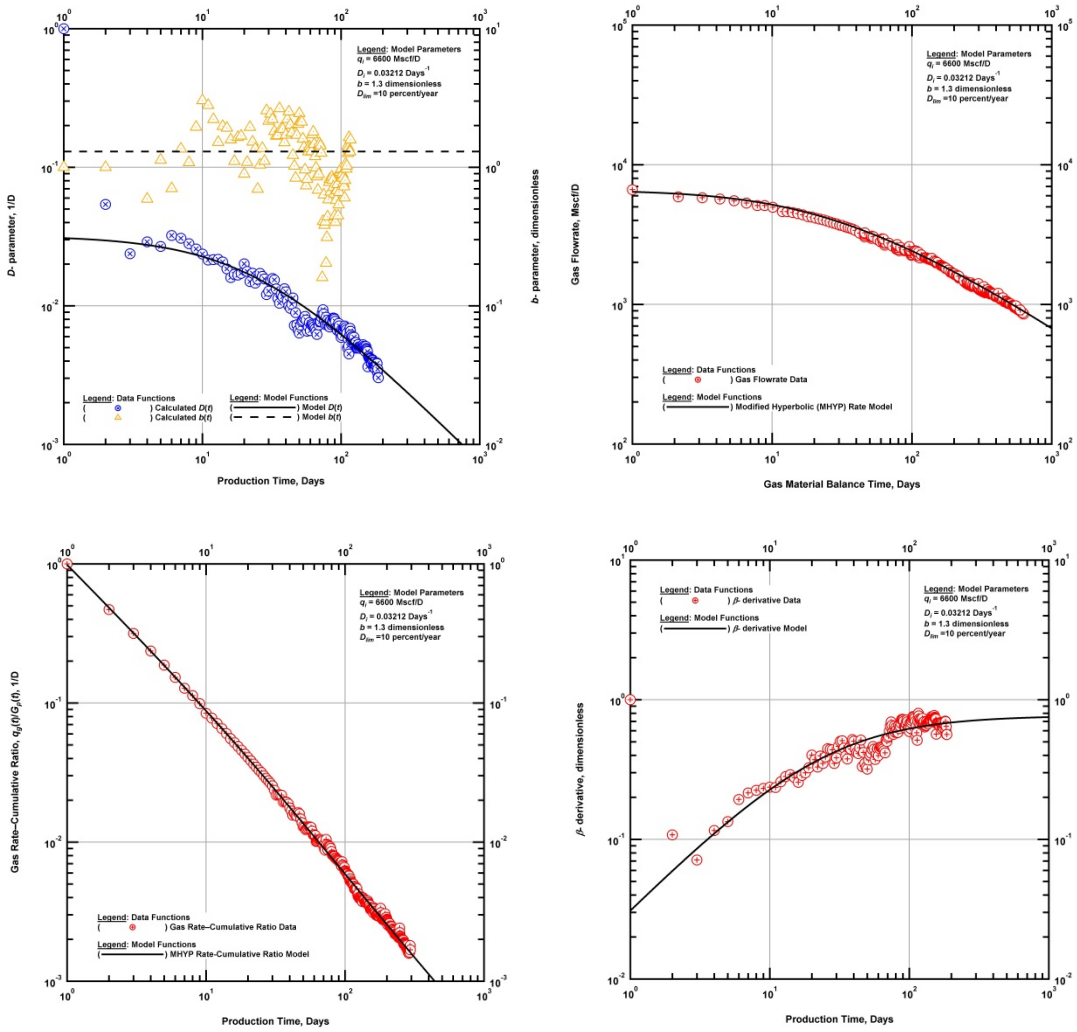

Figure A.4 — Diagnostic Suite Demonstrating Hyperbolic Time-Rate Model Calibration Methodology

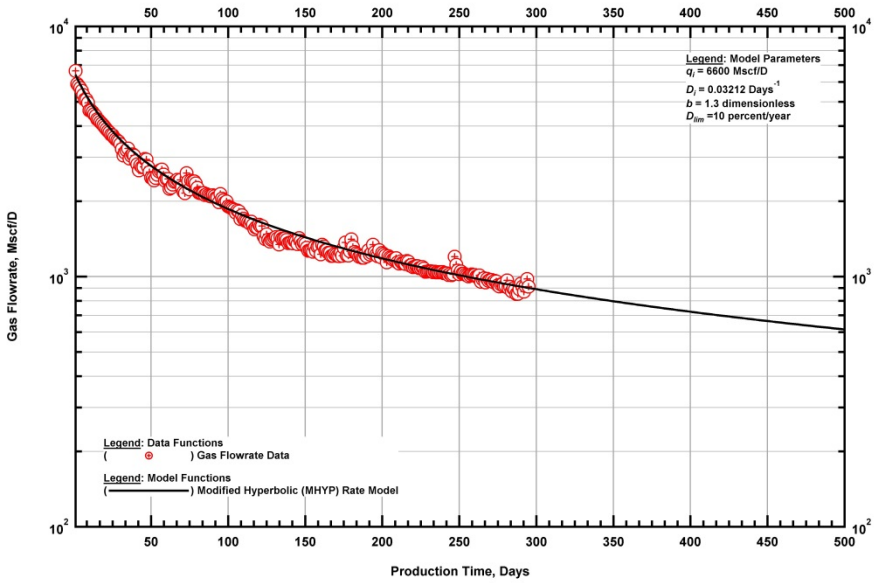

Figure A.5 — Calibrated Modified Hyperbolic Rate Versus Production Time Match

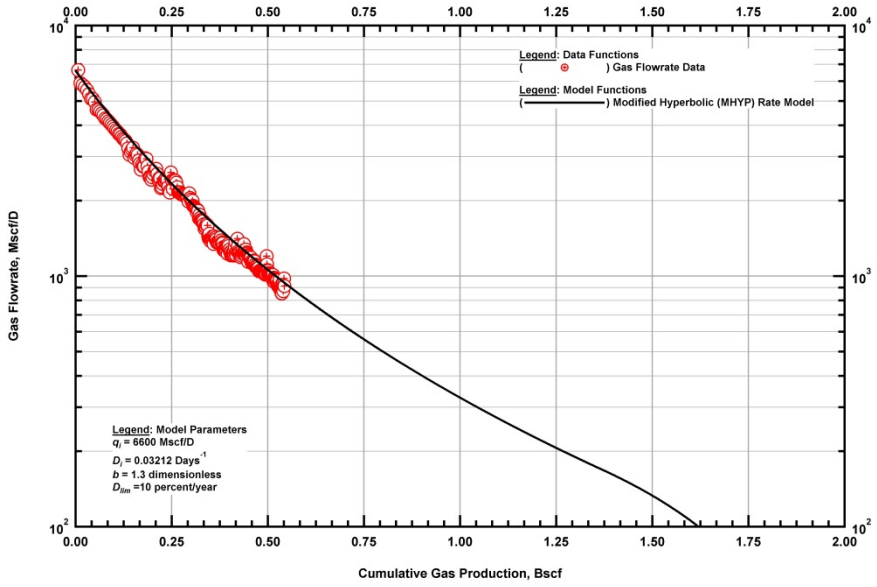

Figure A.6 — Calibrated Modified Hyperbolic Rate Versus Cumulative Gas Production Match

APPENDIX B

POWER-LAW EXPONENTIAL DECLINE CURVE RELATION

This section aims to fully derive the power-law exponential relation introduced by Ilk *et al*. (2008). A schematic "qDb plot" and a brief time-rate application example is included demonstrating the rate and derivative behavior of the model. As with the Arps' (1945) relations, the derivation of the power-law exponential model was based on a base relationship established as a result of observations of the loss-ratio trend on logarithmic coordinates. The mathematical definitions of the loss-ratio and loss-ratio derivative, introduced by Johnson and Bollens (1927), are included below.

$$\frac{1}{D(t)} = -\frac{q(t)}{dq(t)/dt} \quad \text{.....(B.1)}$$

$$b(t) = \frac{d}{dt}\left[\frac{1}{D(t)}\right] = -\frac{d}{dt}\left[\frac{q(t)}{dq(t)/dt}\right] \quad \text{.....(B.2)}$$

where q is flowrate in volume per unit time t, $D(t)$ is the decline rate as a function of time expressed as a percentage decline per unit time, and $b(t)$ is the dimensionless loss ratio derivative as a function of time.

It is important to note that this relationship was derived as a result of a study analyzing the merits and limitations of using Arps' hyperbolic relationship for fractured low-permeability tight gas wells. The model utilizes a best-fit power-law trend of the loss-ratio as a function of time, $D(t)$, which decays to a constant behavior, or exponential decline at late times using a limiting term (*i.e.* D_∞). The model was derived with the goal of creating a "unifying" model relying upon diagnostic relationships for model calibration and providing enough flexibility to model transient, transitional, and boundary dominated flow. From a physical standpoint, the model must be considered entirely empirical at this point in time.

B.1 Derivation of the Power-Law Exponential Decline Relation

Ilk *et al*. (2008) provided a mathematical derivation of the power-law exponential decline based on observations of the loss ratio data defined as Eq. B.1. There basis function differed from that of the exponential or hyperbolic decline in that they defined a decaying power-law function with a constant behavior at relatively late times. The authors introduced the so called "qDb" plot, which is extensively utilized in this work, to simultaneously depict the rate, loss-ratio, and loss-ratio derivative trends and guide model calibration. The basis function from which they began their derivation is provided below.

$$D(t) = D_\infty + D_1 t^{-(1-n)} \quad \text{.....(B.3)}$$

where D_1 is the decline constant at time unit 1, n is the time exponent, t is time, and D_∞ is the limiting decline at infinite time. Rearranging Eq. B.1, we obtain a mathematical relationship describing $D(t)$ as:

$$D(t) = -\frac{1}{q(t)}\frac{dq(t)}{dt} \quad \text{.....(B.4)}$$

Combining Eq. B.4 with the basis function for $D(t)$ provided by Eq. B.3, we arrive at the expression below:

$$\frac{1}{q}\frac{dq}{dt} = -D_\infty - D_1 t^{-(1-n)} \quad \text{.....(B.5)}$$

For simplicity in derivation the (t) notation was dropped. Separating the variables in Eq. B.5 we obtain:

$$\frac{dq}{q} = \left[-D_\infty - D_1 t^{-(1-n)}\right]dt \quad \text{.....(B.6)}$$

Integrating both sides of Eq. B.6 as follows:

$$\int_{\hat{q}_i}^{q(t)} \frac{dq}{q} = -D_\infty \int_0^t dt - D_1 \int_0^t t^{-(1-n)} dt \quad \text{.....(B.7)}$$

where $\hat{q}_i$ refers to the initial rate intercept at time zero and has a different interpretation than q_i used in Arps' models. In order to complete the integral on the left hand side (LHS) of Eq. B.7 the definition of a natural logarithm is recalled:

$$\ln[x] = \int_1^x \frac{dx}{x} \quad \text{.....(B.8)}$$

where x serves as a generic placeholder variable. Utilizing the definition in Eq. B.8 the integration is completed as follows:

$$\ln[q]\Big|_{\hat{q}_i}^{q(t)} = -D_\infty t\Big|_0^t - \frac{D_1}{n} t^n\Big|_0^t \quad \text{.....(B.9)}$$

Substitution of the limits of integration yields:

$$\ln[q(t)] - \ln[\hat{q}_i] = -D_\infty (t-0) - \frac{D_1}{n}(t^n - 0^n) \quad \text{(B.10)}$$

We again recall a logarithmic identity before proceeding in our derivation:

$$\ln[x] - \ln[y] = \ln\left[\frac{x}{y}\right] \quad \text{(B.11)}$$

where y serves as an additional generic placeholder variable. Using Eq. B.11, the LHS of Eq. B.10 simplifies to arrive at the following form:

$$\ln\left[\frac{q(t)}{\hat{q}_i}\right] = -D_\infty t - \frac{D_1}{n} t^n \quad \text{(B.12)}$$

Exponentiation both sides of Eq. B.12 yields:

$$\frac{q(t)}{\hat{q}_i} = \exp\left[-D_\infty t - \frac{D_1}{n} t^n\right] \quad \text{(B.13)}$$

The final time-rate form of power law exponential decline utilizes a single variable, $\hat{D}_i$, in place term representing the division of D_1 and n. This variable has a different interpretation from D_i used in the Arps' models and is defined as follows:

$$\hat{D}_i = \frac{D_1}{n} \quad \text{(B.14)}$$

Combining Eqs. B.13 and B.14 we arrive at the final rate versus time formulation for the power-law exponential decline model.

$$q(t) = \hat{q}_i \exp\left[-\hat{D}_i t^n - D_\infty t\right] \quad \text{(B.15)}$$

The authors proposed the use of the reciprocal of the loss-ratio, $D(t)$, and loss-ratio derivative, $b(t)$, data trends to calibrate the model parameters for forecasting production. We have $D(t)$, namely the basis function, and we have derived the rate versus time model, $q(t)$, but we still need to determine the loss-ratio derivative behavior. In order to determine the $b(t)$ behavior we recall Eq. B.2 which is the definition of the loss-ratio derivative.

$$b(t) = \frac{d}{dt}\left[\frac{1}{D(t)}\right] \quad \text{(B.2)}$$

Combining Eq. B.2 and substituting Eq. B.3 for the $D(t)$ term we obtain:

$$b(t) = \frac{d}{dt}\left[\frac{1}{D_\infty + \hat{D}_i n t^{n-1}}\right] \quad \text{(B.16)}$$

where the $\hat{D}_i$ term is used and the equation is rearranged for simplicity. To complete the derivation, we now define a substitution variable, *x*, as follows:

$$x = D_\infty + \hat{D}_i n t^{n-1} \quad \text{(B.17)}$$

Combining Eqs. B.16 and B.17, we obtain:

$$b(t) = \frac{d}{dt}\left[\frac{1}{x}\right] \quad \text{(B.18)}$$

In order to carry out the derivation we utilize the chain rule defined as:

$$\frac{dD}{dt} = \frac{dD}{dx}\frac{dx}{dt} \quad \text{(B.19)}$$

Applying the chain rule to the RHS of Eq. B.19:

$$b(t) = \frac{d}{dx}\left[\frac{1}{x}\right]\frac{dx}{dt} \quad \text{(B.20)}$$

Recalling our variable of substitution from Eq. B-17 and taking the derivative we obtain:

$$\frac{dx}{dt} = (n-1)\hat{D}_i t^{n-2} \quad \text{(B.21)}$$

Completing the derivative in Eq. B.20 and substituting for our dummy variable, *x*, we arrive at the following expression:

$$b(t) = -\frac{(n-1)nt^{n-2}\hat{D}_i}{\left(D_\infty t + \hat{D}_i n t^{n-1}\right)^2} \quad \text{(B.22)}$$

In an effort to simplify the expression, we expand the numerator and denominator terms:

$$b(t) = -\frac{n^2 t^{n-2}\hat{D}_i - nt^{n-2}\hat{D}_i}{n^2 t^{2n-2}\hat{D}_i^2 + 2nt^{n-1}\hat{D}_i D_\infty + D_\infty^2} \quad \text{.....(B.23)}$$

In order to simplify we recall the following property of exponents:

$$z^{a+b} = z^a z^b \quad \text{.....(B.24)}$$

where *z*, *a*, and *b* are all placeholder variables. Using this identity, we can simplify Eq. B.23 to the following:

$$b(t) = -\frac{n^2 \frac{t^n}{t^2}\hat{D}_i - n\frac{t^n}{t^2}\hat{D}_i}{n^2 \frac{t^{2n}}{t^2}\hat{D}_i^2 + 2n\frac{t^n}{t^1}\hat{D}_i D_\infty + D_\infty^2} \quad \text{.....(B.25)}$$

Multiplying both the numerator and denominator by $1/t^2$ yields the following:

$$b(t) = -\frac{\frac{n^2 t^n \hat{D}_i - nt^n \hat{D}_i}{t^4}}{n^2 \frac{t^{2n}}{t^4}\hat{D}_i^2 + 2n\frac{t^n}{t^3}\hat{D}_i D_\infty + \frac{D_\infty^2}{t^2}} \quad \text{.....(B.26)}$$

Simplifying the denominator of the above expression:

$$b(t) = -\frac{\frac{n^2 t^n \hat{D}_i - nt^n \hat{D}_i}{t^4}}{\frac{n^2 t^{2n}\hat{D}_i^2 + 2nt^{n+1}\hat{D}_i D_\infty + t^2 D_\infty^2}{t^4}} \quad \text{.....(B.27)}$$

Cancelling like terms, simplifying the polynomial expressions, and distributing the negative to the numerator provides the fully simplified $b(t)$ expression for the power-law exponential model.

$$b(t) = \frac{\hat{D}_i (1-n) n t^n}{\left(D_\infty t + \hat{D}_i n t^n\right)^2} \quad \text{.....(B.27)}$$

All of the equations up until this point in the derivation are concerned with the modeling of time-rate data based on the assumption of a constant bottomhole flowing pressure. In keeping with the aim of this work,

namely incorporating pressure data into decline curve analysis, the variable pressure form of the power-law exponential decline is provided below.

The discrete form of the convolution integral is used to account for variations in bottomhole flowing pressure as a function of time. A complete development of the superposition equation is included in Appendix F. The final mathematical form is provided below:

$$q(t)=\sum_{k=1}^{u}(\Delta p_{wf,k}-\Delta p_{wf,k-1})(q_{cp}(t_u-t_{k-1})) \quad \text{.....(B.28)}$$

where Δp_{wf} is the bottomhole pressure drop in units of pressure at a specific point in time and q_{cp} denotes a constant pressure rate solution. This work makes the assumption that the constant pressure rate signature of a well is accurately represented by the pressure drop normalized rate behavior of that well. If this assumption holds, it is proposed that this data trend can be modeled using a pressure drop normalized form of an empirical time-rate decline relation serving as the unknown constant pressure rate solution in Eq. B.28. The pressure drop normalized form of the power-law exponential decline is provided below:

$$q_{cp}(t)\approx\frac{q(t)}{\Delta p(t)}=\left(\frac{\hat{q}_i}{\Delta p}\right)_i\exp\left[-\hat{D}_i t^n-D_\infty t\right] \quad \text{.....(B.29)}$$

Finally, combining Eq. B.28 and Eq. B.29 the superposition form of the power- law exponential decline is obtained:

$$q(t)=\left(\frac{\hat{q}}{\Delta p}\right)_i\sum_{k=1}^{u}(\Delta p_{wf,k}-\Delta p_{wf,k-1})\exp\left[-\hat{D}_i(t_u-t_{k-1})^n-D_\infty(t_u-t_{k-1})\right] \quad \text{.....(B.30)}$$

When calibrating the model parameters for the superposition expression shown in Eq. B.30, we desire the behavior of $D(t)$ and $b(t)$ much as we did for the simple rate versus time expression. These will be calculated using the following modified expressions for the loss-ratio and loss-ratio derivative.

$$\frac{1}{D(t)}=-\frac{q(t)/\Delta p(t)}{d(q(t)/\Delta p(t))/dt} \quad \text{.....(B.31)}$$

$$b(t)=\frac{d}{dt}\left[\frac{1}{D(t)}\right]=-\frac{d}{dt}\left[\frac{q(t)/\Delta p(t)}{d(q(t)/\Delta p(t))/dt}\right] \quad \text{.....(A.32)}$$

Recalling our expressions for $D(t)$ and $b(t)$ provided by B.3 and B.27 we note that they are independent of the initial rate term. As a result, the derivative terms arrived at using the pressure drop normalized rate

form and the time-rate form are identical. This is a result of the assumption that pressure drop normalization of rate data adequately transforms the variable pressure signature of the well to the equivalent constant pressure signature. This has important implications from a diagnostic standpoint and allows the derivative trends to guide calibration regardless of whether time-rate or time-rate-pressure decline methods are utilized provided the constant pressure rate approximation assumption is adequate.

B.2 Power-Law Exponential Type Plots and Application Example

The aim of this section is to provide a cartoon schematic showing the diagnostic behavior of the power-law exponential decline and to demonstrate a simple application example using a variety of plots to aid in model calibration. The first objective is addressed in this appendix by using a type plot of the "qDb" behavior for the power-law exponential model provided below as **Fig. B.1**.

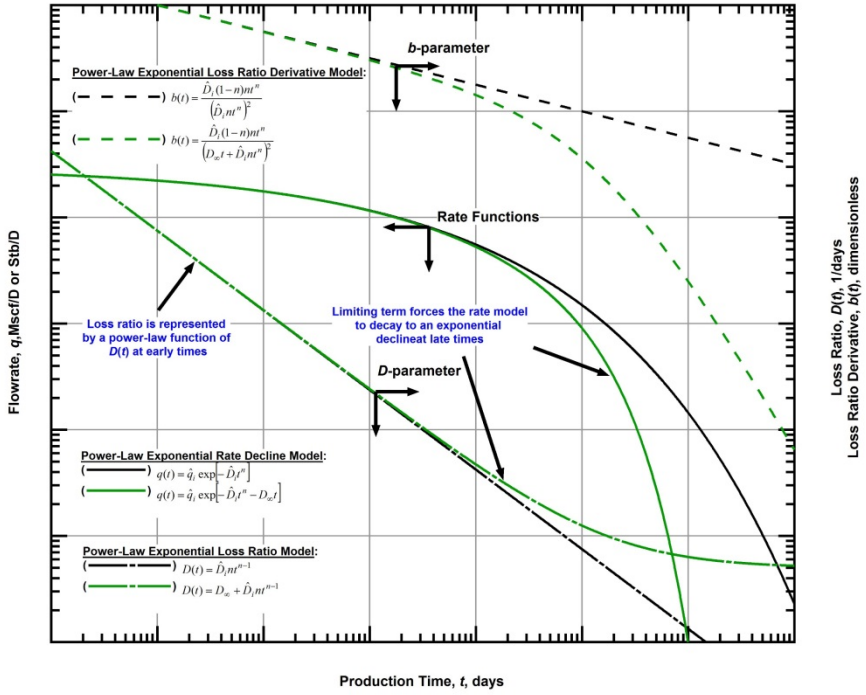

Figure B.1 — Schematic Type Plot of "qDb" Model Behavior for the Power-Law Exponential Decline

The model parameters governing the shape of power-law exponential decline model need to be calibrated in order to generate a forecast of future production performance. Unfortunately, non-uniqueness in match calibration is an unescapable reality for all production analysis techniques and decline curve analysis is no exception. In order to mitigate this issue, it is recommended that a suite of diagnostic plots is used as opposed to solely rate versus time analysis. These additional plots provide further match confirmation and help to ensure that the calibrated model honors well performance characteristics such as prevailing flow regime(s). Included below in **Fig. B.2** is an example of such an approach applied to a field production scenario where the power-law exponential model is calibrated across a suite of plots. The corresponding rate-time and rate-cumulative matches are shown in **Fig. B.3** and **B.4**.

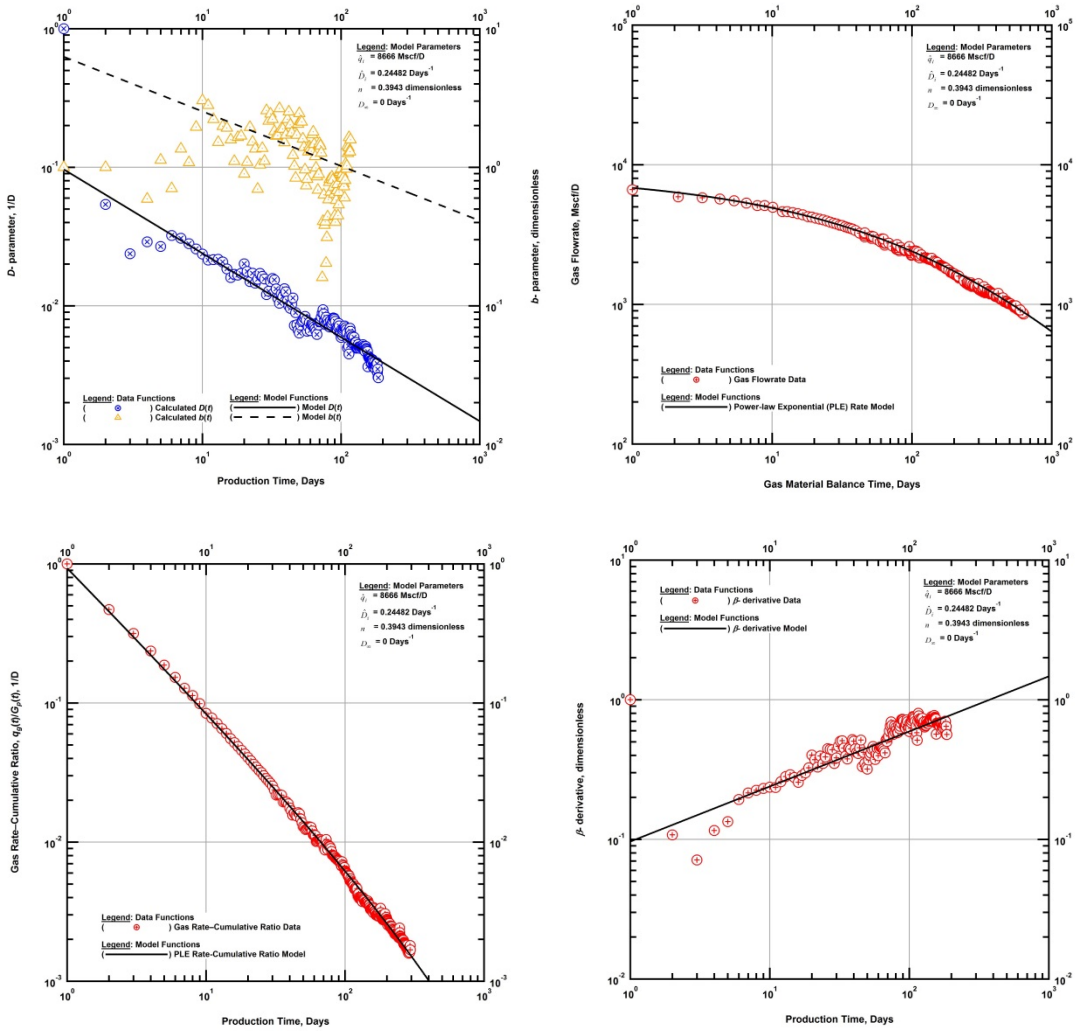

Figure B.2 — Diagnostic Suite Demonstrating Power-Law Exponential Model Calibration Methodology

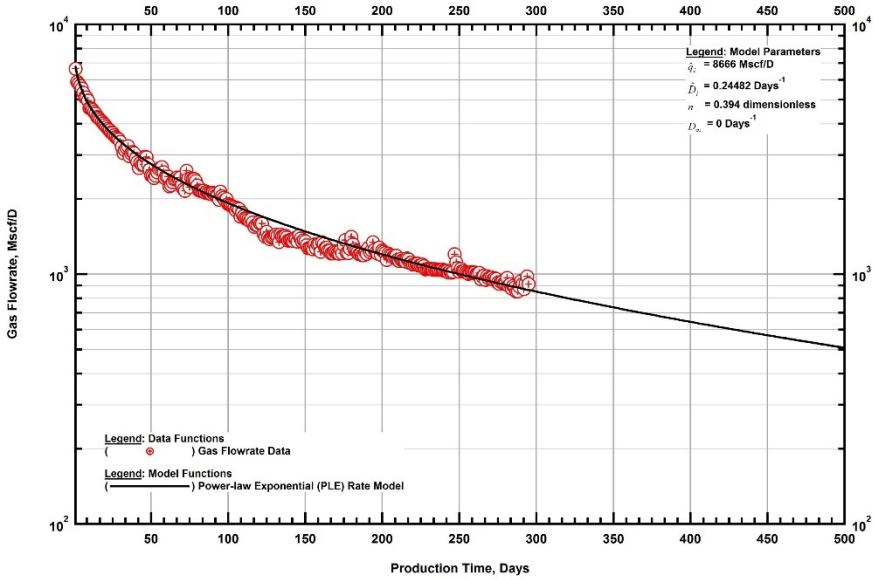

Figure B.3 — Calibrated Power-Law Exponential Rate Versus Production Time Match

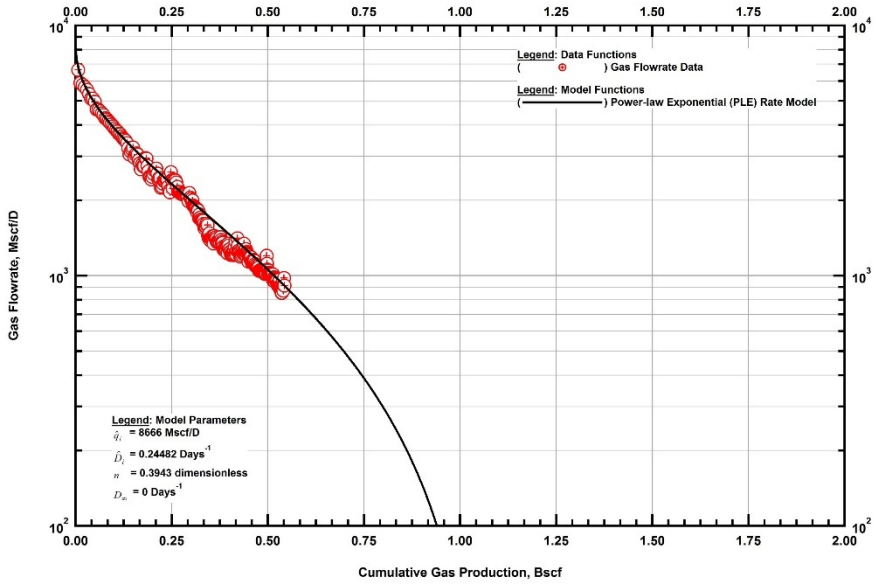

Figure B.4 — Calibrated Power-Law Exponential Rate Versus Cumulative Gas Production Match

APPENDIX C

STRETCHED EXPONENTIAL DECLINE CURVE RELATION

This section aims to fully derive the stretched exponential relation introduced by Valkó (2009). A schematic "qDb plot" and a brief time-rate application example is included demonstrating the rate and derivative behavior of the model. As with each of the decline relations presented in the appendices, the derivation of the stretched exponential model must be considered entirely empirical. In contrast to the Arps' decline relations and the power-law exponential, this model was introduced as a "statistical expression" to model data on a large scale across the Barnett shale gas formation. Additionally, its derivation was not based on empirical observations of the loss-ratio and loss-ratio derivative trends as the Arps' and power-law exponential relations were. While derived independently, this model is mathematically identical to the power-law exponential relation when the limiting term, D_∞, is set equal to zero.

Valkó's original introduction of this model proposed an application workflow for this model analogous to many type curve shifting routines in well test, production, and decline curve analysis. The primary pursuit of the workflow was a straight line on a dimensionless plot of recovery potential (defined in the paper as the one minus the recovery factor) versus dimensionless cumulative production. The model parameters were adjusted accordingly to achieve this goal. It is the opinion of the author that this model has found the most enduring usage for per well reserves forecasts across the industry, aside from the modified forms of Arps' models. It is important to note, however; that the original intent of the model was to analyze performance indicators at a much broader level (*i.e.* basin wide) than typical reserves studies performed on an individual well basis.

C.1 Derivation of the Stretched Exponential Decline Relation

Valkó (2009) provided the conceptual introduction of the stretched exponential decline relation including proposed applications and a summary of all of the relevant mathematical expressions. The defining expressions are all admittedly empirical, however; the new model was based on a non-autonomous differential equation which differed in theoretical form from the Arps' empirical expressions. It is noted that the defining differential equation has found application across various disciplines to describe decay processes analogous to production decline [Kohlrausch (1854) and Kisslinger (1993)]. The defining differential equation proposed by Valkó is provided as follows:

$$\frac{dq}{dt} = -n\left(\frac{t}{\tau}\right)^n \frac{q}{t} \quad \text{.....(C.1)}$$

where τ is a model parameter describing the "characteristic number of periods" and is analogous to the half-life concept, q is the flowrate, and n is the time exponent. We will first derive the rate versus time formulation for this expression by solving the differential equation. We begin by separating variables in Eq. C.1:

$$\frac{dq}{q} = -n\left(\frac{t}{\tau}\right)^n \frac{dt}{t} \quad \text{.....(C.2)}$$

Simplifying the right hand side (RHS) and integrating yields the following:

$$\int_{\hat{q}_i}^{q(t)} \frac{dq}{q} = -n\tau^{-n}\int_0^t t^{n-1}dt \quad \text{.....(C.3)}$$

In order to complete the integral on the left hand side (LHS) of Eq. C.3 the definition of a natural logarithm is recalled:

$$\ln[x] = \int_1^x \frac{dx}{x} \quad \text{.....(C.4)}$$

where x serves as a generic placeholder variable. Utilizing the definition in Eq. C.4 the integration of Eq. C.3 is completed as follows:

$$\ln[q]\Big|_{\hat{q}_i}^{q(t)} = -n\tau^{-n}\frac{t^n}{n}\Big|_0^t \quad \text{.....(C.5)}$$

Simplifying and substitution the limits of integration, we arrive at the following:

$$\ln[q(t)] - \ln[\hat{q}_i] = -\tau^{-n}t^n \quad \text{.....(C.6)}$$

We again recall a logarithmic identity before proceeding in our derivation:

$$\ln[x] - \ln[y] = \ln\left[\frac{x}{y}\right] \quad \text{.....(C.7)}$$

where y serves as an additional generic placeholder variable. Using Eq. C.7, the LHS of Eq. C.6 simplifies to arrive at the following form:

$$\ln\left[\frac{q(t)}{\hat{q}_i}\right] = -\left(\frac{t}{\tau}\right)^n \quad \text{.....(C.8)}$$

Exponentiation both sides of Eq. C.8 yields:

$$\frac{q(t)}{\hat{q}_i} = \exp\left[-\left(\frac{t}{\tau}\right)^n\right] \quad \text{.....(C.9)}$$

The final rate versus time form of the stretched exponential model can be expressed as follows:

$$q(t) = \hat{q}_i \exp\left[-\left(\frac{t}{\tau}\right)^n\right] \quad \text{.....(C.10)}$$

Valkó (2009) proposed an application methodology utilizing a plot of dimensionless cumulative production versus the recovery potential where the parameters are varied in order to achieve a straight line trend and project performance. Keeping with the application methodology advocated throughout the work we venture to derive the reciprocal of the loss-ratio, $D(t)$, and loss-ratio derivative, $b(t)$. These expressions will be used on a "qDb" plot to calibrate the model parameters and extrapolate future production.

In order to derive these expressions, we begin with the definition of the loss-ratio:

$$D(t) = -\frac{1}{q(t)}\frac{dq(t)}{dt} \quad \text{.....(C.11)}$$

We will first evaluate the derivative term on the RHS of Eq. C.11. Isolating the derivative term and substituting Eq. C.10 yields:

$$\frac{dq(t)}{dt} = \frac{d\left\{\hat{q}_i \exp\left[-\left(\frac{t}{\tau}\right)^n\right]\right\}}{dt} \quad \text{.....(C.12)}$$

Simplifying the derivative:

$$\frac{dq(t)}{dt} = \hat{q}_i \frac{d\left\{\exp\left[-\left(\frac{t}{\tau}\right)^n\right]\right\}}{dt} \quad \text{.....(C.13)}$$

To evaluate the derivative term, we must rely on the following identity for differentiation of exponential functions:

$$\frac{d\exp[x]}{dt} = \exp[x]\frac{dx}{dt} \quad \text{.....(C.14)}$$

where x is a dummy variable in this case. Observing Eq. C.13 we define x in the following manner:

$$x = -\left(\frac{t}{\tau}\right)^n \quad \text{.....(C.15)}$$

Simplifying and taking the derivative of Eq. C.15 we arrive at:

$$\frac{dx}{dt} = -\frac{nt^{n-1}}{\tau^n} \quad \text{.....(C.16)}$$

Utilizing the mathematical identity in Eq. C.14 and the derivative expression in Eq. C.16, we can express the Eq. C.13 as the following:

$$\frac{dq(t)}{dt} = -\hat{q}_i \exp\left[-\left(\frac{t}{\tau}\right)^n\right]\frac{nt^{n-1}}{\tau^n} \quad \text{.....(C.17)}$$

Having evaluated the derivative term on the RHS of Eq. C.11, we substitute the rate-time definition, $q(t)$, expressed by Eq. C.10.

$$D(t) = \frac{\hat{q}_i \exp\left[-\left(\frac{t}{\tau}\right)^n\right]}{\hat{q}_i \exp\left[-\left(\frac{t}{\tau}\right)^n\right]}\frac{nt^{n-1}}{\tau^n} \quad \text{.....(C.18)}$$

Cancelling like terms yields the final expression for the reciprocal of the loss-ratio, or $D(t)$:

$$D(t) = \frac{nt^{n-1}}{\tau^n} \quad \text{.....(C.19)}$$

Continuing the derivation, we now aim to solve for the derivative of the loss-ratio, or $b(t)$, trend. This is expressed mathematically as follows:

$$b(t) = \frac{d}{dt}\left[\frac{1}{D(t)}\right] \quad \text{(C.20)}$$

Substituting Eq. C.19 into Eq. C.20:

$$b(t) = \frac{d}{dt}\left[\frac{\tau^n}{nt^{n-1}}\right] \quad \text{(C.21)}$$

Rearranging the derivative term and removing constant terms:

$$b(t) = \frac{\tau^n}{n}\frac{d}{dt}\left[t^{1-n}\right] \quad \text{(C.22)}$$

Carrying out the differentiation yields and simplifying algebraically provides the following final expression for the derivative of the loss-ratio for the stretched exponential model:

$$b(t) = \frac{(1-n)\tau^n}{nt^n} \quad \text{(C.23)}$$

All of the equations up until this point in the derivation are concerned with the modeling of time-rate data based on the assumption of a constant bottomhole flowing pressure. In keeping with the aim of this work, namely incorporating pressure data into decline curve analysis, the variable pressure form of the stretched exponential decline is introduced below.

The discrete form of the convolution integral is used to account for variations in bottomhole flowing pressure as a function of time. A complete development of the superposition equation is included in Appendix F. The final mathematical form is provided below:

$$q(t) = \sum_{k=1}^{u} (\Delta p_{wf,k} - \Delta p_{wf,k-1})(q_{cp}(t_u - t_{k-1})) \quad \text{(C.24)}$$

where Δp_{wf} is the bottomhole pressure drop in units of pressure at a specific point in time and q_{cp} denotes a constant pressure rate solution. This work makes the assumption that the constant pressure rate signature of a well is accurately represented by the pressure drop normalized rate behavior of that well. If this assumption holds, it is proposed that this data trend can be modeled using a pressure drop normalized form of an empirical time-rate decline relation serving as the unknown constant pressure rate solution in Eq. C.24. The pressure drop normalized form of the stretched exponential decline is provided below:

$$q_{cp}(t) \approx \frac{q(t)}{\Delta p(t)} = \left(\frac{\hat{q}_i}{\Delta p}\right)_i \exp\left[-\left(\frac{t}{\tau}\right)^n\right] \quad \text{.....(C.25)}$$

Finally, combining Eq. C.24 and Eq. C.25 the superposition form of the exponential decline is obtained:

$$q(t) = \left(\frac{\hat{q}}{\Delta p}\right)_i \sum_{k=1}^{u} (\Delta p_{wf,k} - \Delta p_{wf,k-1}) \exp\left[-\left(\frac{t_u - t_{k-1}}{\tau}\right)^n\right] \quad \text{.....(C.26)}$$

When calibrating the model parameters for the superposition expression shown in Eq. C.26, we desire the calculated data behavior of $D(t)$ and $b(t)$ much as we did for the simple rate versus time expression. These will be calculated using the following modified expressions for the loss-ratio and loss-ratio derivative.

$$\frac{1}{D(t)} = -\frac{q(t)/\Delta p(t)}{d(q(t)/\Delta p(t))/dt} \quad \text{.....(C.27)}$$

$$b(t) = \frac{d}{dt}\left[\frac{1}{D(t)}\right] = -\frac{d}{dt}\left[\frac{q(t)/\Delta p(t)}{d(q(t)/\Delta p(t))/dt}\right] \quad \text{.....(C.28)}$$

Recalling our expressions for $D(t)$ and $b(t)$ provided by C.19 and C.23 we note that they are independent of the initial rate term. As a result, the derivative terms arrived at using the pressure drop normalized rate form and the time-rate form are identical. This is a result of the assumption that pressure drop normalization of rate data adequately transforms the variable pressure signature of the well to the equivalent constant pressure signature. This has important implications from a diagnostic standpoint and allows the derivative trends to guide calibration regardless of whether time-rate or time-rate-pressure decline methods are utilized provided the constant pressure rate approximation assumption is adequate.

C.2 Stretched Exponential Type Plots and Application Example

The aim of this section is to provide a cartoon schematic showing the diagnostic behavior of the stretched exponential decline and to demonstrate a simple application example using a variety of plots to aid in model calibration. The first objective is addressed in this appendix by using a type plot of the "qDb" behavior for the stretched exponential model provided below as **Fig. C.1**.

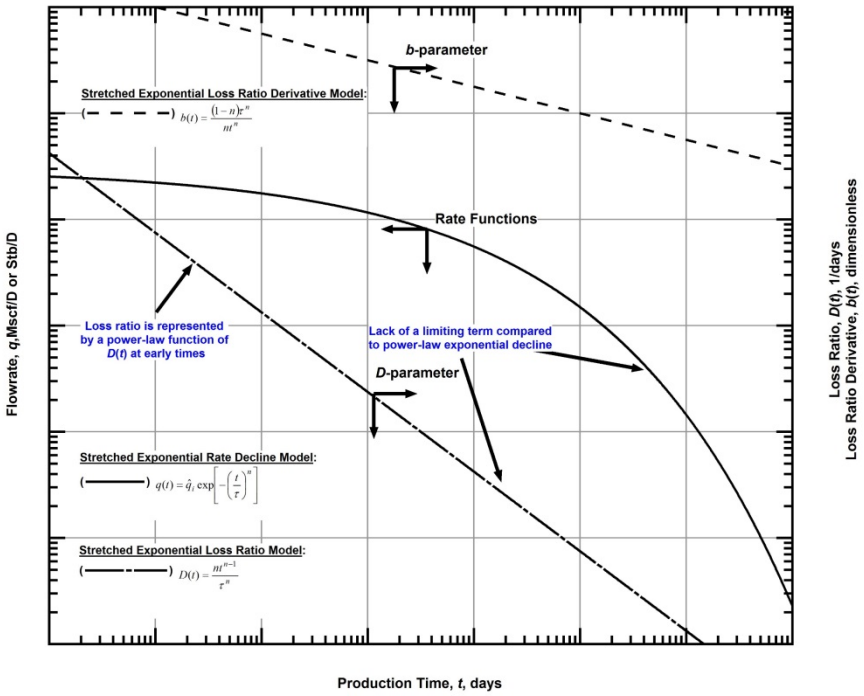

Figure C.1 — Schematic Type Plot of "qDb" Model Behavior for the Stretched Exponential Decline

The model parameters governing the shape of stretched exponential decline model need to be calibrated in order to generate a forecast of future production performance. Unfortunately, non-uniqueness in match calibration is an unescapable reality for all production analysis techniques and decline curve analysis is no exception. In order to mitigate this issue, it is recommended that a suite of diagnostic plots is used as opposed to solely rate versus time analysis. These additional plots provide further match confirmation and help to ensure that the calibrated model honors well performance characteristics such as prevailing flow regime(s). Included below in **Fig. C.2** is an example of such an approach applied to a field production scenario where the stretched exponential model is calibrated across a suite of plots. The corresponding rate-time and rate-cumulative matches are shown in **Fig. C.3** and **C.4**.

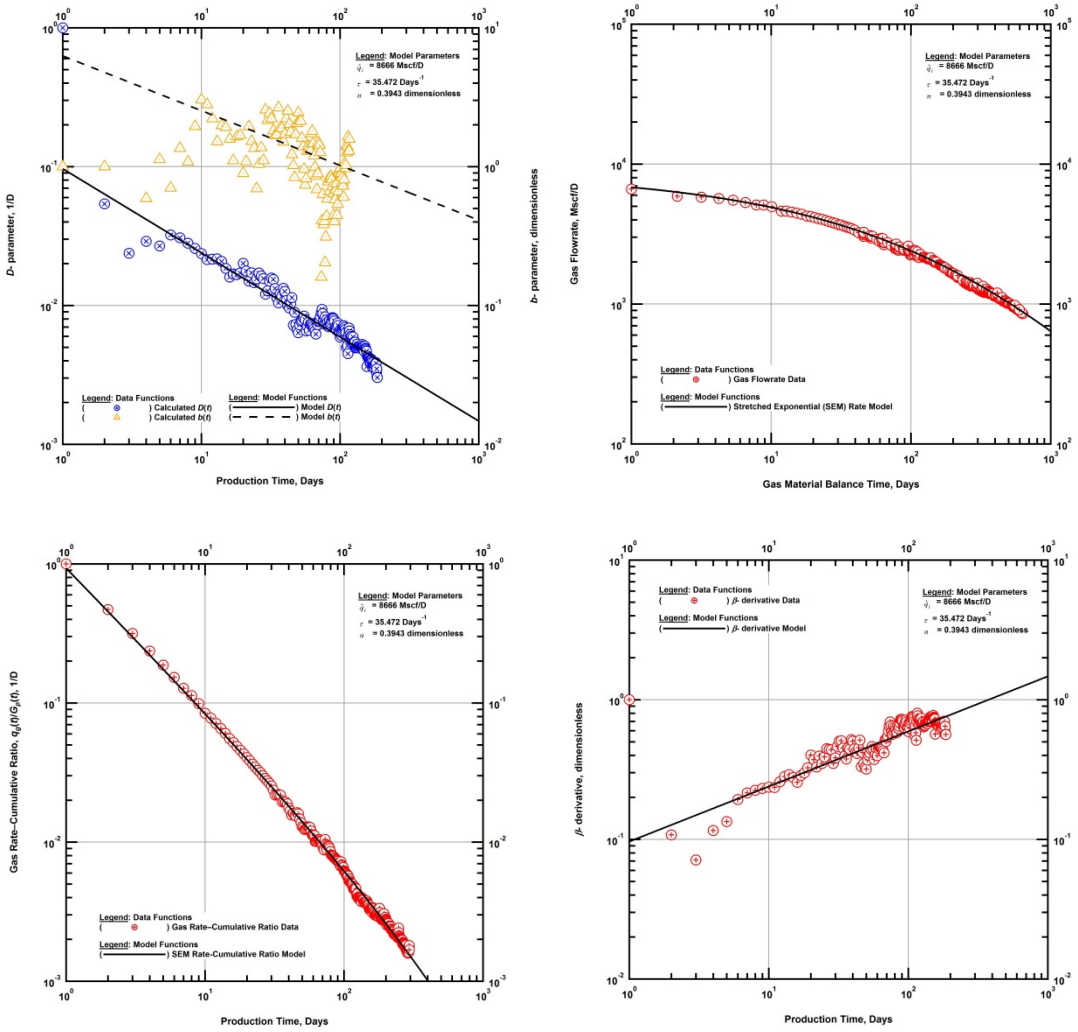

Figure C.2 — Diagnostic Suite Demonstrating Stretched Exponential Model Calibration Methodology

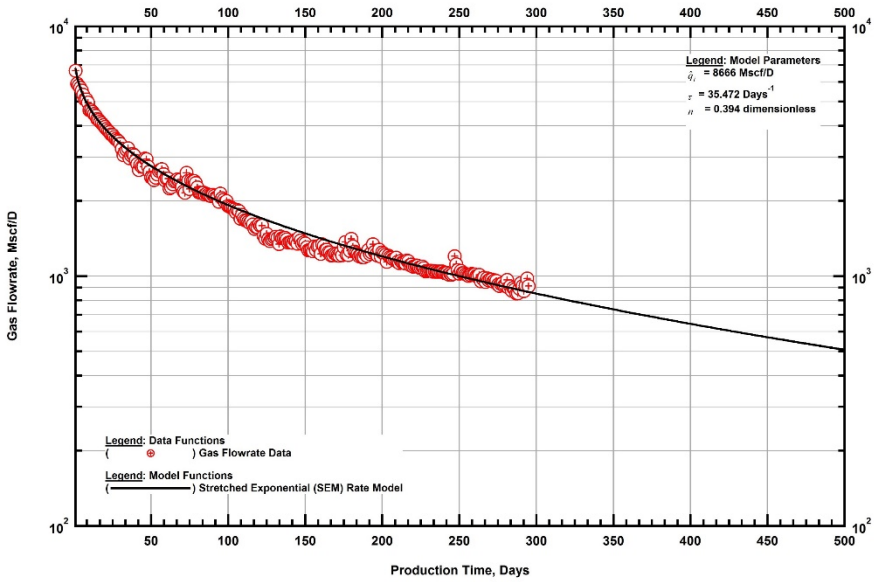

Figure C.3 — Calibrated Stretched Exponential Rate Versus Production Time Match

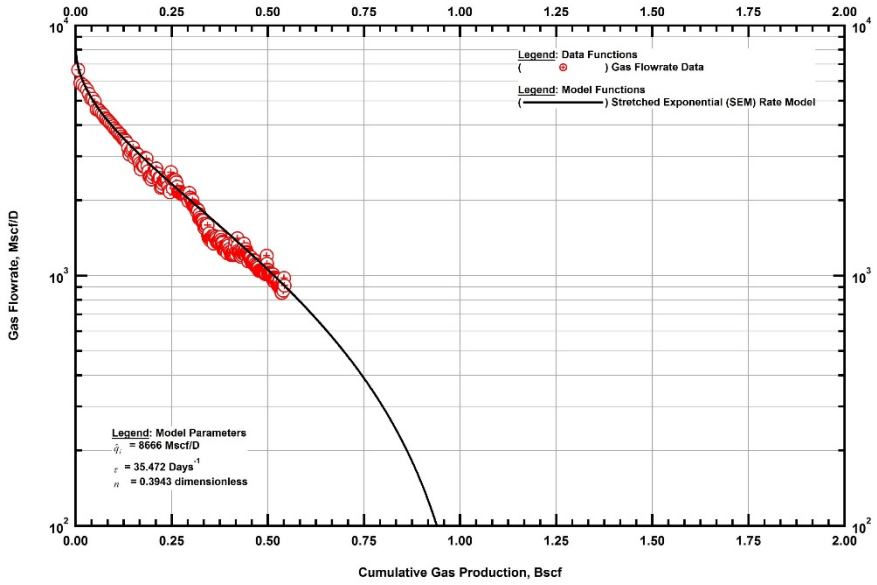

Figure C.4 — Calibrated Stretched Exponential Rate Versus Cumulative Gas Production Match

APPENDIX D

DUONG DECLINE CURVE RELATION

This section aims to fully derive the Duong decline relation introduced by Duong (2011). A schematic "qDb plot" and a brief time-rate application example is included demonstrating the rate and derivative behavior of the model. The defining relationship for this rate versus time model was based on a power law trend describing the rate divided by cumulative production plotted as a function of time. The nature of the model is entirely empirical and the original author suggested its applicability for cases exhibiting long-term linear flow. The defining relationship forming the foundation of this model is presented below.

$$\frac{q(t)}{Q(t)} = at^{-m} \quad \text{.....(D.1)}$$

where q is flowrate in volume per unit time t, Q is the cumulative production expressed as a function of time, and a and m are model parameters controlling the slope and intercept of the described straight line power law expression in logarithmic coordinates.

Along with the defining relation, Duong provided a derivation (which is reproduced here) of the associated closed form rate versus time expression and proposed an application methodology using a best fit power-law trend to define the a and m model parameters. He speculated on physical causes of the long-term linear flow behavior the model is meant to capture and bracketed potential ranges of values for the model parameters based on field examples, past references, and perceived physical phenomena. Finally, he provided comparisons to other rate versus time models and suggested appropriate means of truncating his forecast.

D.1 Derivation of the Duong Decline Relation

Duong (2011) provided a mathematical derivation of the Duong rate-time relation in general terms based on the assumption that the rate-cumulative ratio could be expressed as a general function of time. Duong later went on to propose a defining power-law relationship for this general function. His derivation is reproduced and extended in this section. The generalized basis function from which Duong began his derivation is provided below.

$$\frac{q(t)}{Q(t)} = \varepsilon(t) \quad \text{.....(D.2)}$$

where $\varepsilon(t)$ is an arbitrary function with independent variable time. Rearranging Eq. D.1 to isolate the cumulative production expression we obtain:

$$\frac{q(t)}{\varepsilon(t)} = Q(t) \quad \text{.....(D.3)}$$

Differentiating both sides of Eq. D.3 yields the following:

$$\frac{d}{dt}\left[\frac{q(t)}{\varepsilon(t)}\right] = \frac{d}{dt}Q(t) \quad \text{.....(D.4)}$$

In order to complete the differentiation on the right-hand side (RHS) of Eq. D.4 we present the following identity for rate and cumulative production as a function of time:

$$\int_0^t q(t)dt = Q(t) \quad \text{.....(D.5)}$$

which simply implies that the cumulative production from a well is the area of the curve underneath the rate measured as a function of time. Utilizing this definition we complete the RHS of Eq. D.4:

$$\frac{d}{dt}\left[\frac{q(t)}{\varepsilon(t)}\right] = q(t) \quad \text{.....(D.6)}$$

To complete the left-hand side (LHS) of Eq. D.6, we must recall the quotient rule from fundamental calculus which is reproduced as follows:

$$\frac{d}{dx}\left[\frac{f(x)}{g(x)}\right] = \frac{g(x)f'(x) - f(x)g'(x)}{\left[g(x)\right]^2} \quad \text{.....(D.7)}$$

where $f(x)$ and $g(x)$ are arbitrary functions of an arbitrary independent variable, x, and the apostrophe denotes the first derivative of the functions with respect to x. Utilizing the above definition where $q(t)$ and $\varepsilon(t)$ replace $f(x)$ and $g(x)$, respectively, we complete the differentiation of Eq. D.6 below.

$$\frac{\varepsilon(t)q'(t) - q(t)\varepsilon'(t)}{\left[\varepsilon(t)\right]^2} = q(t) \quad \text{.....(D.8)}$$

Expanding the terms on the RHS yields the following differential equation:

$$\frac{1}{\varepsilon(t)}\frac{dq(t)}{dt}-\frac{q(t)}{\varepsilon(t)^2}\frac{d\varepsilon(t)}{dt}=q(t) \quad \text{.....(D.9)}$$

Separating variables algebraically we obtain the expression below.

$$\frac{dq(t)}{q(t)}=\varepsilon(t)dt+\frac{d\varepsilon(t)}{\varepsilon(t)} \quad \text{.....(D.10)}$$

Integrating both sides from time one to time *t*:

$$\int_1^t\frac{dq(t)}{q(t)}=\int_1^t\varepsilon(t)dt+\int_1^t\frac{d\varepsilon(t)}{\varepsilon(t)} \quad \text{.....(D.11)}$$

The LHS and the second term of the RHS of Eq. D.10 require the following definition of the natural logarithm.

$$\ln[x]=\int_1^x\frac{dx}{x} \quad \text{.....(D.12)}$$

where *x* serves as a generic placeholder variable. Utilizing the definition in Eq. D.12 the integration of Eq. D.11 is partially completed as follows:

$$\ln[q(t)]\Big|_1^t=\ln[\varepsilon(t)]\Big|_1^t+\int_1^t\varepsilon(t)dt \quad \text{.....(D.13)}$$

Substitution of the limits of integration yields:

$$\ln[q(t)]-\ln[q_1]=\ln[\varepsilon(t)]-\ln[\varepsilon(1)]+\int_1^t\varepsilon(t)dt \quad \text{.....(D.14)}$$

where q_1 is the rate evaluated at time unit one and $\varepsilon(1)$ is the arbitrary function evaluated at time unit one. We again recall a logarithmic identity before proceeding in our derivation:

$$\ln[x]-\ln[y]=\ln\left[\frac{x}{y}\right] \quad \text{.....(D.15)}$$

where *y* serves as an additional generic placeholder variable. Using Eq. D.15, we can now simplify Eq. D.14 to arrive at the following form:

$$\ln\left[\frac{q(t)}{q_1}\right] = \ln\left[\frac{\varepsilon(t)}{\varepsilon(1)}\right] + \int_1^t \varepsilon(t)dt \quad \text{.....(D.16)}$$

Isolating the integral term and again utilizing the identity presented as Eq. D.15 we simplify Eq. D.16 as follows.

$$\ln\left[\frac{q(t)\varepsilon(1)}{q_1\varepsilon(t)}\right] = \int_1^t \varepsilon(t)dt \quad \text{.....(D.17)}$$

Exponentiation of both sides of Eq. D.17 and solving for $q(t)$ algebraically provides the following general expression for rate as a function of time.

$$q(t) = q_1 \frac{\varepsilon(t)}{\varepsilon(1)} \exp\left[\int_1^t \varepsilon(t)dt\right] \quad \text{.....(D.18)}$$

Eq. D.18 is the general solution for the Duong model where $\varepsilon(t)$ is an arbitrary function describing the behavior of the rate as function of time divided by the cumulative production as a function of time. The author of the paper proposed the following power-law expression to describe $\varepsilon(t)$, which serves as the defining identify of the Duong decline model.

$$\varepsilon(t) = at^{-m} \quad \text{.....(D.19)}$$

The solution of Eq. D.19 at time one and the integral within the exponential on the RHS of Eq. D.18 are still needed to arrive at the closed form rate-time solution of the Duong model. Both of these terms are provided below.

$$\varepsilon(1) = a\,1^{-m} = a \quad \text{.....(D.20)}$$

$$\int_1^t \varepsilon(t)dt = a\int_1^t t^{-m}dt = \frac{a}{1-m}\left(t^{1-m} - 1\right) \quad \text{.....(D.21)}$$

Combining Eqs. D18 through D.21, we obtain the final rate-time form of the Duong decline model proposed in the original paper.

$$q(t) = q_1 t^{-m} \exp\left[\frac{a}{1-m}(t^{1-m} - 1)\right] \quad \text{.....(D.22)}$$

As with each of the models used in this work, we desire expressions for the reciprocal of the loss-ratio, $D(t)$, and the loss-ratio derivative, $b(t)$. These expressions will be used along with other diagnostic plots to calibrate the Duong model parameters and match the historical production data. We will begin with the derivation of the $D(t)$ equation which requires us to recall the following identity.

$$D(t) = -\frac{1}{q(t)}\frac{dq(t)}{dt} \quad \text{.....(D.23)}$$

Combining Eq. D.22 and D.23 we obtain the following:

$$D(t) = -\frac{1}{q_1 t^{-m} \exp\left[\frac{a}{1-m}(t^{1-m}-1)\right]}\frac{d}{dt}\left\{q_1 t^{-m} \exp\left[\frac{a}{1-m}(t^{1-m}-1)\right]\right\} \quad \text{.....(D.24)}$$

We first isolate and simplify the differentiation component on the RHS of Eq. D.24:

$$\frac{d}{dt}\left\{q_1 t^{-m} \exp\left[\frac{a}{1-m}(t^{1-m}-1)\right]\right\} = q_1 \frac{d}{dt}\left\{t^{-m} \exp\left[\frac{a}{1-m}(t^{1-m}-1)\right]\right\} \quad \text{.....(D.25)}$$

To complete the differentiation we must utilize the definition of the product rule of differentiation, namely:

$$\frac{d}{dx}\left[f(x)g(x)\right] = f'(x)g(x) + f(x)g'(x) \quad \text{.....(D.26)}$$

where $f(x)$ and $g(x)$ are arbitrary functions of an arbitrary independent variable x and the apostrophe denotes the first derivative with respect to x. Observing Eqs. D.25 and D.26 we can define the following placeholder functions.

$$f(t) = t^{-m} \quad \text{.....(D.27)}$$

$$g(t) = \exp\left[\frac{a}{1-m}(t^{1-m}-1)\right] \quad \text{.....(D.28)}$$

To fully complete the differentiation in Eq. D.25 using the product rule we also require expressions for the first derivative with respect to time, t. The expression for $f'(t)$ is expressed below

$$f'(t) = -m t^{-m-1} \quad \text{.....(D.29)}$$

In order to differentiate the second substitution function, namely $g(t)$, we recall the definition of the derivative of an exponential function below.

$$\frac{d\exp[x]}{dt} = \exp[x]\frac{dx}{dt} \quad \text{.....(D.30)}$$

In our case, x and its derivative with respect to time are defined as follows:

$$x = \frac{a}{1-m}(t^{1-m} - 1) \quad \text{.....(D.31)}$$

$$\frac{dx}{dt} = a\, t^{-m} \quad \text{.....(D.32)}$$

Utilizing Eqs. D.30 through D.32, we can define $g'(t)$ as follows:

$$g'(t) = at^{-m}\exp\left[\frac{a}{1-m}(t^{1-m} - 1)\right] \quad \text{.....(D.33)}$$

Utilizing the product rule definition in Eq. D.26 and the expressions for the substitution functions defined by Eqs. D.27, D.28, D.29, and D.33 we can complete the differentiation in Eq. D.25.

$$q_1\frac{d}{dt}\left\{t^{-m}\exp\left[\frac{a}{1-m}(t^{1-m} - 1)\right]\right\} = q_1\left\{-mt^{-m-1}\exp\left[\frac{a}{1-m}(t^{1-m} - 1)\right] + t^{-m}at^{-m}\exp\left[\frac{a}{1-m}(t^{1-m} - 1)\right]\right\}$$
$$\text{.....(D.34)}$$

Simplifying algebraically, we arrive at:

$$q_1\frac{d}{dt}\left\{t^{-m}\exp\left[\frac{a}{1-m}(t^{1-m} - 1)\right]\right\} = q_1t^{-m}\exp\left[\frac{a}{1-m}(t^{1-m} - 1)\right]\left\{-mt^{-1} + at^{-m}\right\} \quad \text{.....(D.35)}$$

Eq. D.35 represents the completed differentiation for the second term in Eq. D.24. Combining Eqs. D.24 and D.35 yields the following for $D(t)$:

$$D(t) = -\frac{q_1t^{-m}\exp\left[\frac{a}{1-m}(t^{1-m} - 1)\right]}{q_1t^{-m}\exp\left[\frac{a}{1-m}(t^{1-m} - 1)\right]}\left[-mt^{-1} + at^{-m}\right] \quad \text{.....(D.36)}$$

With a final simplification we arrive at the following simplified final expression for the reciprocal of the loss-ratio, $D(t)$, for the Duong model:

$$D(t) = mt^{-1} - at^{-m} \quad \text{.....(D.37)}$$

Having derived the reciprocal of the loss-ratio, $D(t)$, for the Duong model, we now continue with our derivation to derive the derivative of the loss-ratio, $b(t)$. The identity recalled below serves as the starting point for this derivation:

$$b(t) = \frac{d}{dt}\left[\frac{1}{D(t)}\right] \quad \text{.....(D.38)}$$

Substituting the expression for $D(t)$, given by Eq. D.37, into Eq. D.38 yields the following:

$$b(t) = \frac{d}{dt}\left[\frac{1}{mt^{-1} - at^{-m}}\right] \quad \text{.....(D.39)}$$

To complete the differentiation on the RHS or Eq. D.39 we again recall the quotient rule identity introduced by Eq. D.7 earlier in this appendix.

$$\frac{d}{dx}\left[\frac{f(x)}{g(x)}\right] = \frac{g(x)f'(x) - f(x)g'(x)}{\left[g(x)\right]^2} \quad \text{.....(D.7)}$$

where $f(x)$ and $g(x)$ again represent arbitrary functions of an arbitrary independent variable x and the apostrophe denotes the first derivative of the aforementioned functions. For this derivation we will let $f(x)$ and $g(x)$ be defined as follows.

$$f(t) = 1 \quad \text{.....(D.40)}$$

$$g(t) = mt^{-1} - at^{-m} \quad \text{.....(D.41)}$$

where the arbitrary independent variable x is represented by time, t, for these expressions. The quotient rule identity also requires the first derivatives of Eqs. D.40 and D.41 with respect to time which are defined as such:

$$f'(t) = 0 \quad \text{.....(D.42)}$$

$$g'(t) = -mt^{-2} + m\,a\,t^{-m-1} \quad \text{.....(D.43)}$$

Utilizing the quotient rule definition provided by Eq. D.7, we can complete the derivation on the RHS of Eq. D.39 by substitution of Eqs. D.40 through D.43.

$$\frac{d}{dt}\left[\frac{1}{mt^{-1}-at^{-m}}\right]=\frac{mt^{-2}-a\,m\,t^{-m-1}}{\left[mt^{-1}-at^{-m}\right]^2} \quad \text{.....(D.44)}$$

Aiming to simplify the expression we expand the denominator as follows:

$$\frac{d}{dt}\left[\frac{1}{mt^{-1}-at^{-m}}\right]=\frac{mt^{-2}-a\,m\,t^{-m-1}}{mt^{-2}-2a\,m\,t^{-1-m}+a^2t^{-2m}} \quad \text{.....(D.45)}$$

Simplifying both the numerator and denominator algebraically:

$$\frac{d}{dt}\left[\frac{1}{mt^{-1}-at^{-m}}\right]=\frac{mt^{-2-m}\left(t^m-a\,t\right)}{t^{-2(1+m)}\left[a^2t^2+m^2t^{2m}-2a\,m\,t^{1+m}\right]} \quad \text{.....(D.46)}$$

Canceling like terms and factoring the bracketed polynomial yields the following simplified expression for the loss-ratio derivative, $b(t)$, for the Duong decline model.

$$b(t)=\frac{mt^m\left[t^m-a\,t\right]}{\left[at-mt^m\right]^2} \quad \text{.....(D.47)}$$

All of the equations up until this point in the derivation are concerned with the modeling of time-rate data based on the assumption of a constant bottomhole flowing pressure. In keeping with the aim of this work, namely incorporating pressure data into decline curve analysis, the variable pressure form of the Duong decline model is provided below.

The discrete form of the convolution integral is used to account for variations in bottomhole flowing pressure as a function of time. A complete development of the superposition equation is included in Appendix F. The final mathematical form is provided below:

$$q(t)=\sum_{k=1}^{u}(\Delta p_{wf,k}-\Delta p_{wf,k-1})(q_{cp}(t_u-t_{k-1})) \quad \text{.....(D.48)}$$

where Δp_{wf} is the bottomhole pressure drop in units of pressure at a specific point in time and q_{cp} denotes a constant pressure rate solution. This work makes the assumption that the constant pressure rate signature of a well is accurately represented by the pressure drop normalized rate behavior of that well. If this assumption holds, it is proposed that this data trend can be modeled using a pressure drop normalized form of an empirical time-rate decline relation serving as the unknown constant pressure rate solution in Eq. D.48. The pressure drop normalized form of the Duong decline is provided below:

$$q_{cp}(t) \approx \frac{q(t)}{\Delta p(t)} = \left(\frac{q_1}{\Delta p}\right)_i t^{-m} \exp\left[\frac{a}{1-m}(t^{1-m}-1)\right] \quad \text{.....(D.49)}$$

Finally, combining Eq. D.48 and Eq. D.49 the superposition form of the Duong decline is obtained:

$$q(t) = \left(\frac{q_1}{\Delta p}\right)_i \sum_{k=1}^{u} (\Delta p_{wf,k} - \Delta p_{wf,k-1})(t_u - t_{k-1})^{-m} \exp\left[\frac{a}{1-m}\left[(t_u - t_{k-1})^{1-m} - 1\right]\right] \quad \text{.....(D.50)}$$

When calibrating the model parameters for the superposition expression shown in Eq. B.50, we desire the behavior of $D(t)$ and $b(t)$ much as we did for the simple rate versus time expression. These will be calculated using the following modified expressions for the loss-ratio and loss-ratio derivative.

$$\frac{1}{D(t)} = -\frac{q(t)/\Delta p(t)}{d(q(t)/\Delta p(t))/dt} \quad \text{.....(D.51)}$$

$$b(t) = \frac{d}{dt}\left[\frac{1}{D(t)}\right] = -\frac{d}{dt}\left[\frac{q(t)/\Delta p(t)}{d(q(t)/\Delta p(t))/dt}\right] \quad \text{.....(D.52)}$$

Recalling our expressions for $D(t)$ and $b(t)$ provided by D.37 and D.47 we note that they are independent of the initial rate term. As a result, the derivative terms arrived at using the pressure drop normalized rate form and the time-rate form are identical (*i.e.* independent of the initial pressure drop normalized rate). This is a result of the assumption that pressure drop normalization of rate data adequately transforms the variable pressure signature of the well to the equivalent constant pressure signature. This has important implications from a diagnostic standpoint and allows the derivative trends to guide calibration regardless of whether time-rate or time-rate-pressure decline methods are utilized provided the constant pressure rate approximation assumption is adequate.

D.2 Duong Type Plots and Application Example

The aim of this section is to provide a cartoon schematic showing the diagnostic behavior of the Duong decline and to demonstrate a simple application example using a variety of plots to aid in model calibration. The first objective is addressed in this appendix by using a type plot of the "qDb" behavior for the Duong model provided below as **Fig. D.1**.

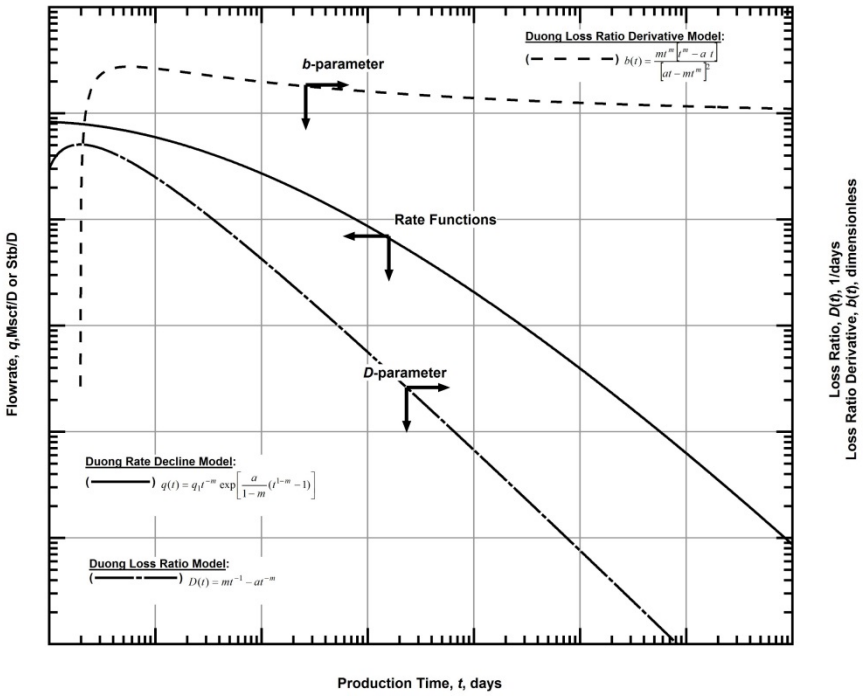

Figure D.1 — Schematic Type Plot of "qDb" Model Behavior for the Duong Decline

The model parameters governing the shape of Duong decline model need to be calibrated in order to generate a forecast of future production performance. Unfortunately, non-uniqueness in match calibration is an unescapable reality for all production analysis techniques and decline curve analysis is no exception. In order to mitigate this issue, it is recommended that a suite of diagnostic plots is used as opposed to solely rate versus time analysis. These additional plots provide further match confirmation and help to ensure that the calibrated model honors well performance characteristics such as prevailing flow regime(s). Included below in **Fig. D.2** is an example of such an approach applied to a field production scenario where the Duong model is calibrated across a suite of plots. The corresponding rate-time and rate-cumulative matches are shown in **Fig. D.3** and **D.4**.

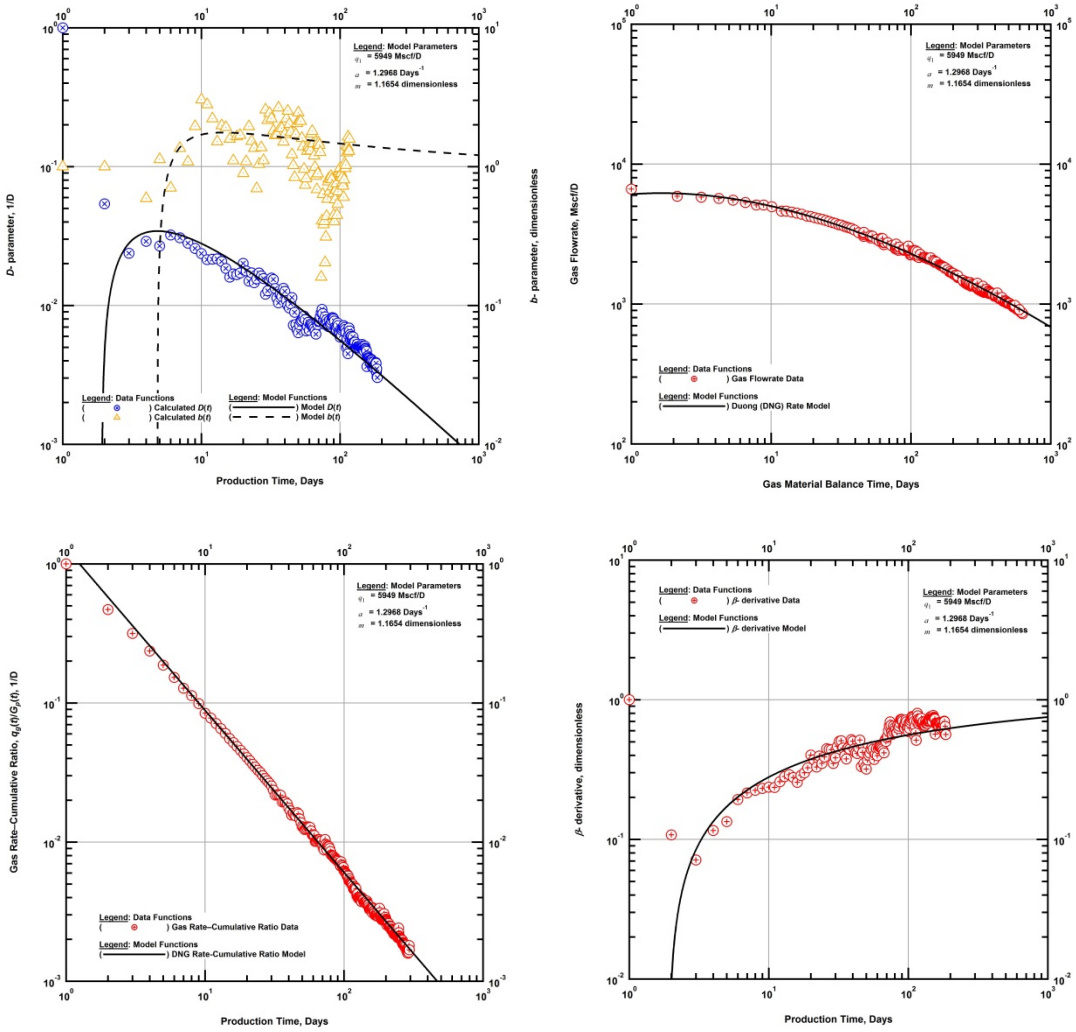

Figure D.2 — Diagnostic Suite Demonstrating Duong Model Calibration Methodology

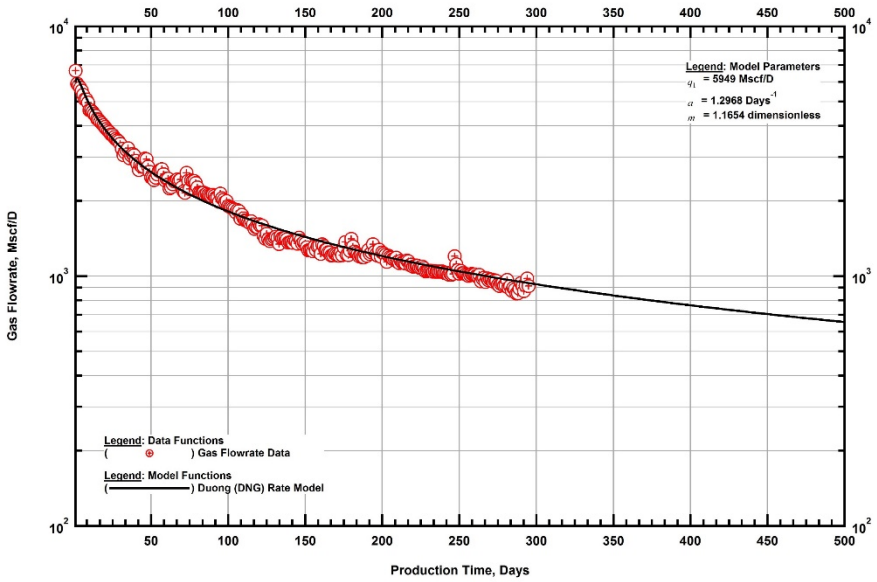

Figure D.3 — Calibrated Duong Rate Versus Production Time Match

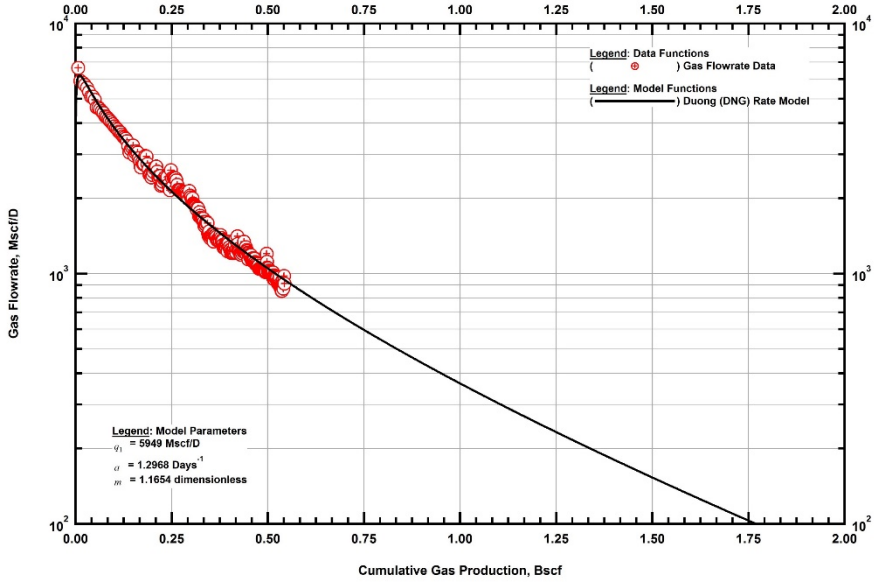

Figure D.4 — Calibrated Duong Rate Versus Cumulative Gas Production Match

APPENDIX E

LOGISTIC GROWTH DECLINE CURVE RELATION

This section aims to fully derive the Logistic Growth decline relation introduced by Clark *et al*. (2011). A schematic "qDb plot" and a brief time-rate application example is included demonstrating the rate and derivative behavior of the model. The defining relationship for this rate versus time model is based on a logistic growth trend of the cumulative hydrocarbon production towards a carrying capacity term, *K*. The nature of the model is entirely empirical; however, the authors suggest that the carrying capacity term be defined by an estimate of the hydrocarbon in place which lends a degree of physical meaning or constraint. The defining relationship forming the foundation of this model is presented below.

$$Q(t) = \frac{Kt^n}{(a + t^n)} \quad \text{.....(E.1)}$$

where *Q* is the cumulative production expressed as a function of time, and *a* and *n* are model parameters controlling the functional behavior of the growth equation.

Along with the defining relation, Clark *et al*. (2011) provided a derivation (which is reproduced here) of the associated closed form rate versus time expression and proposed two application methodologies, one using a regression routine, and one involving linearizing the defining expressions and solving for the *a* and *n* model parameters. Additionally, the authors provided a thorough discussion of generalized logistic growth models across a variety of industries and applications. As a final discussion, the authors provided a complete discourse on the statistical ranges and distributions of the model parameters using a large database of Barnett Shale wells. This is highly beneficial to the unfamiliar practitioner as a quality control measure once analysis has been complete.

E.1 Derivation of the Logistic Growth Decline Relation

Clark *et al*. (2011) provided a defining cumulative production relationship and a closed form rate-time expression in their original paper. A complete mathematical derivation of the rate versus time expression, the reciprocal of the loss-ratio expression, $D(t)$, and the loss-ratio derivative expression, $b(t)$, is presented in this section. As a necessary starting point we reproduce the fundamental relationship given by Eq. E.1 below.

$$Q(t) = \frac{Kt^n}{(a + t^n)} \quad \text{.....(E.1)}$$

Our first derivation is that of the rate as a function of time expression. To begin we define the following identity:

$$\int_0^t q(t)dt = Q(t) \quad \text{(E.2)}$$

where q is the flowrate as a function of time, t. Differentiating both sides with respect to time yields the following:

$$\frac{dQ(t)}{dt} = q(t) \quad \text{(E.3)}$$

Combining Eqs. E.1 and E.3:

$$q(t) = \frac{dQ(t)}{dt} = K\frac{d}{dt}\left[\frac{t^n}{(a+t^n)}\right] \quad \text{(E.4)}$$

To complete the differentiation of the bracketed term on the right-hand side (RHS) of Eq. E.4, we must recall the quotient rule from fundamental calculus which is reproduced as follows:

$$\frac{d}{dx}\left[\frac{f(x)}{g(x)}\right] = \frac{g(x)f'(x) - f(x)g'(x)}{\left[g(x)\right]^2} \quad \text{(E.5)}$$

where $f(x)$ and $g(x)$ are arbitrary functions of an arbitrary independent variable, x, and the apostrophe denotes the first derivative of the functions with respect to x. By observing Eq. E.4, we can define the arbitrary functions and their derivatives as follows:

$$f(t) = t^n \quad \text{(E.6)}$$

$$g(t) = a + t^n \quad \text{(E.7)}$$

$$f'(t) = nt^{n-1} \quad \text{(E.8)}$$

$$g'(t) = nt^{n-1} \quad \text{(E.9)}$$

Observing the structure of Eq. E.5 and combining Eq. E.4 with Eqs. E.6 through E.9, we obtain the following un-simplified expression for flowrate as a function of time.

$$q(t) = K\left[\frac{(a+t^n)(nt^{n-1}) - (t^n)(nt^{n-1})}{(a+t^n)^2}\right] \quad \text{(E.10)}$$

Expanding the numerator term:

$$q(t) = \frac{Kant^{n-1} + Knt^{2n-1} - Knt^{2n-1}}{(a+t^n)^2} \quad \text{(E.11)}$$

Simplifying by cancelling like terms in the numerator yields the final closed form rate versus time expression presented in the original work.

$$q(t) = \frac{Kant^{n-1}}{(a+t^n)^2} \quad \text{(E.12)}$$

Continuing our derivation, we next desire an expression for the reciprocal of the loss-ratio, $D(t)$. We recall the following identity to serve as a starting point.

$$D(t) = -\frac{1}{q(t)}\frac{dq(t)}{dt} \quad \text{(E.13)}$$

Substituting Eq. E.12 into Eq. E.13, we arrive at the following:

$$D(t) = -\frac{Kan(a+t^n)^2}{Kant^{n-1}}\frac{d}{dt}\left[\frac{t^{n-1}}{(a+t^n)^2}\right] \quad \text{(E.14)}$$

Simplifying by cancelling like terms yields:

$$D(t) = -\frac{(a+t^n)^2}{t^{n-1}}\frac{d}{dt}\left[\frac{t^{n-1}}{(a+t^n)^2}\right] \quad \text{(E.15)}$$

Completing the differentiation of the bracketed expression on the RHS of Eq. E.15 again requires the quotient rule defined by Eq. E.5:

$$\frac{d}{dx}\left[\frac{f(x)}{g(x)}\right] = \frac{g(x)f'(x) - f(x)g'(x)}{[g(x)]^2} \quad \text{(E.5)}$$

where we redefine the arbitrary substitution functions and their derivatives as follows:

$$f(t) = t^{n-1} \quad \text{(E.16)}$$

$$g(t) = (a + t^n)^2 \quad \text{(E.17)}$$

$$f'(t) = (n-1)t^{n-2} \quad \text{(E.18)}$$

$$g'(t) = 2nt^{n-1}(a + t^n) \quad \text{(E.19)}$$

Isolating the bracketed term on the RHS of Eq. E.15 and completing the derivation by utilizing the quotient rule and Eqs. E.16 through E.19, we arrive at the following expression:

$$\frac{d}{dt}\left[\frac{t^{n-1}}{(a+t^n)^2}\right] = \left\{\frac{(a+t^n)^2(n-1)t^{n-2} - t^{n-1}2nt^{n-1}(a+t^n)}{\left[(a+t^n)^2\right]^2}\right\} \quad \text{(E.20)}$$

Combining Eqs. E.15 and E.20:

$$D(t) = -\frac{(a+t^n)^2}{t^{n-1}}\left\{\frac{(a+t^n)^2(n-1)t^{n-2} - t^{n-1}2nt^{n-1}(a+t^n)}{\left[(a+t^n)^2\right]^2}\right\} \quad \text{(E.21)}$$

Simplifying algebraically yields the following final expression for the reciprocal of the loss-ratio, $D(t)$, as a function of time:

$$D(t) = \frac{a(1-n) + (1+n)t^n}{t(a+t^n)} \quad \text{(E.22)}$$

The final step in the derivation process is to obtain an expression of the loss-ratio derivative, $b(t)$. The following identity forms the starting point of the derivation:

$$b(t) = \frac{d}{dt}\left[\frac{1}{D(t)}\right] \quad \text{(E.23)}$$

Substituting Eq. E.22 into Eq. E.23:

$$b(t) = \frac{d}{dt}\left[\frac{t(a+t^n)}{a(1-n) + (1+n)t^n}\right] \quad \text{(E.24)}$$

Completing the differentiation on the RHS of Eq. E.24 requires both the quotient rule identity defined previously and the product rule definition. Both are included below for reference.

$$\frac{d}{dx}\left[\frac{f(x)}{g(x)}\right]=\frac{g(x)f'(x)-f(x)g'(x)}{\left[g(x)\right]^2} \quad \text{(E.5)}$$

$$\frac{d}{dx}\left[p(x)u(x)\right]=p'(x)u(x)+p(x)u'(x) \quad \text{(E.25)}$$

where $p(x)$ and $u(x)$ are arbitrary functions of an arbitrary independent variable, x, and the apostrophe denotes the first derivative of the functions with respect to x. By observing Eq. E.4, we can define arbitrary functions, $f(t)$ and $g(t)$, as follows:

$$f(t)=t(a+t^n) \quad \text{(E.26)}$$

$$g(t)=a(1-n)+(1+n)t^n \quad \text{(E.27)}$$

We must use the product rule definition provided by Eq. E.25 to obtain the first derivative with respect to time, t, for Eq. E.26 and E.27. Doing so yields the following results.

$$f'(t)=a+t^n+nt^n \quad \text{(E.28)}$$

$$g'(t)=n(1+n)t^{n-1} \quad \text{(E.29)}$$

We are now able to complete the differentiation on the RHS of Eq. E.24 by utilizing the quotient rule and the expressions defined in Eqs. E.26 through E.29. The result is the following un-simplified form of the loss-ratio derivative expression:

$$b(t)=\frac{(a(1-n)+(1+n)t^n)(a+t^n+nt^n)-t(a+t^n)n(1+n)t^{n-1}}{(a(1-n)+(1+n)t^n)^2} \quad \text{(E.30)}$$

Simplifying algebraically yields the following final expression for the loss-ratio derivative as a function of time for the logistic growth model.

$$b(t)=\frac{a^2(1-n)-2a(n^2-1)t^n+(n+1)t^{2n}}{[a(1-n)+(n+1)t^n]^2} \quad \text{(E.31)}$$

All of the equations up until this point in the derivation are concerned with the modeling of time-rate data based on the assumption of a constant bottomhole flowing pressure. In keeping with the aim of this work, namely incorporating pressure data into decline curve analysis, the variable pressure form of the Logistic Growth decline model is provided below.

The discrete form of the convolution integral is used to account for variations in bottomhole flowing pressure as a function of time. A complete development of the superposition equation is included in Appendix F. The final mathematical form is provided below:

$$q(t)=\sum_{k=1}^{u}(\Delta p_{wf,k}-\Delta p_{wf,k-1})(q_{cp}(t_u-t_{k-1})) \quad \text{.....(E.32)}$$

where Δp_{wf} is the bottomhole pressure drop in units of pressure at a specific point in time and q_{cp} denotes a constant pressure rate solution. This work makes the assumption that the constant pressure rate signature of a well is accurately represented by the pressure drop normalized rate behavior of that well. If this assumption holds, it is proposed that this data trend can be modeled using a pressure drop normalized form of an empirical time-rate decline relation serving as the unknown constant pressure rate solution in Eq. E.48. The pressure drop normalized form of the Logistic Growth model is provided below:

$$q_{cp}(t)\approx\frac{q(t)}{\Delta p(t)}=\left(\frac{K}{\Delta p}\right)_i\frac{nat^{n-1}}{(a+t^n)^2} \quad \text{.....(E.33)}$$

Finally, combining Eq. E.32 and Eq. E.33 the superposition form of the Logistic Growth model is obtained:

$$q(t)=\left(\frac{K}{\Delta p}\right)_i\sum_{k=1}^{u}(\Delta p_{wf,k}-\Delta p_{wf,k-1})\frac{na(t_u-t_{k-1})^{n-1}}{[a+(t_u-t_{k-1})^n]^2} \quad \text{.....(E.34)}$$

When calibrating the model parameters for the superposition expression shown in Eq. E.34, we desire the behavior of $D(t)$ and $b(t)$ much as we did for the simple rate versus time expression. These will be calculated using the following modified expressions for the loss-ratio and loss-ratio derivative.

$$\frac{1}{D(t)}=-\frac{q(t)/\Delta p(t)}{d(q(t)/\Delta p(t))/dt} \quad \text{.....(E.35)}$$

$$b(t)=\frac{d}{dt}\left[\frac{1}{D(t)}\right]=-\frac{d}{dt}\left[\frac{q(t)/\Delta p(t)}{d(q(t)/\Delta p(t))/dt}\right] \quad \text{.....(E.36)}$$

Recalling our expressions for $D(t)$ and $b(t)$ provided by E.22 and E.31 we note that they are independent of the carrying capacity term, K. As a result, the derivative terms arrived at using the pressure drop normalized rate form and the time-rate form are identical (*i.e.* independent of the initial pressure drop normalized carrying capacity). This is a result of the assumption that pressure drop normalization of rate data adequately transforms the variable pressure signature of the well to the equivalent constant pressure signature. This has important implications from a diagnostic standpoint and allows the derivative trends to guide calibration regardless of whether time-rate or time-rate-pressure decline methods are utilized provided the constant pressure rate approximation assumption is adequate.

E.2 Logistic Growth Type Plots and Application Example

The aim of this section is to provide a cartoon schematic showing the diagnostic behavior of the Logistic Growth model and to demonstrate a simple application example using a variety of plots to aid in model calibration. The first objective is addressed in this appendix by using a type plot of the "qDb" behavior for the Logistic Growth model provided below as **Fig. E.1**.

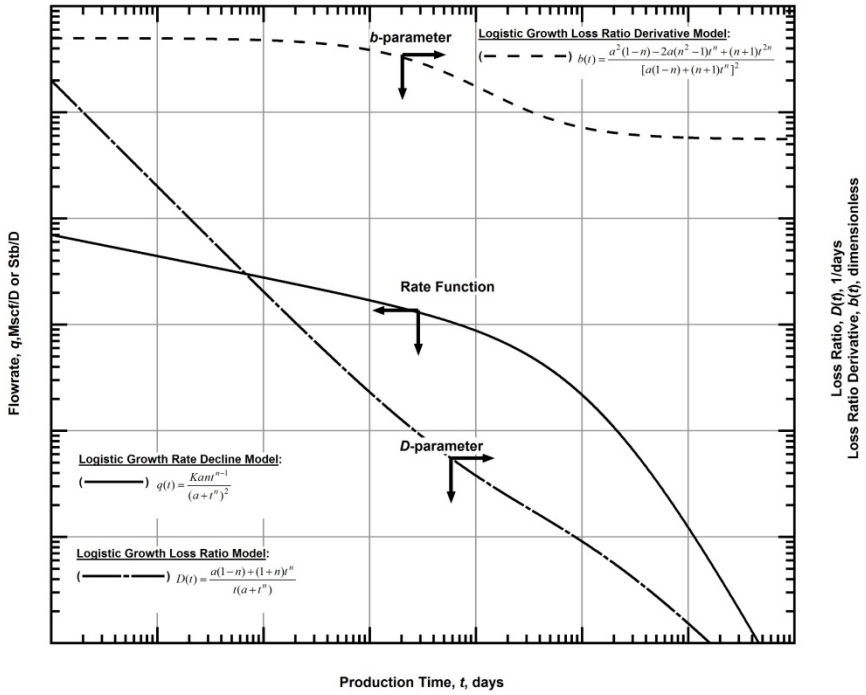

Figure E.1 — Schematic Type Plot of "qDb" Model Behavior for the Logistic Growth Decline Model

The model parameters governing the shape of Logistic Growth model need to be calibrated in order to generate a forecast of future production performance. Unfortunately, non-uniqueness in match calibration is an unescapable reality for all production analysis techniques and decline curve analysis is no exception. In order to mitigate this issue, it is recommended that a suite of diagnostic plots is used as opposed to performing solely rate versus time analysis. These additional plots provide further match confirmation and help to ensure that the calibrated model honors well performance characteristics such as prevailing flow regime(s). Included below in **Fig. E.2** is an example of such an approach applied to a field production scenario where the Logistic Growth model is calibrated across a suite of plots. The corresponding rate-time and rate-cumulative matches are shown in **Fig. E.3** and **E.4**.

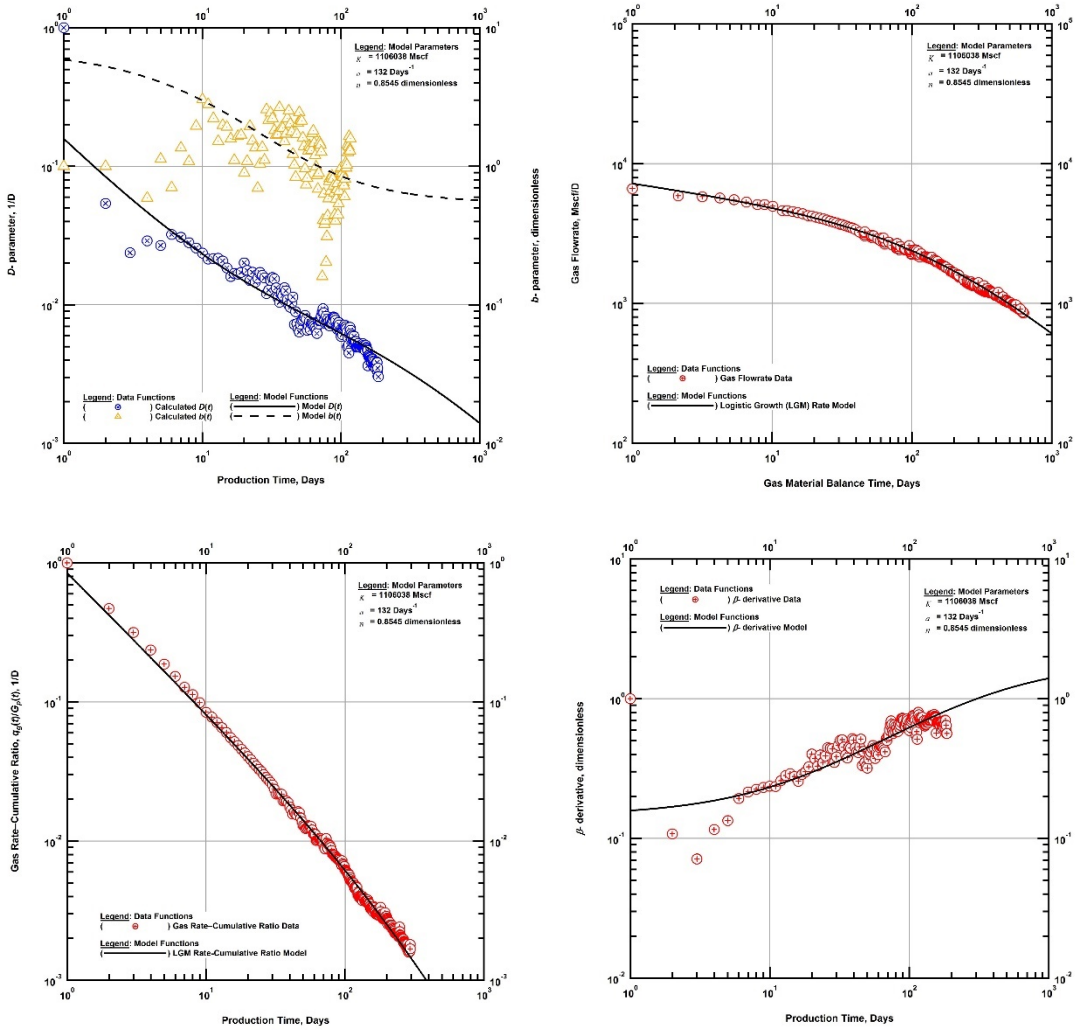

Figure E.2 — Diagnostic Suite Demonstrating Logistic Growth Model Calibration Methodology

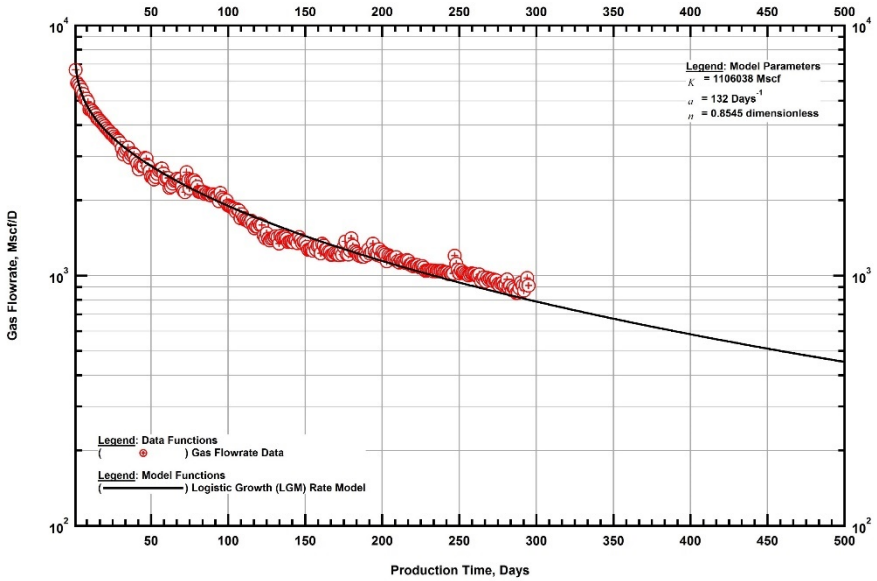

Figure E.3 — Calibrated Logistic Growth Rate Versus Production Time Match

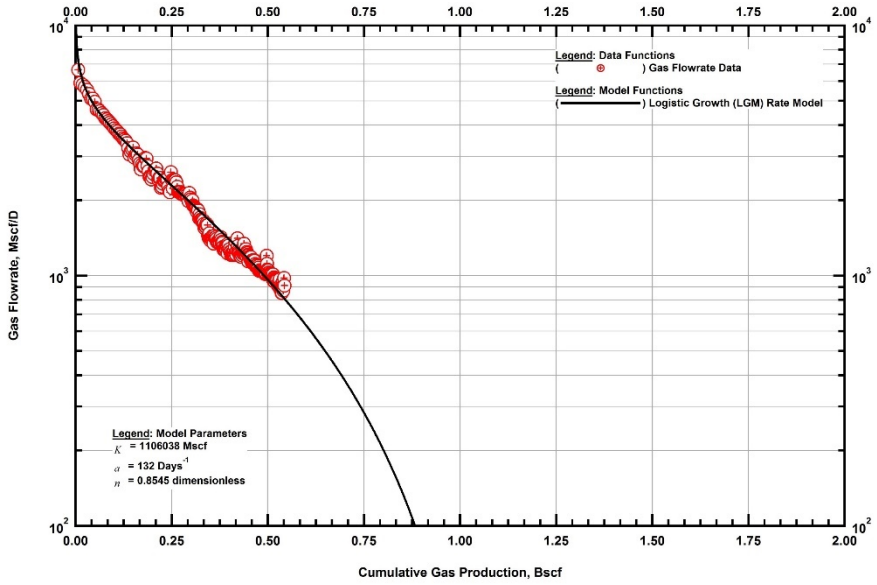

Figure E.4 — Calibrated Logistic Growth Rate Versus Cumulative Gas Production Match

APPENDIX F

DERIVATION OF THE CONVOLUTION INTEGRAL

This appendix works through the derivation of both the discrete and continuous forms of the convolution equation describing the rate response to variable pressure drop conditions. The principle of superposition is now utilized to describe the rate as a function of time by considering the individual rate responses corresponding to the pressure drop steps. For reference the principle of superposition, as defined in Haberman (2004), is stated as follows:

> *If arbitrary variables u_1* and *u_2 satisfy a linear homogenous equation, then an arbitrary linear combination of them, $c_1u_1+c_2u_2$ where c_1 and c_2 are arbitrary constants, also satisfies the same linear homogeneous equation.*

The above definition was included to emphasize the need for linearity (or transformations such as pseduopressure or pseudotime) when applying the superposition principle. With the definition above in mind we assume a linear system (*e.g.* slightly compressible oil flow) and proceed to describe the rate as a function of time as follows:

$$q(t) = q_1 + q_2 + q_3 + \cdots + q_n \quad \text{(F.1)}$$

We now use a proportionality relation to make the assertion that rate response due to a change in pressure drop over a particular interval, q_j, is equivalent to the unit rate response had a constant reference pressure, p_r, been maintained throughout the productive life of the well. This is expressed mathematically as:

$$\frac{q_j}{\left(p_i - p_{wf,j}\right)} = \frac{q_u(t - t_{j-1})}{\left(p_i - p_r\right)} \quad \text{(F.2)}$$

For mathematical simplicity we now define a variable, q_{cp}, to represent the constant pressure rate response described by the right hand side of Eq. F.2.

$$q_{cp}(t - t_{j-1}) = \frac{q_u(t - t_{j-1})}{\left(p_i - p_r\right)} \quad \text{(F.3)}$$

Combining Eqs. F.2 and F.3 and solving for q_j we arrive at:

$$q_j = q_{cp}(t - t_{j-1})(p_i - p_{wf,j}) \quad \text{(F.4)}$$

Substituting Eq. F.4 into Eq. F.1 yields the following relation describing the rate response due to variable discrete changes in pressure drop.

$$q(t) = q_{cp}(t-t_0)(p_i - p_{wf,1}) + q_{cp}(t-t_1)(p_i - p_{wf,2}) + q_{cp}(t-t_2)(p_i - p_{wf,3}) + \cdots + q_{cp}(t-t_n)(p_i - p_{wf,n-1}) \quad \text{..... (F.5)}$$

Alternatively Eq. F.5 can be expressed as a summation as follows:

$$q(t) = \sum_{j=1}^{n} \left(p_i - p_{wf,j}\right) q_{cp}\left(t - t_{j-1}\right) \quad \text{..... (F.6)}$$

The discretized form of the convolution equations presented above is useful in a practical sense by resolving the changing pressure drop as a function of time into discrete steps. From a theoretical standpoint, however, we now aim to obtain an integral form describing the rate response as a result of continuous pressure drop changes. Before proceeding the following variables of substitution are introduced:

$$\tau = t_{j-1} \quad \text{.....(F.7a)}$$

$$\Delta\tau = t_j - t_{j-1} \quad \text{..... (F.7b)}$$

Substituting the variables of substitution and multiplying the right hand side of Eq. F.6 by $\Delta\tau/\Delta\tau$ yields:

$$q(t) = \sum_{j=1}^{n} \frac{\Delta p_{wf}}{\Delta\tau} q_{cp}\left(t-\tau\right)\Delta\tau \quad \text{..... (F.8)}$$

We now utilize the definition of a derivative and considering the limit as $\Delta\tau$ approaches zero:

$$q(t) = \lim_{\Delta\tau\to 0} \sum_{j=1}^{n} \frac{\Delta p_{wf}}{\Delta\tau} q_{cp}\left(t-\tau\right)\Delta\tau \quad \text{..... (F.9)}$$

Evaluating the limit and simplifying yields the following definition of the convolution integral for continuously varying pressure drops.

$$q(t) = \int_0^t \Delta p'_{wf}(\tau)\, q_{cp}\left(t-\tau\right) d\tau \quad \text{..... (F.10)}$$

The definition provided by Eq. F.10 varies slightly from that introduced in the body of this work. We will now prove the equivalence of Eq. F.10 and Eq. F.11, the latter of which was introduced in the body of this work and is reproduced below.

$$q(t) = \int_0^t \Delta p_{wf}(\tau) q_{cp}^{'}(t-\tau) d\tau \quad \text{..... (F.11)}$$

Integration by parts is used to transfer between the two forms of the convolution integral. The definition of integration by parts using dummy variables is as follows:

$$\int u dv = uv - \int v du \quad \text{..... (F.12)}$$

For the problem considered here we define the dummy variables u and v along with their derivatives as such:

$$u = q_{cp}(t-\tau) \quad \text{.....(F.13a)}$$

$$du = -q_{cp}^{'}(t-\tau) d\tau \quad \text{..... (F.13b)}$$

$$dv = \Delta p_{wf}^{'}(\tau) d\tau \quad \text{.....(F.13c)}$$

$$v = \Delta p_{wf}(\tau) \quad \text{..... (F.13d)}$$

Combining Eq. 13 and Eq. 12 and evaluating the equation at its limits yields the following equation.

$$\int_0^t \Delta p_{wf}^{'}(\tau)\, q_{cp}(t-\tau) d\tau = \left[q_{cp}(0)\Delta p_{wf}(t) - q_{cp}(t)\Delta p_{wf}(0)\right] + \int_0^t \Delta p_{wf}(\tau)\, q_{cp}^{'}(t-\tau) d\tau \quad \text{..... (F.14)}$$

Utilizing our understanding of initial reservoir conditions we know that $q_{cp}(0) = 0$ and $\Delta p_{wf}(0) = 0$. Simplifying Eq. F.14 provides the continuous form of the convolution integral used to model rates effected by variable pressure drop conditions.

$$q(t) = \int_0^t \Delta p_{wf}(\tau)\, q_{cp}^{'}(t-\tau) d\tau \quad \text{..... (F.15)}$$